PHOTOPHYSICOCHEMICAL STUDIES OF PHENYLTHIO PHTHALOCYANINES: INTERACTION WITH GOLD NANOPARTICLES AND APPLICATIONS IN DYE SENSITISED SOLAR CELLS AND OPTICAL LIMITING

A thesis submitted in fulfilment of the requirements for the degree of

MASTER OF SCIENCE

Of

RHODES UNIVERSITY

By

SHAUN FORTEATH

December 2011

DEDICATION

To my parents, Anthony and Suzette Forteath

***"The important thing is not to stop questioning. Curiosity has its own reason for existing."* – Albert Einstein**

ACKNOWLEDGEMENTS

To my supervisor, Prof. Tebello Nyokong, whose guidance, expertise, understanding and patience, added considerably to my experience.

To my co-supervisor, Dr. Edith Antunes, without whose motivation and guidance I would not have completed this thesis, you are truly invaluable.

Thanks also to Prof. Derck Schlettwein and the entire research group at Justus-Liebig University Giessen for their generosity and support during my stay.

To my parents, I thank you for your constant love, support, encouragement and persuasion to continue studying and understand the true value of education and rewards of perseverance.

To my friends, whose patience and humour have kept me going throughout this experience.

I thank all my friends and colleagues in the S22 research group and the Rhodes University Chemistry Department staff and postgraduate students.

Financial support from the Nanotechnology Innovation Centre (NIC), in association with the Department of Science and Technology and Mintek, is gratefully acknowledged.

ABSTRACT

The syntheses, spectroscopic characterisation, photophysical and photochemical studies have been conducted for a variety of phenylthio substituted phthalocyanines (Pcs). Comparisons have been made taking into consideration the influence of the central metal ion, solvent properties and substituent type. The optical limiting properties were also determined for all the Pcs synthesised.

A low-symmetry metallophthalocyanine complex was similarly characterised and the photoelectrochemical parameters determined when used as a sensitiser of nanoporous ZnO. The symmetric analogue was conjugated to gold nanoparticles to determine the influence of interactions on its photophysical properties and distinct differences occurred in the absorption and fluorescence spectra suggesting successful formation of conjugates.

CONTENTS

LIST OF ABBREVIATIONS

AFM	atomic force microscopy
APCE	absorbed photon to current conversion efficiency
CD-RW	rewriteable compact disc
D149	5-[[4-[4-(2,2-diphenylethenyl)phenyl]-1,2,3-3a,4,8b-hexahydro-cyclopent[*b*]indol-7-yl]methylene]-2-(3-ethyl-4-oxo-2-thioxo-5-thiazolidinylidene)-4-oxo-3-thiazolidineacetic acid
DBN	1,5-diazabicyclo[4.3.0]non-5-ene
DBU	1,8-diazabicyclo[5.4.0]undec-7-ene
DCM	dichloromethane
DCTB	*trans*-2-[3-(4-tert-butylphenyl)-2-methyl-2-propenylidene]malononitrile
DFWM	degenerate four-wave mixing
DMAE	*N*,*N*-dimethylaminoethanol
DMF	*N*,*N*-dimethylformamide
DMSO	dimethylsulfoxide
DNA	deoxyribonucleic acid
DSC	differential scanning calorimetry
DSSC	dye sensitised solar cells
EPR	enhanced permeability and retention
F	fluorescence
FF	fill-factor
FT-IR	Fourier transform infra-red
FTO	fluorine-doped tin oxide

HOMO	highest occupied molecular orbital
HRTEM	high resolution tunnelling electron microscopy
IC	internal conversion
IPCE	incident photon to current conversion efficiency
IR	infra-red
ISC	intersystem crossing
IV	current-voltage
LUMO	lowest unoccupied molecular orbital
MRI	magnetic resonance imaging
MPc	metallophthalocyanine
N3	Ru(4,4'-dicarboxylic acid-2,2'-bipyridine)$_2$(NCS)$_2$
Nd:YAG	neodymium-doped yttrium aluminium garnet
NIR	near infra-red
NLO	nonlinear optics
NMR	nuclear magnetic resonance
NP	nanoparticles
OC	octacarboxy
OE	octaestrone
OMP	octa(methyl-phenoxy)
OP	octaphenoxy
P	phosphorescence
Pc	phthalocyanine
Ph	phenyl
PDT	photodynamic therapy
RDE	rotating disc electrode

ROS	reactive oxygen species
SDA	structure directing agent
SEM	scanning electron microscopy
SPR	surface plasmon resonance
STM	scanning tunnelling microscopy
TBAI	tetrabutylammonium iodide
TBO	toluidine blue O
TBP	tetra(*tert*-butylphenoxy)
TCSPC	time-correlated single photon counting
TEM	tunnelling electron microscopy
THF	tetrahydrofuran
THG	third harmonic generation
TLC	thin-layer chromatography
TMP	tetramercaptopyridyl
TNCDP	*tris*-(naptho)-2-(carboxy)
TRES	time-resolved emission spectra
TOABr	tetraoctylammonium bromide
UV-vis	ultraviolet-visible
VR	vibrational relaxation
XPS	X-ray photoelectron spectroscopy
XRD	powder X-ray diffraction spectroscopy

LIST OF SYMBOLS

α	non-peripheral position/linear absorption coefficient
β	peripheral position/full width at half maximum
β_1	intensity-dependent absorption coefficient
γ	second-order hyperpolarisability
Δ	heating/change
ε	molar extinction coefficient
ε_0	permittivity of free space
η	quantum efficiency
η_0	linear refractive index
θ	angle
λ	wavelength
μ	ligand bridging
ν	frequency
π	double bond/numerical value
ρ	density
σ	single bond
τ	lifetime
τ_F	fluorescence lifetime
τ_T	triplet state lifetime
$\chi^{(3)}$	third-order susceptibility
ω	frequency
Φ	quantum yield
Φ_F	fluorescence quantum yield
Φ_I	intersystem crossing quantum yield

Φ_{Pd}	photodegradation quantum yield
Φ_T	triplet state quantum yield
A/abs	absorbance/absorption
C	concentration
c	speed of light
D	core diameter
d	mean particle size
E	energy
f	Lorentz local-field enhancement factor
F	area under fluorescence emission curve
F_{in}	incident fluence
h	Planck's constant
I_{in}	incident light intensity
I_{out}	transmitted light intensity
I_{sc}	short circuit current density
k	rate constant
k_F	fluorescence rate constant
k_{ISC}	intersystem crossing rate constant
k_{IC}	internal conversion rate constant
k_d	photodegradation rate constant
N	number of atoms
N_A	Avogadro's constant
n	refractive index
M	atomic weight
S	irradiated cell area

S_0	singlet ground state
S_1	singlet excited state
t	time
T	transmittance
T_1	triplet excited state
V	volume
V_{oc}	open circuit voltage
w_0	waist radius at focus

LIST OF FIGURES

LIST OF SCHEMES

LIST OF TABLES

1. INTRODUCTION

This chapter gives a general overview of metallophthalocyanines and nanoparticles, including synthesis and basic properties. An overview of photodynamic therapy, dye sensitised solar cells and nonlinear optics is also given. The characterisation techniques used in this thesis are also summarised.

1.1 Metallophthalocyanine Chemistry

Intense research has been conducted on phthalocyanines (Pcs) ever since their initial characterisation by Linstead and Robertson in the 1930s [1,2]. Linstead conceived the term 'phthalocyanine' as a result of its structural origin from phthalic acid precursor and 'cyanine' which refers to their blue colour. Metallophthalocyanines (MPcs) are planar, tetrapyrolic, macrocyclic aromatic compounds which absorb strongly in the red region of the visible spectrum due to their highly conjugated 18-π electron system (Figure 1.1). Variations in the type, number and position of substituents (either α-non-peripheral substitution, β-peripheral substitution or axial substitution) attached to the MPc macrocycle or the central metal, greatly influence the chemical properties that make these molecules applicable in a diverse range of fields.

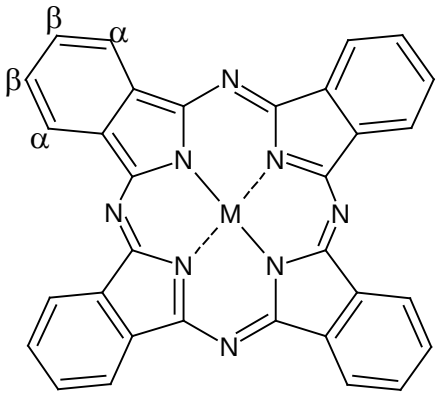

Figure 1.1. Molecular structure of metallophthalocyanine showing α- and β-positions

Originally used as dyes and pigments in the paint, textile and printing industries [3] due to their low reactivity, low solubility and high thermal stability, phthalocyanines have had recent renewed interest in high-technology applications [4] due to their high degree of aromaticity, synthetic flexibility and ability to be adapted to a wide range of

applications. These applications include use as electrocatalysts [5] and photocatalysts [6,7], as photoconductors in laser printing devices, for optical data storage in the form of rewriteable optical media (CD-RW) [8], use in Langmuir-Blodgett thin films [9,10], field effect transistors [11], liquid crystals [12,13], electrophotography [14], gas sensors [15], low-dimensional metals and semi conductors [16,17], molecular electronics and photonics [18], electrochromism in display devices [5], photovoltaics and solar cells [19,20], nonlinear optics [21,22] and in medicine as photosensitisers in photodynamic therapy (PDT) [23-25].

1.1.1 Phthalocyanine syntheses

1.1.1.1 Symmetrical phthalocyanines

Cyclotetramerisation reactions (Scheme 1.1) have primarily been performed to synthesise Pcs, with phthalonitriles (1,2-dicyanobenzene) (a) [26] most often as precursors, but phthalic anhydrides (b) [27], phthalimides (c) [28], 1,3-diiminoisoindolines (d), phthalic acids (e) [29], phthalamides (f), and o-cyanobenzamide (g) are also used. The success of the synthetic approach is dependant on several factors including precursors, metal salt, solvent, temperature, base and catalyst, with the use of phthalonitrile as precursors considered the simplest approach with highly pure products obtained.

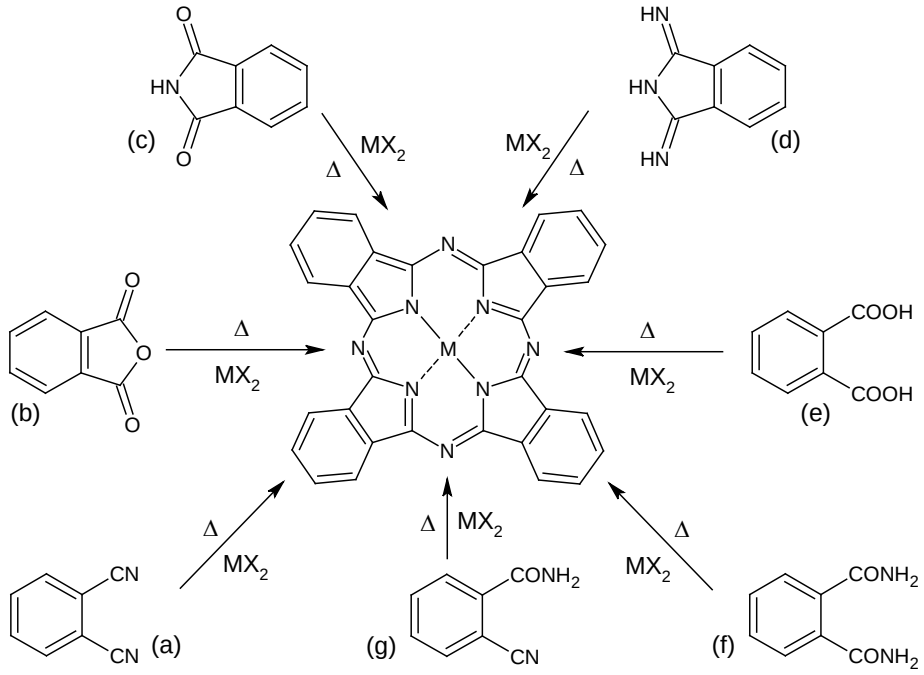

Scheme 1.1. Synthesis of phthalocyanines from different precursors

Phthalonitriles are often cyclised at high temperature in the presence of a metal salt and a basic solvent, such as *N*,*N*-dimethylaminoethanol (DMAE). Alcoholic solvents e.g. 1-pentanol in combination with bases such as 1,8-diazabicylo[5.4.0]undec-7-ene (DBU), 1,5-diazabicyclo[4.3.0]non-5-ene (DBN), piperidine or cyclohexylamine can also be used [30]. Labile metals such as lithium or sodium may be used for synthesis of free base H_2Pcs or MPcs with large central metals, with the labile metal ions easily exchanged to form the desired MPc [31]. Much initial research was focussed on the effect of changes at the α- and/or β-positions, with modifications of the peripherally fused benzene rings resulting in a number of analogues including 2,3-anthracocyanines and 1,2- [32] and 2,3-naphthalocyanines. Replacing the peripheral fused benzene rings with other fused ring systems has led to analogues including fluoranthocyanine, perylenophthalo-cyanine [33], phenanthrocyanine [34] and triphenylocyanine with tetrapyrido- [35], tetrapyrazino- [35], thiopheno- [36], and dithioleporphoryazines [37] containing peripheral heteroatoms.

1.1.1.2 Low-symmetry AAAB type phthalocyanines

Condensation reactions of two different precursors is the most common method for forming compounds with AAAA, AAAB, AABB, ABAB, ABBB and BBBB structures (Scheme 1.2). Adjusting the ratio of the precursors can optimise the formation of the AAAB structure, which can then be separated by chromatography. A 3:1 ratio for two precursors of similar reactivity is commonly used for the formation of the AAAB type Pc [38-40] with a mixture of products obtained in the following predicted percentages: AAAA (33 %), AAAB (44 %) and 23 % for other cross-condensation products. A:B molar ratios of up to 9:1 may be used when the reactivity of B exceeds that of A [41,42].

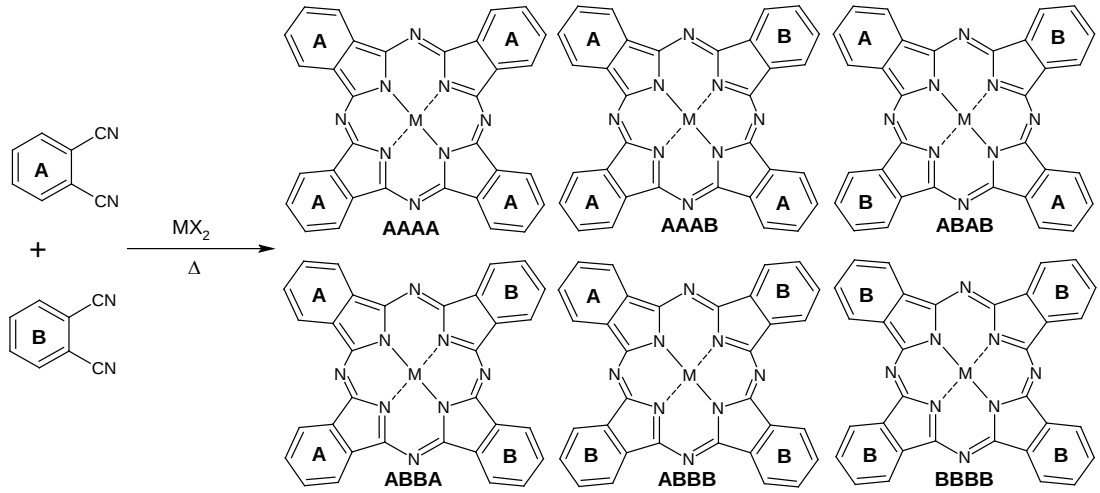

Scheme 1.2. Products anticipated for a mixed condensation of two phthalonitriles

The other methods used to selectively synthesise low-symmetry phthalocyanines are (i) the ring expansion of a subphthalocyanine [43,44] and (ii) the use of a polymer support which preferentially reacts with the B precursor through the peripheral substituent [45-48]. The statistical condensation of two different phthalonitriles was employed in this work.

1.1.1.3 Phthalocyanines synthesised in this work

In this thesis a novel low-symmetry (AAAB) ZnPc derivative containing a single carboxylic acid group (COOH) and three phenylthio (SPh) substituents (Figure 1.2 a) and novel symmetrical (AAAA) GePc derivative containing four phenylthio substituents and two axial hydroxy ligands (Figure 1.2 b) were synthesised and characterised. The reported [49] symmetric Zn and H_2Pcs containing four phenylthio substituents (Figure 1.2 b) were also synthesised and characterised.

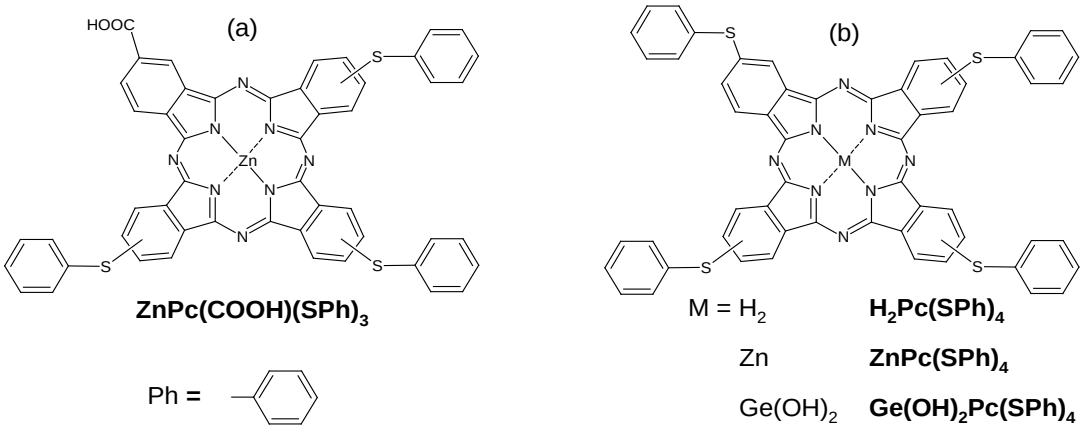

Figure 1.2. Structures of synthesised (a) low-symmetry, and (b) symmetrical Pcs

The carboxylic acid group allows for anchoring of the Pc to ZnO for applications in dye sensitised solar cells (DSSCs), and linking to bio-molecules [50-52] and other supports [53,54] is also possible. The bulky phenylthio substituents are beneficial in reducing aggregation [55,56] due to their ability to impose steric repulsion. The Q band absorbance of the Pc becomes red-shifted due to the presence of the electron donating sulfur atoms [55-66]. Conjugation to gold electrode and gold nanoparticle surfaces is also possible through the sulfur atoms [57-67]. The higher number of delocalised π-electrons contributed by the phenylthio rings have been reported to increase the ability of Pcs to create photocurrent [68]. The low-symmetry nature of

the phthalocyanine is also expected to have improved performance in DSSCs due to improved directionality of its electronic orbitals in the excited state, provided by the electron-donating phenylthio "push" groups and electron-withdrawing carboxylic acid "pull" group [68,69]. This "push-pull" mechanism is also useful in nonlinear optics [70]. ZnPc and GePc derivatives show long triplet state lifetimes (τ_T) and high triplet quantum yields (Φ_T) [71-77] required for PDT and optical limiting which are the focus of this work.

1.1.2 Ground state electronic absorption spectra of phthalocyanines

1.1.2.1 Origins of spectra

The dominant bands observed in the absorption spectra of monomeric MPcs are the intense Q band (Q_{00}) at 600-750 nm [78,79], and the less intense broad Soret or B band consisting of the B_1 and B_2 bands at ~ 350 nm [78-80]. One or two weak vibronic bands (Q_{vib}) accompany the Q band (Figure 1.3), with additional bands below 300 nm in UV-transparent solvents, such as dichloromethane (DCM) or chloroform ($CHCl_3$), referred to as N, L and C, in order of increasing energy [81,82].

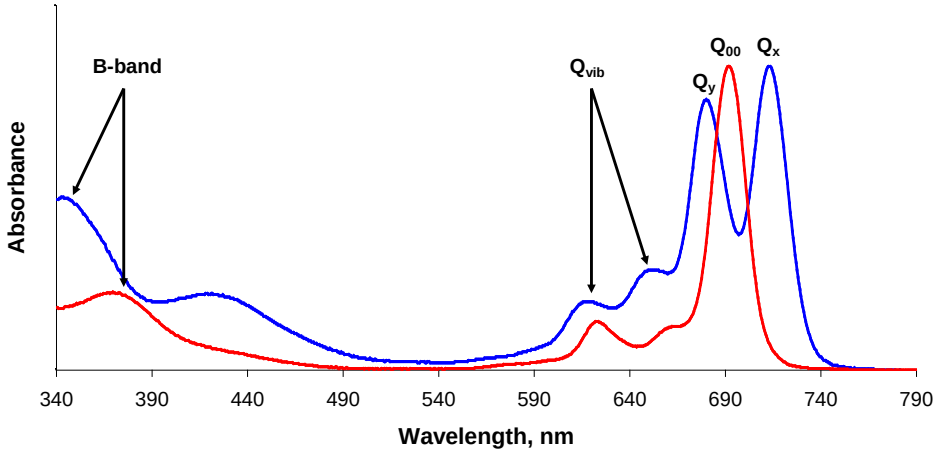

Figure 1.3. Typical ground state electronic absorption spectra of a free base H_2Pc (blue) and symmetrical MPc (red)

The origin of these bands can be explained using Gouterman's four-orbital model [83], which considers four frontier molecular orbitals: Highest occupied molecular orbital-1 (HOMO-1), HOMO, lowest unoccupied molecular orbital (LUMO) and LUMO+1 account for transitions that give rise to the first two allowed transitions in the UV-visible spectrum (Figure 1.4). The Q and B bands both generally arise from π-π* (x/y polarised) transitions, where the Pc Q band (Q_{00}) is the result of a transition from the a_{1u} (HOMO) to the degenerate e_g (LUMO) orbital while the transition from a_{2u} and b_{2u} to e_g results in the B band absorptions (B_1 and B_2).

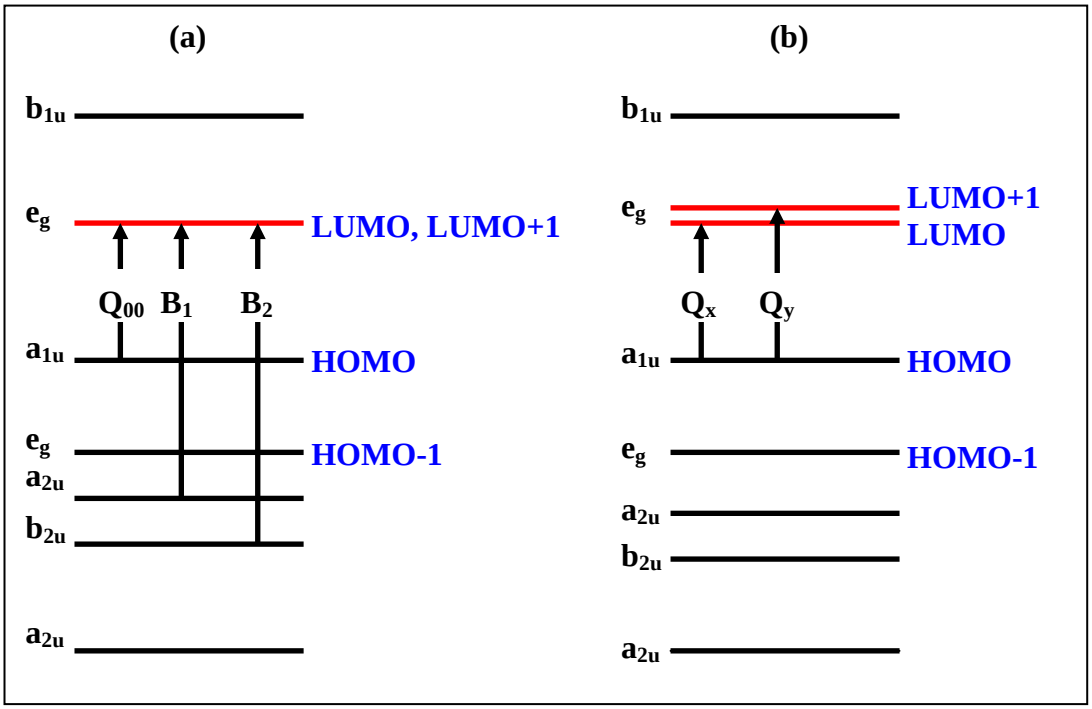

Figure 1.4. Electronic transitions (a) in symmetrical MPcs showing the origin of the $Q_{(00)}$ band and B_1 and B_2 absorption bands [84] and (b) in symmetry lowered MPcs showing the origin of the Q_x and Q_y bands

The absorption spectra of Pcs are sensitive to changes in central metal, solvent, substitution pattern and aggregation [84-86]. Metal free Pcs are characterised by D_{2h}

symmetry, increased symmetry to D_{4h} can be obtained by the introduction of a metal that fits into the Pc cavity (3.96 Å) [87], maintaining the planarity of the molecule and resulting in a reduction in the number of allowed electronic transitions. Large metal ions which often do not fit into the Pc cavity can lower the symmetry to C_{4v}. Solvents of different polarity, affect the shape, position and intensity of absorption bands. Increase in solvent polarity [88], the use of conjugated or aromatic solvents [89], or the use of coordinating solvents, such as *N,N*-dimethylformamide (DMF), dimethylsulfoxide (DMSO) and pyridine, red shifts the Q band, with the coordinating solvents resulting in interactions which stabilise the LUMO [90]. The non coordinating nature of acidic solvents, such as DCM and chloroform, favours the formation of Pc aggregates [90,91] and can affect ring oxidation, at times resulting in demetallation [72,85,92] or protonation [71].

1.1.2.2 Phthalocyanine aggregation

MPc aggregation is recognised by broadening and/or splitting of the Q band and a hypsochromic (blue) or bathochromic (red) shift [93] indicating the presence of additional electronic levels of the aggregates due to non-covalent, π-π interactions between the conjugated Pc rings. Aggregates could be formed in a number of ways including direct linkage or bridging between two or more Pc rings [94], covalent bonding involving the metal as μ-oxo links [79], sandwich-type complex formation [95,96] and weak association in which peripheral substituents hold two Pc rings that are adjacent in space [97,98]. The tendency for Pcs to aggregate is dependent on the central metal and axial ligands, position and type of substituents on the Pc periphery as well as the solvent properties [99,100] and coordinating power [49]. Bulky substituents impose steric repulsion [55,56], particularly at the α-position of the Pc ring, and reduce the tendency to aggregate; they may also distort the Pc ring from

planarity to reduce aggregation [101]. In polar solvents such as water and methanol (MeOH), Pcs are prone to aggregation driven by hydrophobic interactions [94,102] due to their large π-system [102]. Cofacial Pc dimers, referred to as H-aggregates, result in a blue-shift with the overlapping of energy levels increasing radiationless excited state deactivation leading to aggregates being photoinactive. Co-planar Pc arrangements, give rise to red-shifted absorption characteristic of J-aggregates, which are observed in some molecules, usually under certain conditions such as the nature of the solvent and substituents attached to Pc ring periphery [103]. Unlike H-aggregates, J-aggregates are photoactive [101].

1.1.3 Photophysical properties

The photophysical properties of Pcs are of particular importance in PDT, optical data storage systems as red or near-infrared (NIR) light absorbers, nonlinear optics (NLO), photoconductors and in solar cells. The Jablonski diagram [104-106] (Figure 1.5) explains the origin of the radiative (fluorescence (F), phosphorescence (P)) and non-radiative (internal conversion (IC), vibrational relaxation (VR), intersystem crossing (ISC)) photophysical properties [105].

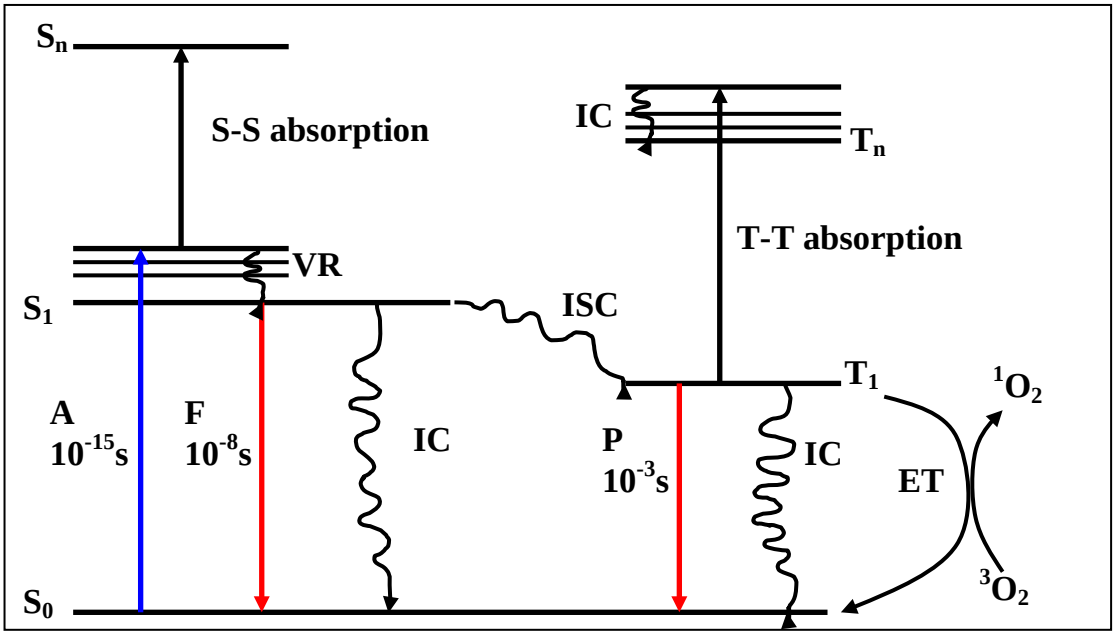

Figure 1.5. Modified Jablonski diagram showing the transition between the singlet ground state (S_0) and electronic excited states (S_1 and T_1). A = absorption, F = fluorescence, VR = vibrational relaxation, IC = internal conversion, ISC = intersystem crossing, P = phosphorescence. S_1 = singlet excited state and T_1 = triplet excited state.

1.1.3.1 Fluorescence spectra, quantum yields and lifetimes

MPc fluorescence properties such as fluorescence intensity, fluorescence quantum yield (Φ_F) and fluorescence lifetimes (τ_F) are influenced by aggregation, solvent properties, concentration, nature of the central metal, substituent type and photo-induced energy transfer [28]. Fluorescence in MPcs is usually short lived, of the order of 10^{-8} s, and is reduced in the presence of paramagnetic metals and metals of high atomic number, an effect in response to the heavy atom effect. These types of compounds encourage ISC, a spin-forbidden process, which occurs as a consequence of spin-orbit coupling. In general, the excitation spectra [107] are similar to the corresponding absorption spectra in MPc complexes. Conformational reorganisation on excitation may however lead to alteration in the shape of the spectra due to a

difference in the nuclear arrangement of the ground and excited states due to changes in the structure of the absorbing molecule. This is typical of MPcs with reduced symmetry as a result of protonation or the presence of large central metals prone to demetallation [71,108].

Quantum yields (Φ) are used to give a measure of the efficiency of a photophysical or photochemical process. Fluorescence quantum yields (Φ_F) are determined by steady-state fluorescence measurements and give a measure of the efficiency of an emission process. Φ_F is defined by a ratio of the number of fluorescing molecules to the number of photons absorbed. Relative Φ_F can be determined by a comparative method using a standard reference [109,110], whereby the Φ_F of an unknown substance is related to that of a sample with a known Φ_F value (standard) using Equation 1.1 [109]:

$$\Phi_F = \Phi_{F(Std)} \frac{F . A_{Std} . n^2}{F_{Std} . A . n_{Std}^2} \qquad (1.1)$$

where Φ_{std} is the fluorescence quantum yield of the standard; F and F_{std} refer to the areas under the fluorescence emission curves of the MPc and reference respectively; A and A_{std} are the absorbances of the sample and reference, respectively, at the excitation wavelength and n and n_{std} are the refractive indices of the solvents used for the sample and standard, respectively. A number of techniques exist to determine fluorescence lifetimes [111-114], with time domain measurements more commonly used [112,115]. The equipment used for time-domain measurements is based on gating the fluorescence signal using either time-correlated single-photon counting

(TCSPC) [113,116] or gated image intensifiers [112] techniques. Figure 1.6 shows a typical fluorescence decay curve for ZnPc, obtained using a TCSPC set-up. Determinations can also be made using the absorbance and emission spectra of MPcs [74,117] in the PhotochemCAD software package [118].

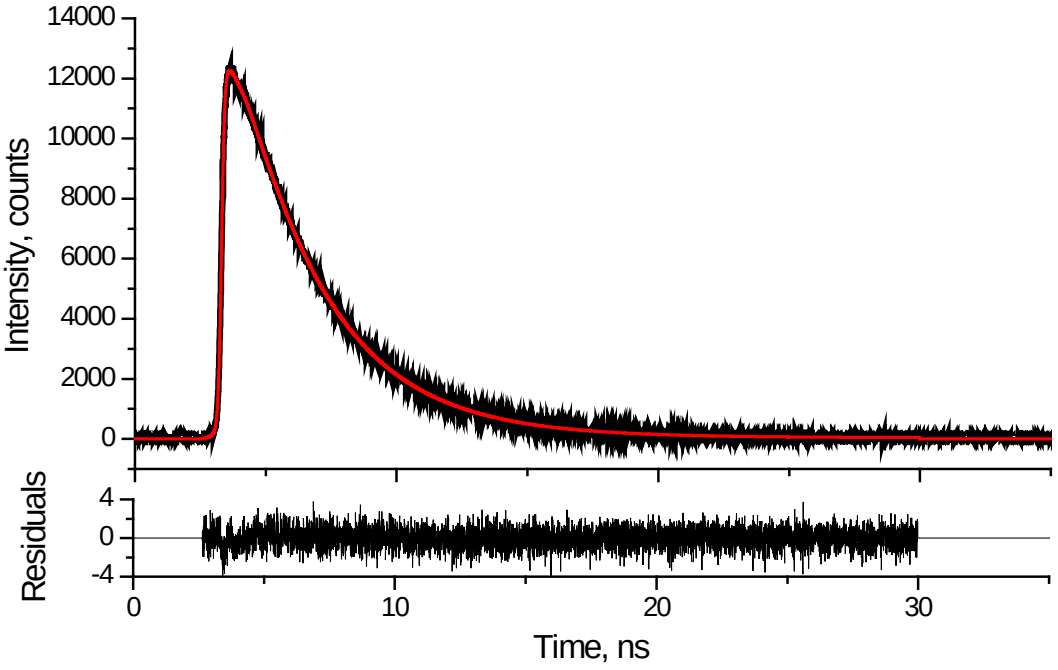

Figure 1.6. Fluorescence decay curve of ZnPc in DMSO (unpublished work)

The fluorescence lifetimes of MPcs are usually of the order of a few nanoseconds (10^{-9} s). Table 1.1 lists the photophysical properties of some ZnPc derivatives [72,108,119-124]. Figure 1.7 shows the structures of the low-symmetry Pcs listed in Table 1.1. The results show a strong dependence on the choice of substituents. The table shows that the photophysicochemical studies relating to low-symmetry MPc derivatives are also quite sparse, hence the aim of this thesis for ZnPc derivatives.

Table 1.1. Photophysical and photochemical properties of synthesised ZnPcs and selected low-symmetry and symmetrical ZnPc derivatives in DMSO

Complex[a]	Φ_T	τ_T (μs)	Φ_F	Φ_{Pd} (x10^5)	**Ref**
Low-symmetry					
ZnPc-COOH	0.82	230	0.16	0.11	[119]
ZnPcTTBI	0.82	180	0.097	0.07	
ZnPcTNC			0.05		[120]
ZnPcTNCDP			0.12		
ZnPcTFMP	0.74	240	0.20		[121]
Symmetrical					
ZnPcTMP	0.73	160	0.10	0.31	[119]
$ZnPc(COOH)_4$[b]	0.50	600	<0.01		[123]
ZnPc	0.65 [122]	350	0.20	2.61	
$ZnPc(NO_2)_4$	0.62	310	0.022		
$ZnPc(SO_3^-)_4$	0.86	470	0.07	4.03	
ZnPcTBP	0.85	160	0.14	3.33	[72,108]
ZnPcOMP	0.63	370	0.24	2.12	
ZnPcOE			0.19	275	
ZnPcOP			0.17 [71]	2.53 [124]	

[a] TMP = tetramercaptopyridyl; TBP = tetra(*tert*-butylphenoxy); OMP = octa(methyl-phenoxy); OP = octaphenoxy; OE = octaestrone

[b] 0.1 M NaOH/EtOH (1:1) as solvent

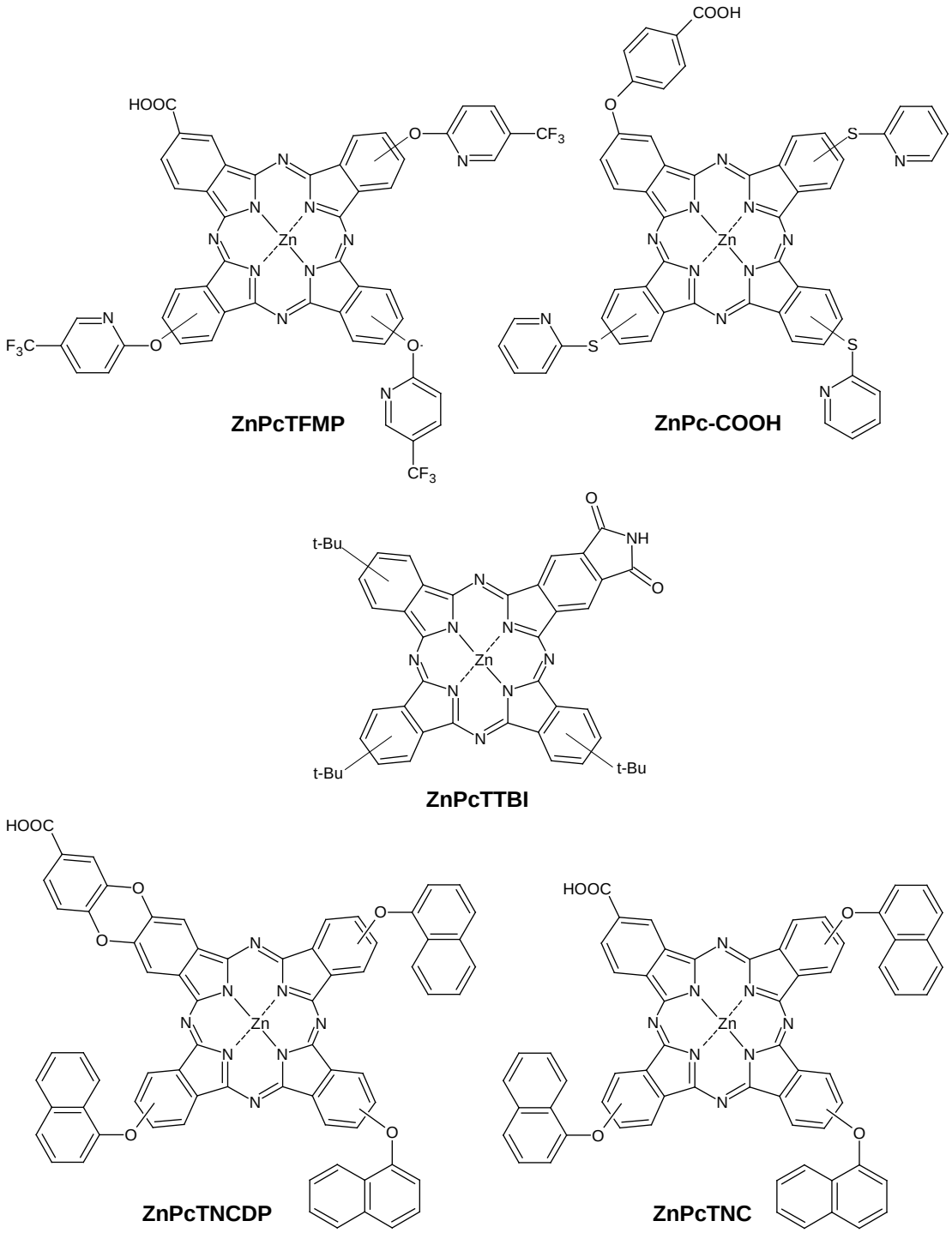

Figure 1.7. Structures of low-symmetry ZnPc derivatives

1.1.3.2 Triplet quantum yields and lifetimes

Laser flash photolysis is often used to determine the triplet state properties of MPcs, and involves the rapid introduction of an intense pulse of light, using a laser source, into an MPc solution, followed by analysis of the time-evolved electronic absorption signal. The relative population of (Φ_T) and the time spent (τ_T) in the triplet state (T_1) can be determined. The technique monitors the absorption from the T_1 state to a higher T_n state (Figure 1.5) [106,125]. Flash photolysis also provides information on the excited state lifetime of transient species. A typical triplet state decay curve is shown (Figure 1.8). The triplet quantum yield (Φ_T) may be determined by the comparative method using Equation 1.2 [122]:

$$\Phi_T = \Phi_T^{Std} . \frac{\Delta A_T . \varepsilon_T^{Std}}{\Delta A_T^{Std} . \varepsilon_T} \qquad (1.2)$$

where ΔA_T and ΔA_T^{Std} are the changes in the triplet state absorbances of the sample and the standard, respectively and Φ_T^{Std} is the triplet quantum yield for the standard in the respective solvent. ε_T and ε_T^{Std} are the triplet state molar extinction coefficients for the sample and the standard respectively, and are determined using the singlet depletion method [126] Equations 1.2 a and 1.2 b.

$$\varepsilon_T = \varepsilon_S \frac{\Delta A_T}{\Delta A_S} \qquad (1.2\ a)$$

$$\varepsilon_T^{Std} = \varepsilon_S^{Std} \frac{\Delta A_T^{Std}}{\Delta A_S^{Std}} \qquad (1.2\ b)$$

The triplet state lifetime (τ_T) is determined by the time resolved absorption measurement described above. Fitting of the triplet decay curves (as shown in Figure 1.8), using OriginPro 8 software has been used in this work for determination of the lifetimes of the MPc transients.

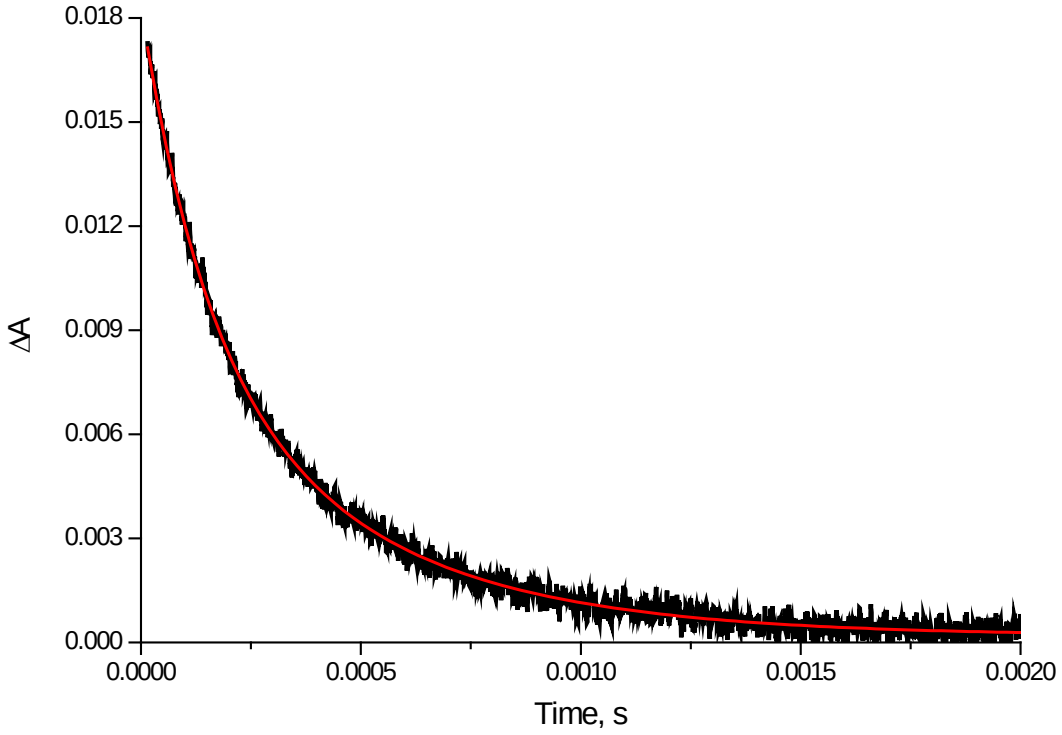

Figure 1.8. Typical triplet state decay curve of ZnPc standard

MPc triplet lifetimes are in the range between micro-seconds (μs) and milliseconds (ms) (Table 1.1). The forbidden $T_1 \rightarrow S_0$ transition accounts for this longer lifetime. The triplet state properties of phthalocyanines are sensitive to changes that deactivate fluorescence. The Φ_T and Φ_F values of MPcs in solution are influenced by the nature of the central metal ion; heavy diamagnetic or paramagnetic metal ions are known to enhance the triplet state yield. Diamagnetic metal ions such as Zn^{2+} also promote long lived lifetimes. Shortened lifetimes are experienced in the presence of heavy and paramagnetic metals due to the presence of low-lying d-orbitals which endorse

quenching of the T_1 state via charge transfer processes. Substitution with heavy atoms also result in high Φ_T. However, the $T_1 \rightarrow S_0$ transition may be enhanced as a result of heavy atom induced structural deformation. Increased molecular rigidity promotes fluorescence due to the decrease of non-radiative electronic energy 'leaking' [127]. Solvent properties such as polarity, viscosity, refractive index and temperature may also influence this rigidity. Low Φ_F values are often predicted for aggregated MPcs [128,129] and on the departure of molecular symmetry from D_{4h} in symmetry-lowered Pc analogues [44,130]. The photophysical and photochemical properties associated with symmetrically substituted ZnPc derivatives have been reported extensively [13,71,72,75-77]. The influence of the properties of solvents used is reported in this thesis. As Table 1.1 shows, photophysical studies have been conducted on very few unsymmetrically substituted ZnPc complexes. The Φ_T values of $ZnPc(SPh)_3(COOH)$ are compared in this thesis to those of the symmetrical analogues, $ZnPc(SPh)_4$ and $ZnPc(COOH)_4$ [123], and unmetallated $H_2Pc(SPh)_4$ and $Ge(OH)_2Pc(SPh)_4$. As stated above unsymmetrical MPcs are expected to improve performance in for example dye sensitised solar cells (DSSCs) and nonlinear optics (NLO).

1.1.4 Photodegradation

Photodegradation is the photochemical induced oxidative degradation of a molecule into lower molecular weight fragments [131] and is used to determine the stability of MPc molecules to light, and is thus important for light-requiring applications of interest in this work such as DSSCs and NLO. The ability of macrocyclic metal complexes to react with singlet oxygen has been reported [132-134], thus photodegradation is often considered a singlet oxygen mediated process, but photoreduction is also possible in Sn [74,135] and GePc derivatives [74,136]. The

photodegradation process generally involves oxidative attack of the MPc excited triplet state macrocycle by singlet oxygen via a Diels-Alder cycloaddition mechanism, the product being the respective substituted phthalimide (Scheme 1.3) [132,133].

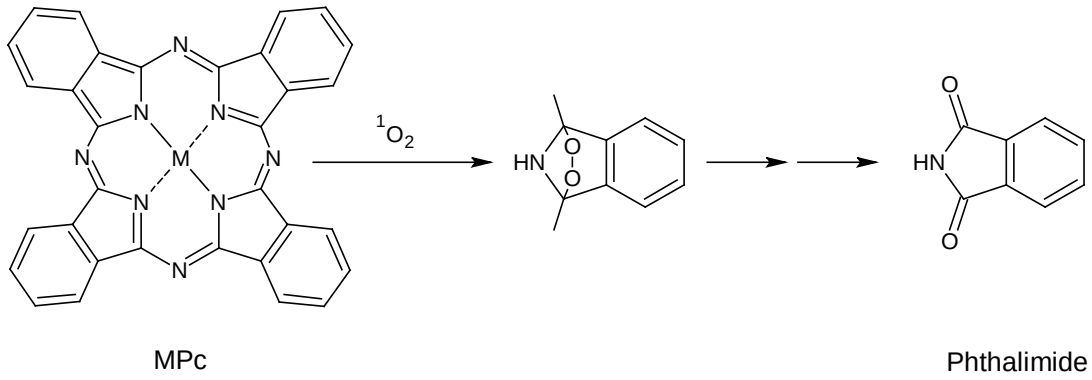

Scheme 1.3. [4+2] cycloaddition reaction of MPc with singlet oxygen ($^1O_2$)

Photodegradation depends on the MPc structure i.e. nature of substituents attached to the ring periphery and central metal, solvent, light intensity and the concentration of singlet oxygen since it is a singlet-oxygen mediated process. Electron-donating substituents on the Pc ring were reported to bring about rapid photodegradation, while electron-withdrawing substituents stabilise the Pc ring, reducing photodegradation yields owing to the difficulty in oxidising the MPc ring [124,137,138]. Substitution at the non-peripheral (α) positions of the macrocycle are known to result in a stabilising effect compared to the peripheral (β) positions [137]. Photodegradation is increased in chlorinated solvents such as chloroform and DCM as a result of their low basicity, leaving the MPc molecule open to oxidative attack [72,92,139]. Strongly coordinating, highly solvating basic solvents, such as DMSO, permit axial coordination to the central metal atom thus partly shielding the MPc molecule from oxidative attack [140]. Photodegradation rates are also reduced in the presence of

some singlet oxygen quenchers due to their ability to react with singlet oxygen [124,138]. Equation 1.3 is employed for the determination of photodegradation quantum yields [72]:

$$\Phi_{Pd} = \frac{(C_0 - C_t)VN_A}{I_{abs}St} \qquad (1.3)$$

where C_0 and C_t refer to the respective MPc derivative's concentrations (M) before and after irradiation, respectively; V is the reaction volume, N_A the Avogadro's number; I_{abs} the overlap integral of the radiation source intensity and the absorption of the MPc in the region of the interference filter transmittance [136], S is the irradiated cell area (2.0 cm^2) and t is the irradiation time, in seconds. The photochemical properties of ZnPc derivatives are quite widespread [71,72,76,77]. The aim in this thesis is to study the photochemical behaviour of the MPc complexes.

1.2 Dye sensitised solar cells

Dye sensitised solar cells (DSSCs) are a class of solar power devices that are environmentally friendly and relatively cheap, and involve the sensitisation of a wide band gap semiconductors such as ZnO or TiO_2 by organic dye molecules [141]. Moser, at the University of Vienna, discovered charge transfer from photoexcited dyes into semiconductors more than 100 years ago [142]. He observed enhancement in the photoelectric effect, in the presence of erythrosine, first detected on silver plates by Becquerel [143]. The first commercially viable DSSCs however, were only produced in 1991 by O'Regan and Grätzel [144] utilising sintered TiO_2 nanoparticles as substrate, after the discovery of the photocatalytic properties of TiO_2 for the hydrolysis of water by Fujishima and Honda were published in 1972 [145]. Photoexcitation of the dye (Figure 1.9, step a) results in the injection of an electron into the conduction band of the oxide (step b). Electron donation from the electrolyte containing a redox system, such as the iodide/triiodide couple (step c), restores the original state of the dye. Reduction of triiodide at the counter electrode regenerates the iodide (step d), with electron migration through the external load completing the circuit (step e) [146].

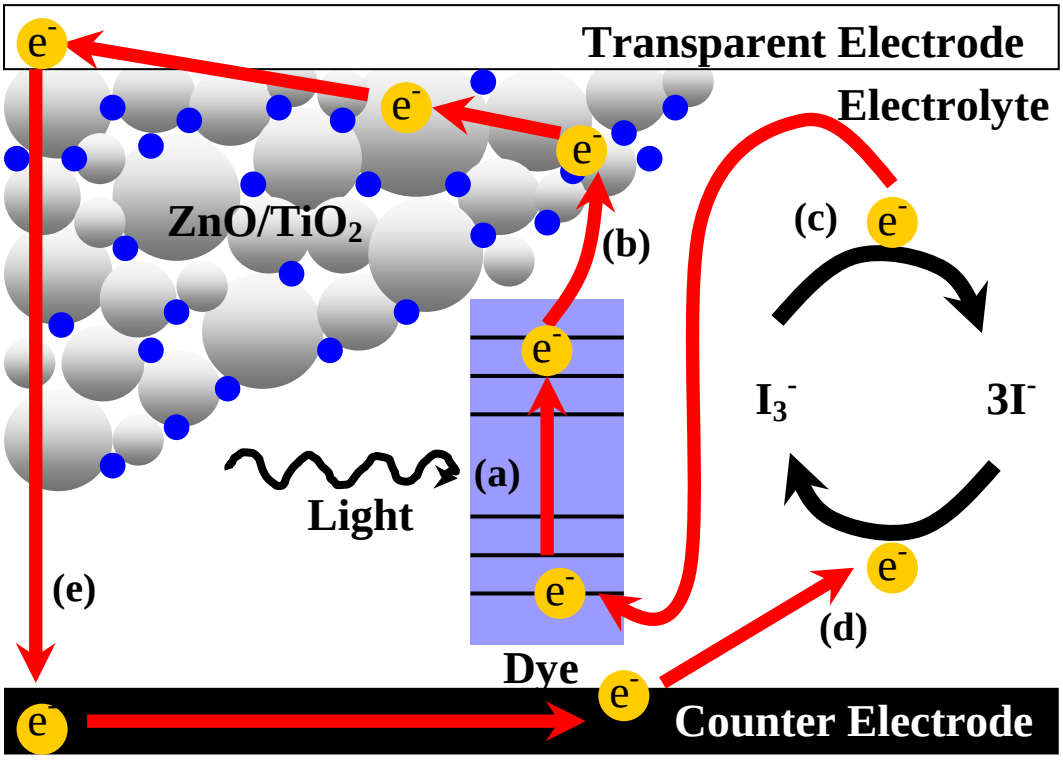

Figure 1.9. Diagrammatic representation of working principle of a DSSC

1.2.1 TiO_2 and ZnO as substrates

O'Regan and Grätzel first produced DSSCs with light-to-electric energy conversion yields of 7.1-7.9% in simulated solar light and 12% in diffuse daylight in 1991 [144]. They did so by using a paste of nano-particles of TiO_2 sintered at 450°C, producing a thin, highly porous film with a high surface roughness. This film was then sensitised with a monolayer of a ruthenium complex, the produced DSSC showed high stability as well as fast electron injection, and paved the way for practical development. The most efficient DSSCs produced, with efficiencies above 11%, are those of TiO_2 sensitised with Ru tris-bipyridyl (N3 dye) type complexes, structure shown in Figure 1.10 [147]. The drawback of such cells is the need for high temperatures for film formation, preventing development of solar cells on flexible plastic substrates. This was overcome by the development of ZnO films that could be produced and sensitised under mild conditions.

Highly crystalline ZnO thin films can be produced by cathodic electrodeposition methods. Electrochemical reduction of molecular oxygen can be utilised to induce precipitation of ZnO, with eosin Y added as a catalyst and structure directing agent producing ZnO films with high roughness factors, increasing the available surface area for sensitiser molecule binding [148]. The eosin Y molecules could be desorbed in mild alkaline KOH solution, with readsorption of the dye resulting in higher electrochemical performance [149]. The best performing photosensitiser on ZnO is the indoline dye, 5-[[4-[4-(2,2-diphenylethenyl)phenyl]-1,2,3-3a,4,8b-hexahydro-cyclopent[*b*]indol-7-yl]methylene]-2-(3-ethyl-4-oxo-2-thioxo-5-thiazolidinylidene)-4-oxo-3-thiazolidineacetic acid (D149) (Figure 1.10), with efficiencies of over 5 % obtained [150,151] (Table 1.2).

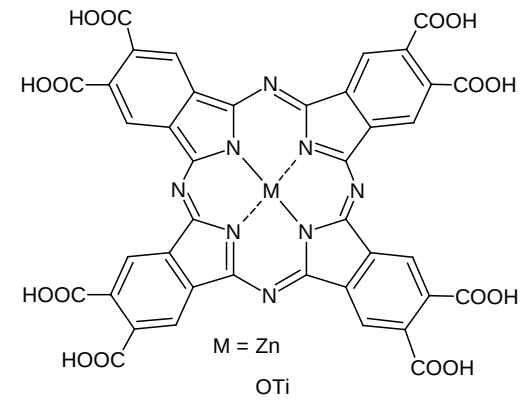

ZnPcOC; OTiPcOC

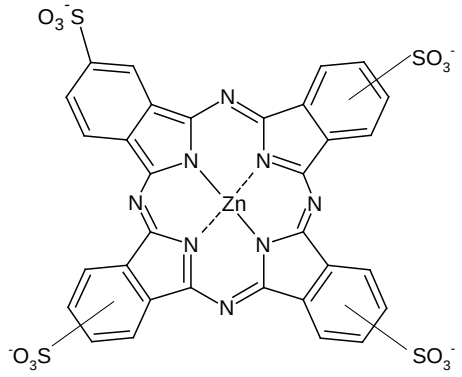

ZnPcTS

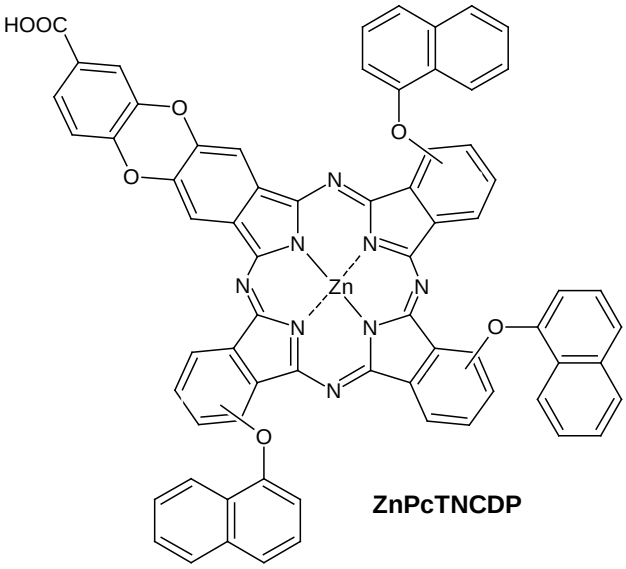

ZnPcTNCDP

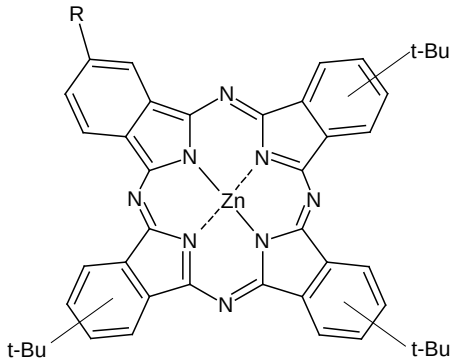

R = -COOH **TT1**

= HOOC COOH **PCH001**

= COOH **TT5**

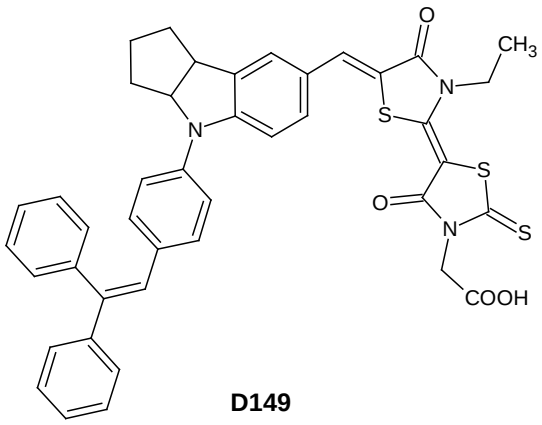

D149

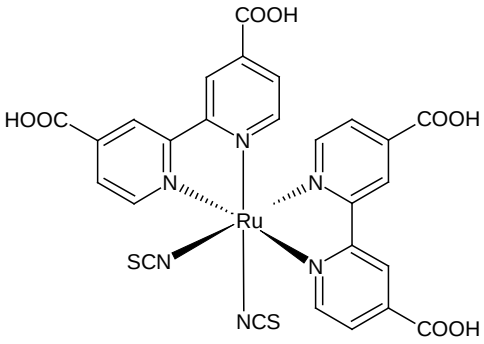

N3 Dye

Figure 1.10. Structures of selected dyes used for DSSCs

1.2.2 Use of phthalocyanines in dye sensitised solar cells

Metallophthalocyanines are potentially useful in the production of photovoltaic cells as they absorb intensely in the red and near infra-red regions of the solar spectrum, are stable and non toxic, and are easily oxidised and reduced. Much research has focussed on designing Pcs suitable for use in DSSCs, with particular interest in the nature of the linkage to the semiconductor surface, the properties of the substituents, and the effects these have on the directionality of the Pc in the excited state [152-156]. Carboxylic or sulfonic groups on the MPcs, not only increase their water solubility, but also allow covalent bonds to form with the hydroxide groups on the ZnO surface [152]. Decreasing the size of the link between the phthalocyanine ring and the carboxylic acid has been reported to improve performance on TiO_2, with insulating and flexible linkers shown to result in poor electronic coupling [153]. Part of the energy absorbed by the Pc can be transformed into heat as a result of non-radiative processes of excited state deactivation, rather than in separation of charge. It was found that photothermal conversion is most probably due to the presence of mobile long-chains which contribute to the loss of energy, with the deactivation being the thermal conversion to the ground state [68]. Thus in this work COOH is directly attached to the Pc ring without a linker in $ZnPc(SPh)_3(COOH)$.

Table 1.2 lists some MPcs used as sensitisers of ZnO [154,156]. The highest efficiencies obtained thus far for ZnPc derivatives on ZnO are 0.33%, 0.15% and 0.48% for zinc(II)- octacarboxy (ZnPcOC) [154], -tetrasulfo (ZnPcTS) [155] and -*tris*-(naptho)-2-(carboxy) (ZnPcTNCDP) phthalocyanines [156] respectively (Structures shown in Figure 1.10). The relatively low efficiency of cells incorporating phthalocyanines appears to be due to aggregation, solubility problems and lack of

directionality in the excited state [69]. Novel low-symmetry zinc phthalocyanines (TT1, PCH001 and TT5) that contain *tert*-butyl and carboxylic acid groups that act as "push" and "pull" groups, respectively, have been designed [153,157] and using these sensitisers on TiO_2, high conversion efficiencies for Pcs of 3.05% (PCH001), 3.10% (TT5) and 3.52% (TT1) were obtained (Table 1.2). The function of the carboxylic acid groups was for attachment onto the semiconductor surface and to provide electronic coupling between excited-state wave function of the phthalocyanine and the conduction-band of the semiconductor. The purpose of the three *tert*-butyl groups was to enhance the solubility, to minimise the aggregation, and to tune the LUMO level of the Pc, providing directionality in the excited state. Based on these observations, $ZnPc(SPh)_3(COOH)$ with a similar "push-pull" mechanism was employed with the hope of improving efficiency in DSSCs.

Table 1.2. Photoelectrochemical parameters of sensitisers of ZnO at an incident photon flux of 10^{16} $s^{-1}.cm^{-2}$ (IPCE, APCE) or conditions close to AM 1.5 (FF, η).

Sensitiser	IPCE (%)	APCE (%)	I_{sc} ($mA.cm^{-2}$)	V_{oc} (mV)	FF (%)	η (%)	Ref.
ZnPcOC	14.98	44.1			46	0.33	[154]
ZnPcTNCDP	30.9	34.6	3.1	420	37	0.48	[156]
PCH001[a]	75.0		6.5	635	74	3.05	[157]
TT5[a]	65.0		6.8	613	74	3.10	[153]
TT1[a]	85.0		7.6	617	75	3.52	[153]
OTiPcOC	50.6	62.8			36	0.45	[156]
D149	12.2		12.23	691	66	5.56	[151]
N3 Dye[a]	>80	98	18.2	720	73	10.0	[147]

[a] TiO_2 used as semiconductor substrate

1.2.3 Parameters for dye sensitised solar cells

The incident photon to current conversion efficiency (IPCE) and absorbed photon to current conversion efficiency (APCE), calculated in Equations 1.4 [158] and 1.5 [159], indicate how well the cells convert light into current.

$$IPCE = 1240 \times \frac{I_{(\lambda)}}{P_{in} \times \lambda} \tag{1.4}$$

$$APCE = \frac{IPCE}{1 - 10^{-abs(\lambda)}} \tag{1.5}$$

where $I_{(\lambda)}$ is the current density (mA/cm^2) at the photoexcitation wavelength (λ), P_{in} is the incident light power density (mW/cm^2) and $1 - 10^{-abs}$ is the light harvesting efficiency at the monochromatic absorbance of the photosensitiser. The short-circuit current (I_{sc}) and open-circuit voltage (V_{oc}) are the maximum current and voltage respectively from a solar cell (Figure 1.11).

The fill factor (FF), is a parameter which, in conjunction with V_{oc} and I_{sc}, determines the maximum power from a solar cell, and is defined as the ratio of the maximum power (V_{Pmax} x I_{Pmax}) from the solar cell to the 'dummy' power output (V_{oc} x I_{sc}), Equation 1.6 [160]:

$$FF = \frac{I_{P\max}.V_{P\max}}{I_{sc}.V_{oc}} \tag{1.6}$$

The quantum efficiency of a solar cell (η) is the ratio of charge carriers collected by the solar cell to the number of photons of a given energy shining on the solar cell and is calculated in Equation 1.7 [160]:

$$\eta = \frac{I_{P\max}.V_{P\max}}{\mathrm{E\ x\ A_c}} \tag{1.7}$$

where $I_{Pmax}.V_{Pmax}$ is the maximum power point on the IV curve (Figure 1.11), E (W/m^2) is the input light irradiance under standard test conditions (AM 1.5) and A_c (m^2) is the surface area of the solar cell.

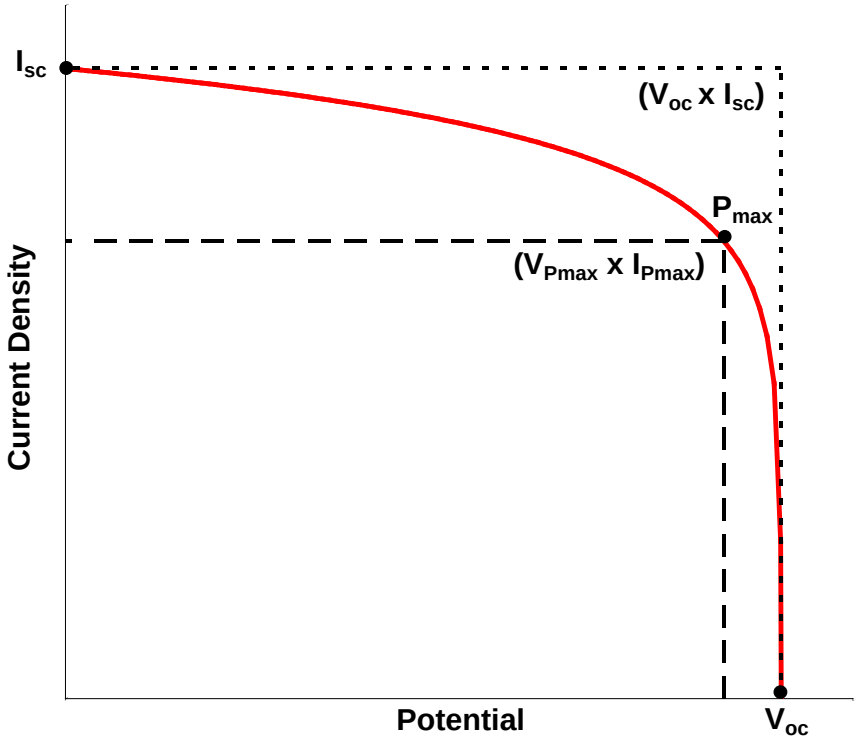

Figure 1.11. Typical IV curve showing origin of parameters

1.3 Nonlinear optics

Nonlinear optics (NLO) is the branch of optics that describes the behaviour of light in nonlinear media, in which the dielectric polarisation responds nonlinearly to the electric field. The mechanism present in all materials arises from perturbation of the electronic distribution in the material by the electric field of the incident light. At low intensities, this is the mechanism for linear polarisability, at high intensities, the electron distribution no longer follows the applied field, resulting in both second and third-order nonlinear susceptibilities [89]. Nonlinear processes can be classified into two main categories, parametric and non-parametric. Macroscopic parametric processes are described in Equation 1.8:

$$P = \chi^{(1)}E + \chi^{(2)}EE + \chi^{(3)}EEE + \ldots \quad (1.8)$$

where $\chi^{(1)}$, $\chi^{(2)}$ and $\chi^{(3)}$ are the linear, quadratic (first-order) and cubic (second-order) susceptibility tensors respectively. The molecular polarisation for microscopic parametric processes is described in Equation 1.9:

$$p = \alpha E + \beta EE + \gamma EEE + \ldots \quad (1.9)$$

α, β and γ being the linear polarisation and the quadratic and cubic hyperpolarisabilities respectively. Non-parametric processes are resonant and rely on light-induced changes in the population of the energy levels of the system.

There is a larger variety of third-order parametric effects, described by $\chi^{(3)}$ (ω: ω_1, ω_2, ω_3) susceptibilities [161], in comparison to those related to second-order.

Experimental techniques used to study third-order NLO processes and to measure susceptibilities include: third harmonic generation (THG) [162], which involves electronic processes and measures $\chi^{(3)}$ (3ω: ω, ω, ω); degenerate four-wave mixing (DFWM) [161], which may include other contributions (thermal, non-parametric, etc.) and measures $\chi^{(3)}$ (ω: ω, - ω, ω); and Z-scan [163], which may respond to mechanisms similar to DFWM and measures nonlinear refraction and absorption. Parametric and non-parametric effects contribute to nonlinear refraction and absorption, and have practical relevance in relation to optical limiting [164].

Optical limiting is a nonlinear effect consisting of a decrease in the transmittance of a sample under high intensity or fluence illumination and has applications for sensor protection including the human eye. The ideal behaviour (Figure 1.12) involves transmitted intensity remaining constant (or decreasing) above a certain illumination intensity, with a linear decrease of the initial constant transmittance above the threshold [70].

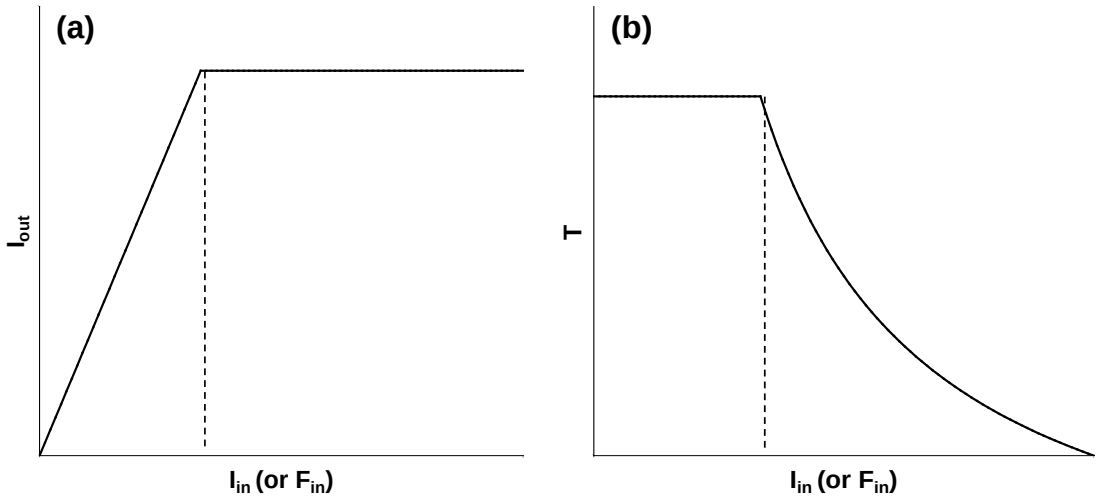

Figure 1.12. Ideal behaviour of an optical limiter: (a) transmitted intensity I_{out} vs. incident intensity I_{in} (or fluence F_{in}); (b) transmittance T versus I_{in} (or F_{in}).

Phthalocyanines have found application in NLO, and optical limiting in particular, as they have two-dimensional π-electron delocalisation and their structure can be modified by addition of suitable substituents and different central metals of different oxidation states to fine tune the NLO response. They also have advantages over inorganic materials as they have large nonlinearities, ultrafast response times and easy and economic processability for the preparation of thin films [164-169].

Under illumination an initial photon of around 550 nm is absorbed at the ground state level S_0 (Figure 1.5) of the Pc to a high vibrational level S_1' of the singlet excited state S_1 (Q band). Rapid decay into a lower energy triplet T_1 state occurs, and another photon may be absorbed exciting the system to a higher triplet level T_2. One-photon transitions from S_1 to S_2 are also possible [70]. Optical limiting properties of a number of ZnPc derivatives [170] are shown in Table 1.3.

Table 1.3. Optical limiting parameters of some ZnPc derivatives [170]

Pc Structure	**Im{$\chi^{(3)}$} (esu)**	**Im{γ} (esu)**
ZnPc(*t*Bu)$_4$	(1.1 ± 0.2) x 10^{-11}	(7.3 ± 1.4) x 10^{-33}
ZnPc(C_6H_{13})$_8$	(1.5 ± 0.3) x 10^{-11}	(8.6 ± 1.7) x 10^{-33}
ZnPc($C_{10}H_{21}$)$_8$	(9.1 ± 1.8) x 10^{-12}	(6.9 ± 1.3) x 10^{-33}
ZnPc($Ciso_5H_{11}$)$_8$	(1.5 ± 0.3) x 10^{-11}	(7.9 ± 1.5) x 10^{-33}
ZnPc($C_3H_7OSO_2$)$_8$	(5.4 ± 1.0) x 10^{-12}	(3.2 ± 0.6) x 10^{-33}
ZnPc($C_3H_7OSO_2$)$_6$(I)	(5.7 ± 1.1) x 10^{-12}	(3.2 ± 0.6) x 10^{-33}
ZnPc(*t*Bu)$_3$(C≡CH)	(1.3 ± 0.2) x 10^{-11}	(8.3 ± 1.6) x 10^{-33}
ZnPc(*t*Bu)$_3$(C≡C)CoPc(*t*Bu)$_3$	(2.1 ± 0.4) x 10^{-12}	(2.6 ± 0.5) x 10^{-33}
ZnPc(*t*Bu)$_3$(C≡C)ZnPc(*t*Bu)$_3$	(4.6 ± 0.8) x 10^{-12}	(5.8 ± 1.1) x 10^{-33}

The parameters for determining the suitability of Pcs for optical limiting are the imaginary third-order susceptibility, Im{$\chi^{(3)}$}, and the imaginary second-order hyperpolarisability, Im{γ}. Im{$\chi^{(3)}$} is directly related to the intensity-dependent absorption coefficient β_1, and is calculated using Equation 1.10 [170]:

$$\mathrm{Im}\{\chi^{(3)}\} = \frac{\eta_0^{\,2}\varepsilon_0 c\lambda\beta_1}{2\pi} \qquad (1.10)$$

where η_0 is the linear refractive index, c is the speed of light ($m.s^{-1}$), ε_0 is the permittivity if free space ($C.V^{-1}.m^{-1}$) and λ is the wavelength of the laser used (m). The relationship between Im{$\chi^{(3)}$} and Im{γ} takes concentration into account and is calculated using Equation 1.11 [170]:

$$\mathrm{Im}\{\gamma\} = \frac{\mathrm{Im}\{\chi^{(3)}\}}{f^4 C_{mol} N_A} \qquad (1.11)$$

where f is the Lorentz local-field enhancement factor and is defined as $f = (\eta_0^2 + 2)/3$, C_{mol} is the molar concentration of the solution and N_A is Avagadro's constant. The aim in this thesis is to determine the suitability of the synthesised complexes for optical limiting applications and to determine the effect of the central metal and solvents on the optical limiting parameters.

1.4 Conjugates of phthalocyanines with gold nanoparticles

Conjugates of gold nanoparticles (AuNPs) and Pcs may be used for drug delivery in photodynamic therapy (PDT).

1.4.1 Basics of photodynamic therapy

PDT has developed as an alternative for the discriminative destruction of cancerous tumours [171]. The superior attributes of MPcs, allow for their use in PDT [23,24,172]. These include red or near infra-red absorption, non-toxicity, with low skin photosensitising potency, selective localisation in tumours, efficient singlet oxygen generation and appreciable fluorescence for visualisation. PDT is a non-invasive, oxygen dependant treatment using a specific wavelength of light to excite light-sensitive (photosensitiser) dyes within target cells to generate cytotoxic derivatives of oxygen (e.g. O_2 ($^1\Delta_g$), O_2^-, $O_2^{\cdot}$, and $OH^{\cdot}$). The highly reactive nature of these species are limited to the immediate vicinity of the photosensitiser. The cytotoxic oxygen species are produced by one of two processes, namely Type I and Type II processes (Scheme 1.4), mediated by the excited triplet state of the photosensitiser.

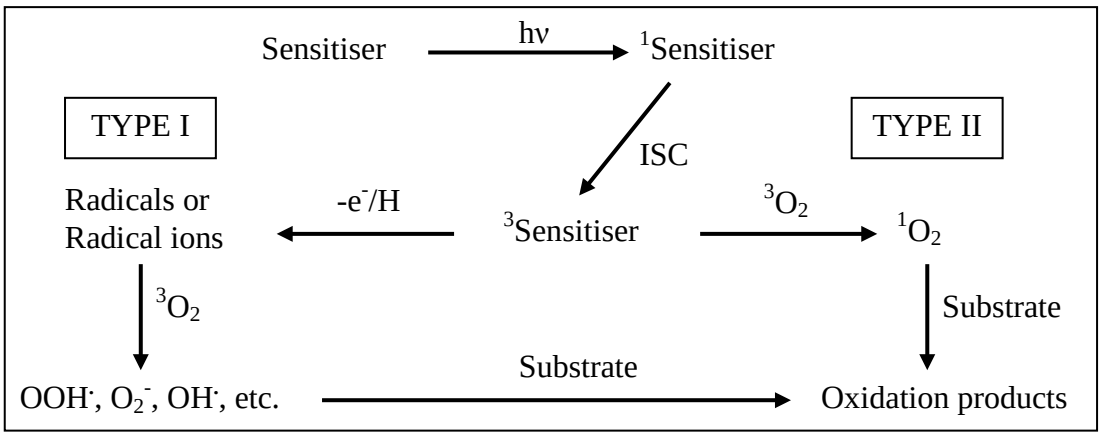

Scheme 1.4. Photosensitisation during photodynamic therapy

It is difficult to distinguish between the two reaction mechanisms in PDT, with contribution from both Types I and II processes probable. Type I mechanism involves electron/hydrogen transfer directly from the photosensitiser, producing ions or radicals which then react rapidly, usually with oxygen, producing highly reactive oxygen species (ROS). Direct interaction of the excited triplet state photosensitiser with ground state molecular oxygen, in Type II reactions, results in the photosensitiser returning to its singlet ground state (S_0) and the formation of reactive singlet oxygen. Studies suggest that singlet oxygen (Type II mechanism) is the mediator in PDT [171].

1.4.2 Nanoparticles in photodynamic therapy

Nanoparticles are routinely defined as particles with sizes between about 1 and 100 nm that show properties that are not found in bulk samples of the same material [173]. They have found applications in biology and medicine as fluorescent biological labels [174-177], magnetic resonance imaging (MRI) contrast enhancers [178], as probes of DNA structure [179] and in tissue engineering [180,181]. Other uses include applications in drug and gene delivery [182,183], detection of pathogens [184] and proteins [185], tumour destruction via heating (hyperthermia) [186], in the separation and purification of biological molecules and cells [187] and in phagokinetic studies [188].

Nanoparticles have been employed in multi-functional medicines as their surfaces can be modified with different functional groups including photosensitisers and targeting moieties. The nanoparticles are expected to concentrate at the target site due to the enhanced permeability and retention (EPR) effect [189] and can be irradiated locally, with higher concentrations of ROS thus produced by the photosensitiser at the site.

The administered nanoparticles may act as photosensitisers, carriers of photosensitisers, light antennas for photosensitisers (up- and down-converters) or as carriers of multiple functions. Studies have shown that quantum dots alone are capable of producing singlet oxygen and ROS [190-193], the overall quantum yields were however low and cadmium-based quantum dots are toxic. ZnPcs have been used as photosensitisers attached to up-converting nanoparticles and caused cell death upon irradiation due to the production of ROS [194,195]. The most promising results of increased PDT efficacy compared to the free photosensitising molecules has been observed in the study of photosensitiser-doped silica nanoparticles [196] and gold nanoparticle/photosensitiser conjugates [57]. A number of photosensitising molecules have been conjugated to gold nanoparticles including toluidine blue O (TBO) [197], porphyrins [198] and chlorins [199] after the initial conjugation with a phthalocyanine [57]. Gold nanoparticles (AuNPs) are attractive as they are non-toxic [200,201] and are already used in therapy. AuNPs are linked to the higher yielding $ZnPc(SPh)_4Pc$ in this work, and the photophysical behaviour of the conjugate is studied.

1.4.2.1 Synthesis of gold nanoparticles

Generally, gold nanoparticles are produced in a solvent by reduction of chloroauric acid ($HAuCl_4$). A reducing agent, usually sodium borohydride ($NaBH_4$), causes dissolved Au^{3+} ions to be reduced to neutral gold atoms (Au^0). The solution becomes supersaturated as more gold atoms form and gold gradually starts to nucleate and grow into particles. To prevent aggregation, stabilising agents are usually added to bind to the nanoparticle surface. A number of synthetic methods have been developed including aqueous syntheses of citrate stabilised nanoparticles by the so called Turkevich method [202], using nanoparticles seeds with hydroquinone as the reducing agent in the Perrault method [203] and using HCl and NaOH as stabilisers of ‘naked’

nanoparticles in the Martin method [204]. The nanoparticles produced in this report were synthesised following the Brust method (Scheme 1.5) in which the nanoparticles are produced in an organic solvent with tetraoctylammonium bromide (TOABr) used as both a phase-transfer catalyst and stabilising agent [205].

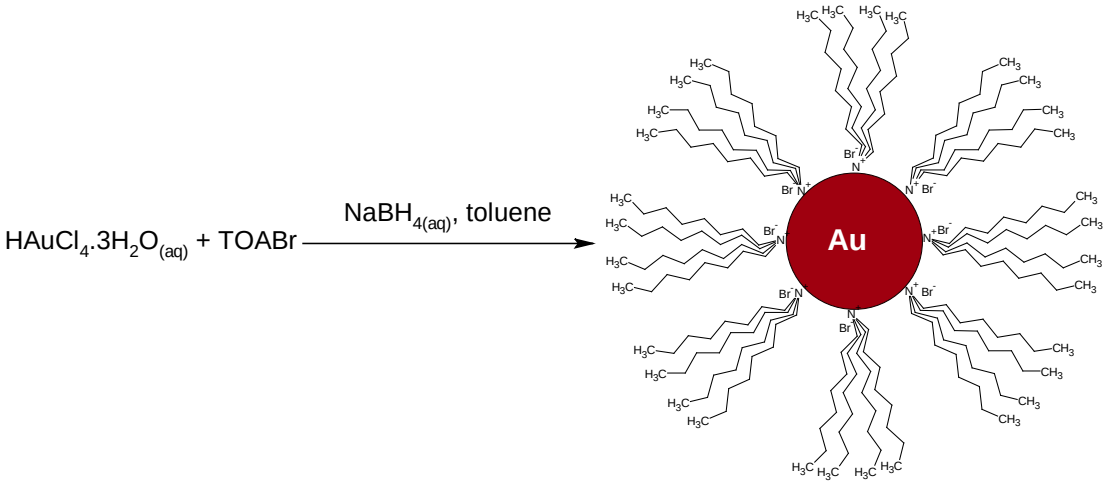

Scheme 1.5. General synthesis of TOABr stabilised AuNPs using Brust method

The concentration of the freshly synthesised nanoparticles in solution can be determined using Equation 1.12 [206]:

$$C = \frac{N_{Total}}{N.V.N_A} \qquad (1.12)$$

where N_{Total} is the number of atoms in the initial amount of gold salt added to the reaction, V is the volume of the reaction solution in litres, N_A is Avogadro's constant and determining the number of gold atoms in each nanoparticle, N is calculated using Equation 1.13 [206]:

$$\mathrm{N} = \frac{\pi \rho D^3}{6\,\mathrm{M}} \tag{1.13}$$

where ρ is the density for face centred cubic gold (19.3 g/cm^3), M the atomic weight of gold and D the average core diameter determined form high resolution tunnelling electron microscopy (HRTEM) or powder X-ray diffraction (XRD).

The size of the nanoparticles can be controlled by changing the relative ratios of the reactants, but the most important parameter for tuning the properties for a specific application is the shape of nanoparticle. Gold nanorods [207-211], nanoplates [212-215], branched [216] and platonic nanoparticles including cubes [217] and faceted spheres [218] have been synthesised.

1.4.2.2 Methods of characterising gold nanoparticles

A wide variety of characterisation and analytical techniques, other than those discussed, applies to nanostructure materials. Imaging by microscopy and analysis by spectroscopy are in general the two techniques for characterisation of nanomaterials. Structural information relating to the crystal lattice can be acquired using XRD [219,220]. The mean particle size can be determined using the Scherrer equation [221], Equation 1.14:

$$d(\mathrm{\AA}) = \frac{k\lambda}{\beta Cos\,\theta} \tag{1.14}$$

where k is an empirical constant (0.9), λ is the X-ray source wavelength (1.5405 Å for Cu), β is the full width at half maximum of the diffraction peak, and θ is the angle of

the peak. Surface analysis and depth profiling can be conducted using X-ray photoelectron spectroscopy (XPS). High-resolution images of the sample surface can be obtained using scanning electron microscopy (SEM) and structure and morphological fine structural details can be probed using transmission electron microscopy (TEM). Surface topological information and imaging of the surface structure can be provided by atomic force microscopy (AFM) and scanning tunneling microscopy (STM) methods. Other commonly employed techniques include solid-state nuclear magnetic resonance spectroscopy (NMR) and differential scanning calorimetry (DSC). In this thesis, XRD, XPS and UV-vis and fluorescence spectroscopies, and TEM and AFM microscopy have been used to investigate the structural properties of the gold nanoparticles.

UV-vis electronic absorption spectroscopy is often employed for analysis of the optical properties that accompany nanoparticles. The cherry-red to purple colour of AuNP solutions is attributed to surface plasmon oscillations in the conduction band of the gold. d-Electrons in the gold are free to move, with no scattering expected for particles smaller than ~50 nm. All the interactions with light are expected to be on the surface, with light of wavelengths larger than the nanoparticle size setting up standing resonance conditions. The electron density in the particle polarises to one surface and oscillates in resonance with the light's frequency as the wave front of the light passes (Figure 1.13) [222].

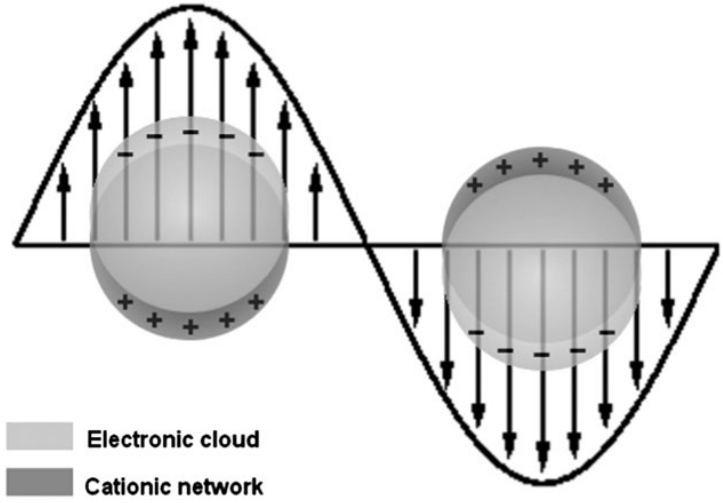

Figure 1.13. Schematic description of electronic cloud displacements in nanoparticles under the effect of an electromagnetic wave [222]

The shape, size, capping material and other chemically bonded molecules affect the surface plasmon resonance (SPR) band peak (Figure 1.14) due to changes in the nature of the nanoparticle surface [223].

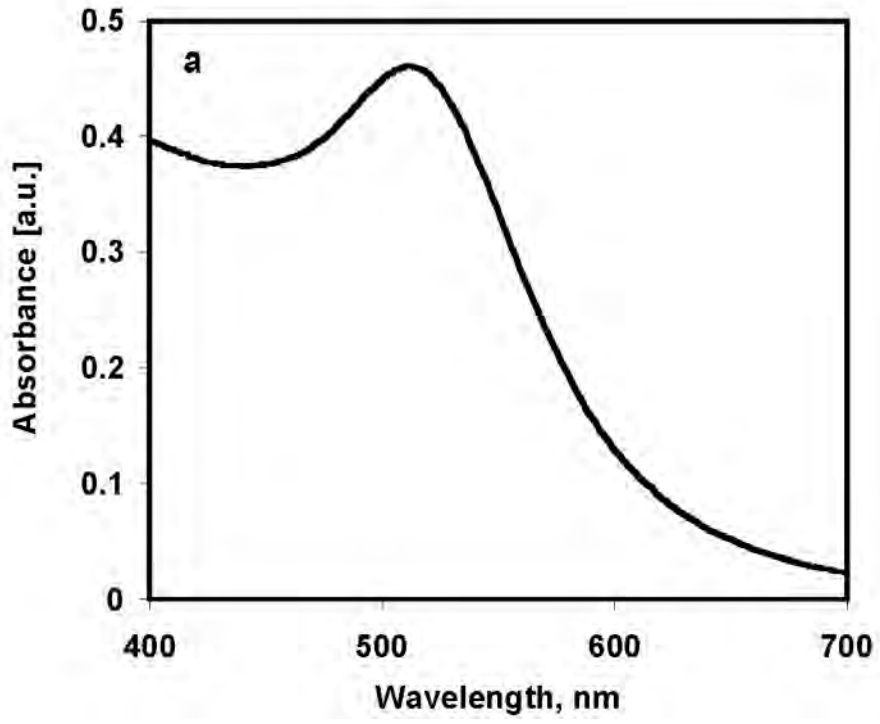

Figure 1.14. Typical absorption spectrum of AuNPs [224]

The molar extinction coefficient (ε) of the SPR peak of the nanoparticles in solution is related to the size of the nanoparticles using Equation 1.15 [206]:

$$\ln\varepsilon = k \ln D + a \tag{1.15}$$

where k = 3.32111, a = 10.80505, and D is the core diameter of the nanoparticles.

1.4.3 Synthesis of phthalocyanine-nanoparticle conjugates

A ligand exchange approach has been successfully employed in a number of reports [57-61,66,67,225] resulting in the conjugation of phthalocyanines to gold nanoparticles. This approach involves stirring the nanoparticles with appropriately substituted Pc molecules, allowing for the replacement of the stabiliser with the phthalocyanine molecule, through binding of sulphur or nitrogen atoms of the Pc substituents with the gold surface (Scheme 1.6).

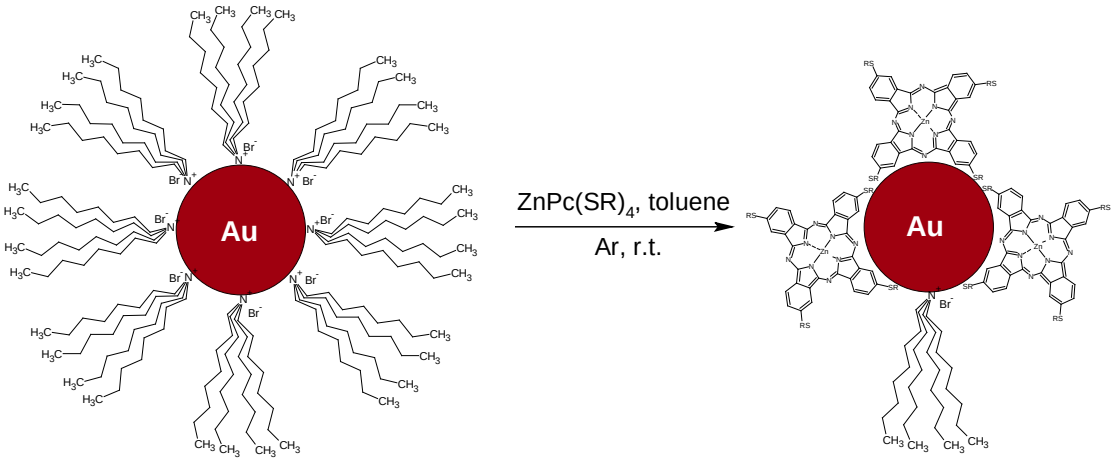

Scheme 1.6. General conjugation of Pcs to TOABr-AuNPs

A number of techniques can be employed to determine the nature of the bound molecules. These include fluorescence techniques, such as time correlated single

photon counting (TCSPC) and time resolved emission spectra (TRES). Gold nanoparticles are known to quench fluorescence of bound dyes. Decreased fluorescence quantum yields (Φ_F) and lifetimes (τ_F) are often observed. Table 1.4 shows some MPc complexes containing SH, S-S, RS or NH_2 groups which have been coordinated to AuNPs. These complexes are still limited, hence the study of the $ZnPc(SPh)_4$-AuNP conjugate in this work. As stated above AuNPs decrease fluorescence of MPc complexes, this work will show an opposite effect.

Table 1.4. Phthalocyanines conjugated to AuNPs

Structure	**Ref.**
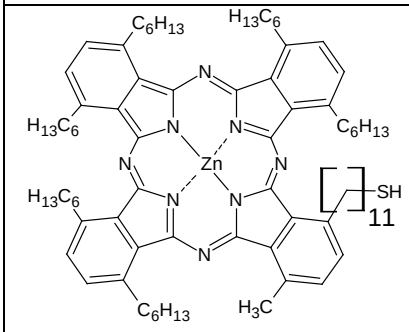	[57]
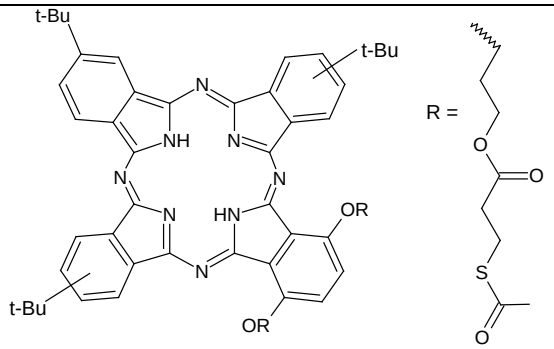	[58]
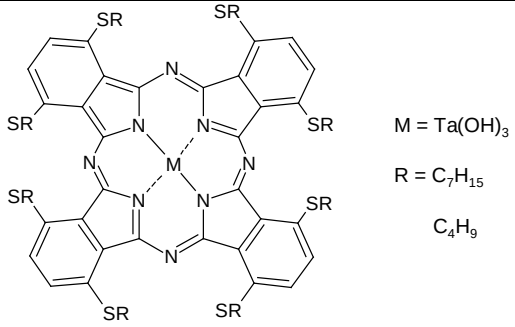	[59]

Structure	**Ref.**
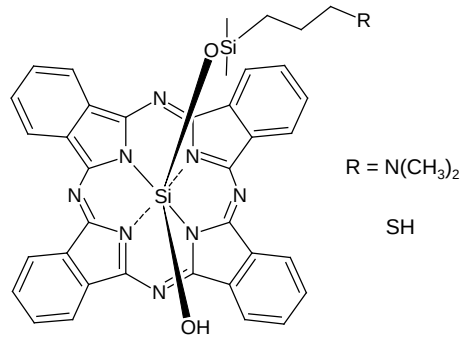	[60,61]
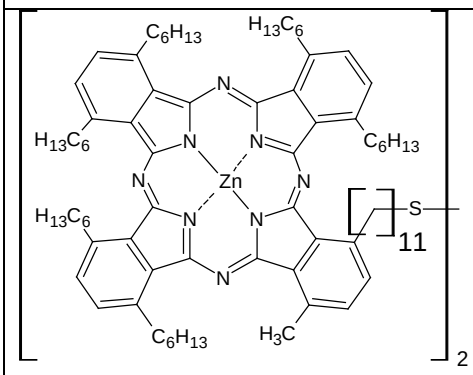	[66]
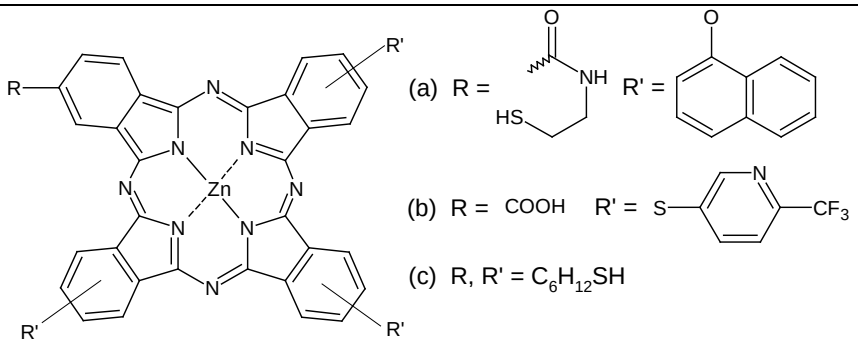	[67]
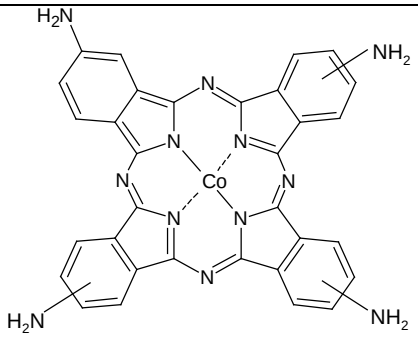	[225]

1.5 Summary of aims

The photophysical and photochemical properties are compared between the synthesised low-symmetry $ZnPc(COOH)(SPh)_3$ and symmetric $ZnPc(SPh)_4$ derivatives, as well as between the symmetric $ZnPc(SPh)_4$, $Ge(OH)_2Pc(SPh)_4$ and $H_2Pc(SPh)_4$ derivatives. The effect of different solvents on the spectra and fluorescence are highlighted. The photophysical parameters are also compared to those of differently substituted ZnPc and GePc derivatives. The optical limiting properties of the synthesised Pcs are determined and compared in different solvents. GePc complexes are known to be good optical limiters, hence $Ge(OH)_2Pc(SPh)_4$ is employed in this work. The low-symmetry $ZnPc(COOH)(SPh)_3$ derivative is also tested as a photosensitiser of ZnO to determine its suitability for use in DSSCs. The higher yielding $Zn(SPh)_4Pc$ is conjugated to gold nanoparticles to determine the effect of conjugation on the spectra and the fluorescence behaviour of the Pc in different solvents.

2. EXPERIMENTAL

Incorporated in this chapter are the experimental procedures used during the course of the study i.e. all synthetic procedures and methods of characterisation for the molecules and nanoparticles used in this work are reported.

2.1 Materials

For synthesis and characterisation: Germanium tetrachloride, zinc acetate, 1,8-diazabicyclo[5.4.0]undec-7-ene (DBU), gold(III) chloride trihydrate, lithium, sodium borohydride, tetraoctylammonium bromide (TOABr) and deuterated tetrahydrofuran (THF-d_8) were purchased from Sigma-Aldrich. Zinc chloride was obtained from Chimica. Column chromatography was performed on silica gel 60 (0.04-0.063 mm) from Merck, dianion HP 20 resin obtained from Aldrich and Bio-Beads S-X1 beads from Bio-Rad.

Photophysicochemistry: Unsubstituted zinc phthalocyanine was purchased from Sigma-Aldrich.

Photoelectrochemistry: Acetonitrile and potassium iodide were purchased from Roth, iodine was obtained from Scharlau and ethylene carbonate was obtained from Fluka. Eosin Y and tetrabutylammonium iodide (TBAI) were purchased from Sigma-Aldrich. The glue for electrode preparation was obtained form Araldite (Nichiban Co. Ltd.), a silver paste was obtained from DOTITE (Fujikura Kasei).

Solvents: Dimethylsulfoxide (DMSO), ethanol, methanol, dichloromethane (DCM), chloroform, tetrahydrofuran (THF), acetone, pyridine, n-pentanol, benzene, toluene and dimethylformamide (DMF) were obtained from SAARChem and dried according to reported procedures [226] before use. Uvasol® DMSO (spectroscopic grade) was purchased from Merck for TCSPC, z-scan and laser flash photolysis studies.

2.2 Equipment and Instrumental

1. Proton nuclear magnetic resonance (^{1}HNMR) spectra were recorded using a Bruker AMX 600 MHz NMR spectrometer.
2. Fourier transform infra-red (FT-IR) spectra were recorded on a Perkin–Elmer Spectrum 100 ATR FT-IR spectrometer.
3. Elemental analysis was performed using a Vario-Elementar Microcube ELIII CHNS Analyser.
4. Mass spectral data was collected with a Bruker AutoFLEX III Smartbeam TOF/TOF mass spectrometer. The instrument was operated in positive ion mode using a m/z range of 400 – 3000 amu. The voltage of the ion sources were set at 19 and 16.7 kV for ion sources 1 and 2 respectively, while the lens was set at 8.50 kV. The reflector 1 and 2 voltages were set at 21 and 9.7 kV respectively. The spectra were acquired using *trans*-2-[3-(4-tert-butylphenyl)-2-methyl-2-propenylidene]malononitrile (DCTB) as the MALDI matrix, using a N_2 laser.
5. UV–visible (UV-vis) spectra were recorded on a Shimadzu UV-2550 spectrophotometer.
6. Fluorescence excitation and emission spectra were recorded on a Varian Eclipse spectrofluorimeter using a 1 cm path-length cuvette at room temperature.
7. A laser flash photolysis system (Figure 2.1) was used for the determination of triplet decay kinetics. The excitation pulses were produced by a Quanta-Ray Nd:YAG laser (1.5 J/9 ns), pumping a Lambda Physik FL 3002 dye laser (Pyridin 1 in methanol). The analysing beam source was from a Thermo Oriel 66902 xenon arc lamp, and a Kratos Lis Projekte MLIS-X3 photomultiplier

tube was used as the detector. Signals were recorded with a two-channel, 300 MHz digital real time oscilloscope (Tektronix TDS 3032C); the kinetic curves were averaged over 256 laser pulses.

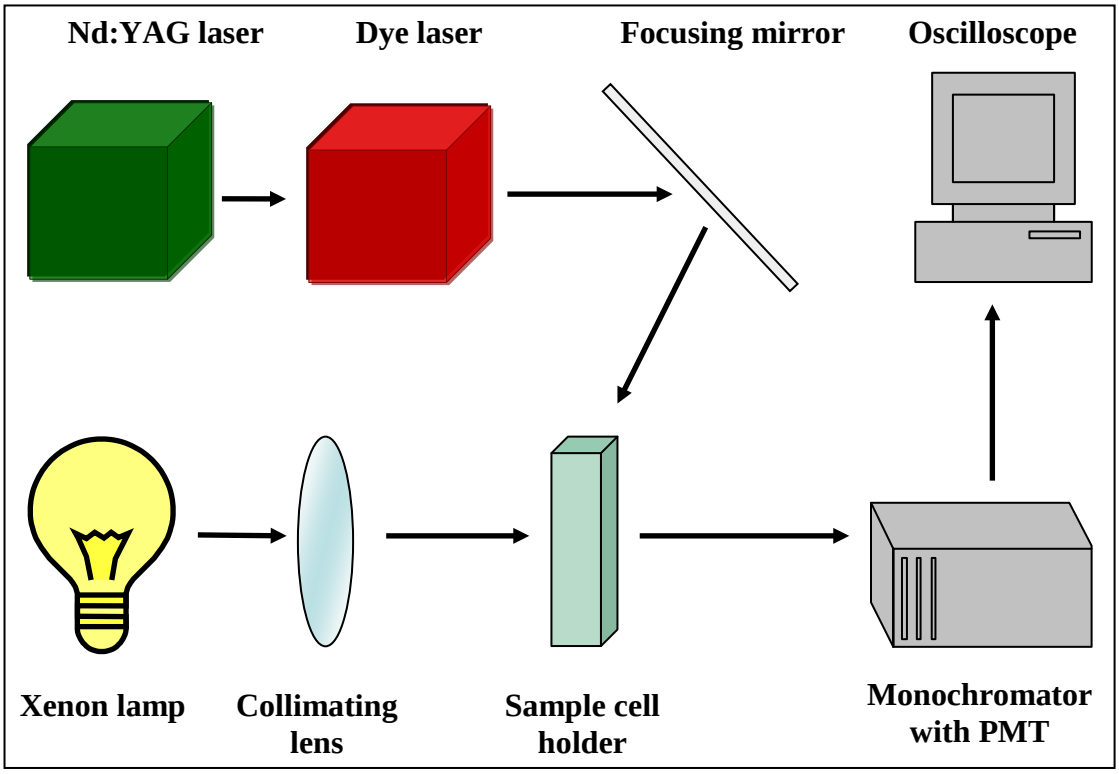

Figure 2.1. Schematic representation of a laser flash photolysis set-up

8. Fluorescence lifetimes were measured using a time correlated single photon counting setup (TCSPC) (FluoTime 200, Picoquant GmbH) with a diode laser (LDH-P-670 with PDL 800-B, Picoquant GmbH, 670 nm, 20 MHz repetition rate, 44 ps pulse width). Fluorescence was detected under the magic angle with a peltier cooled photomultiplier tube (PMA-C 192-N-M, Picoquant) and integrated electronics (PicoHarp 300E, Picoquant GmbH). A monochromator with a spectral width of about 8 nm was used to select the required emission wavelength band. The response function of the system,

which was measured with a scattering Ludox solution (DuPont), had a full width at half-maximum (FWHM) of 300 ps. All luminescence decay curves were measured at the maximum of the emission peak and lifetimes were obtained by deconvolution of the decay curves using the FluorFit Software program (PicoQuant GmbH, Germany). The support plane approach [125] was used to estimate the errors of the decay times.

9. For photodegradation studies (Figure 2.2) the solution was irradiated with light emitted from a 300 W, 120 V halogen photo optic lamp and passed through a 600 nm glass cut-off filter (Schott) and a water filter to filter off ultraviolet and infrared radiations respectively. An interference filter (Intor, 700 nm with a band width of 40 nm) was additionally placed in the light path before the sample, hence ensuring excitation at the Q band only (660 to 740 nm). Light intensities were measured with a POWER MAX 5100 (Molelectron detector incorporated) power meter.

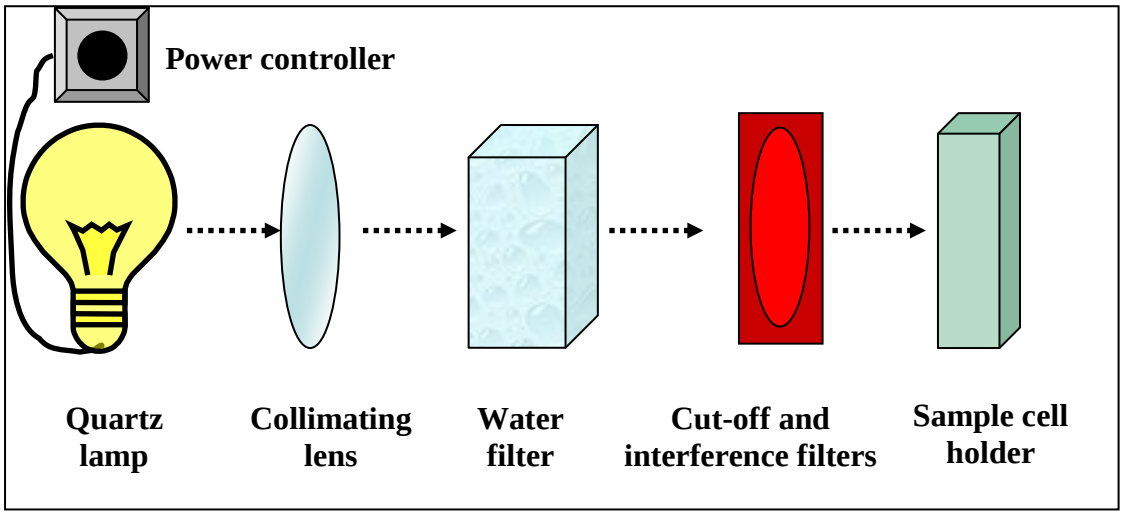

Figure 2.2. Schematic representation of a photodegradation set-up

10. The Z-scan equipment (Figure 2.3) employed in this work was fabricated at the University of Stellenbosch in South Africa. All experiments described in this study were performed using Nd:YAG laser (Quanta-Ray, 1.5 J/ 9 ns) at 532 nm. The laser was operated at its second harmonic, 532 nm, with a pulse repetition rate of 10 Hz, energy range of 0.1 μJ – 0.1 mJ.

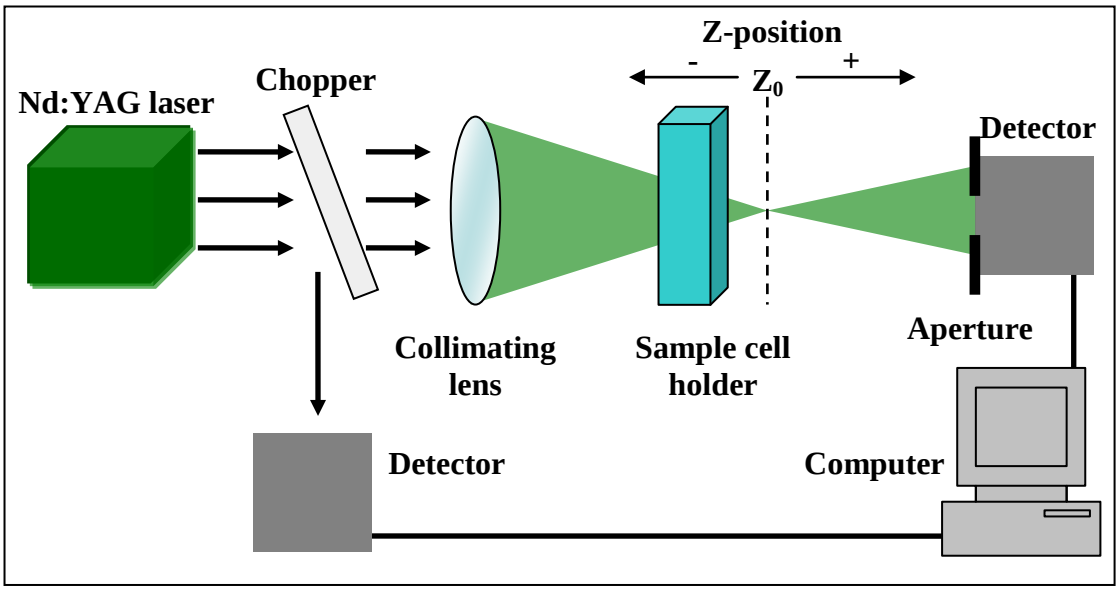

Figure 2.3. Schematic representation of Z-scan set-up

11. Confocal laser microscope images were obtained at Justus-Liebig University of Giessen, Germany using a Keyence VK-9700 Laser scanning microscope.
12. Scanning electron microscope (SEM) images were obtained using a JEOL JSM 840 scanning electron microscope.
13. Transmission electron microscope (TEM) images were obtained using a JEOL JEM 1210 transmission electron microscope at 100 kV accelerating voltage.
14. Atomic force microscopy (AFM) images were recorded in the non-contact mode in air with a CP-11 Scanning Probe Microscope from Veeco Instruments (Carl Zeiss, South Africa) at a scan rate of 1 Hz. The images were obtained

using a spring constant range of 20 –80 N/m, and resonant frequency range of 217–276 Hz.

15. X-ray powder diffraction (XRD) patterns were recorded on a Bruker D8, Discover equipped with a proportional counter, using Cu-K radiation (λ = 1.5405 Å, nickel filter). Data were collected in the range from $2\theta = 5°$ to 100°, scanning at 1° min^{-1} with a filter time-constant of 2.5 s per step and a slit width of 6.0 mm. Samples were placed on a silicon wafer slide. The X-ray diffraction data were treated using the commercially available Eva (evaluation curve fitting) software. Baseline correction was performed on each diffraction pattern by subtracting a spline fitted to the curved background.

16. X-ray photoelectron spectroscopy (XPS) measurements were performed with a Kratos Axis Ultra Xray Photelectron Spectrometer equipped with a monochromated Al Kα source. The base pressure was below 3 x 10^{-7} Pa. XPS experiments were recorded with 75 W power source using hybrid-slot spectral acquisition mode and an angular acceptance angle of ± 20°. The analyser axis made an angle of 90° with the specimen surface, with the specimen surface making an angle of 45° with the X-ray angle. Charge neutraliser was used due to the insulating surface used to prepare the sample. The elemental analysis and metal core level were recorded with a step of 1 eV and pass energy of 160 eV. XPS data analysis was performed with Kratos version 2 program.

2.3 Methods

2.3.1 Fluorescence and triplet yields and lifetimes

Fluorescence quantum yields were determined using Equation 1.1, with unsubstituted ZnPc in DMSO (Φ_F = 0.20) used as a standard [72]. For each study at least two independent experiments were performed for quantum yield determinations. Both the sample and the standard were excited at the same relevant wavelength.

For the laser flash photolysis experiments, the MPc solution (A ~ 1.5) was bubbled with nitrogen for 30 mins in a 1 cm path-length spectrophotometric cell and irradiated at the Q band using the laser flash photolysis system as described above. Triplet quantum yields (Φ_T) were calculated using Equation 1.2, unsubstituted ZnPc in DMSO (Φ_T = 0.65) [122] was used as the standard. Triplet lifetimes were determined by exponential fitting of the kinetic curves using OriginPro 8 software.

2.3.2 Photodegradation quantum yields

Photodegradation quantum yields (Φ_{Pd}) were determined using a solution of the MPc (~ 2.5 ml) in a 1 cm path-length spectrophotometric quartz cell and illuminated at the Q band region using a 300 W General electric quartz lamp as described above (represented in Figure 2.2). The wavelength of the interference filter was chosen such that it was close to the Q band absorption of the MPcs of interest. The steady reduction in the Q band absorption intensity with irradiated time was recorded and used for the calculation of Φ_{Pd} (Equation 1.3).

2.3.3 Photoelectrochemical measurements

The preparation of ZnO thin films was performed at the Justus-Liebig University Giessen, Germany. For the deposition of ZnO in the presence of eosin Y, FTO doped conductive glass substrate (Asahi-Glas, Cond. 10 Ω/cm^2, with transparency > 85 % in visible region) was cut to a size of 2.5 cm x 2.5 cm. The substrate (FTO) was cleaned ultrasonically in acetone, iso-propanol and distilled water for 10 minutes each before being mounted to the holder. The substrate was then etched in 45 % HNO_3 for 2 min and finally rinsed with distilled water. A conventional three electrode system, consisting of a rotating disc electrode (RDE) as a working electrode, RedRod (Radiometer) reference electrode (0 mV vs. Ag|AgCl) and zinc rod as a counter electrode was employed. The electrochemical cell was filled with electrolyte (110 ml ultrapure water containing 0.1 M of KCl) and saturated with O_2 gas (99 %) by purging the solution with oxygen at a rate of 400 ml/min for approximately 15 minutes. The electrolyte was heated to 72°C using circulating thermostated water surrounding the cell and the substrate was mounted on the rotating electrode holder, contacted by an electrically conductive tape and fixed by insulating tape leaving an uncovered circular active electrode area of 2 cm diameter. A constant potential of -1.06 V vs. the reference electrode was applied (Wenking potentiostat LPG0, Bank Elektronik) and a rotating speed of 500 rpm (Radiometer CTV101) was set. This started the electrochemical activation of the substrate, during which oxygen was reduced at the working electrode and the current density gradually became more negative. After this, 1 ml of an aqueous $ZnCl_2$ solution was added to the electrolyte such that the concentration of zinc chloride in the electrolyte was 5 mM. This initiated the growth of a compact (i.e. non-porous) zinc oxide film (the so-called blocking layer). After 5 minutes of blocking layer deposition, 1 ml of an aqueous eosinY solution was added

such that the concentration of eosinY in the electrolyte was 50 µM. The addition of eosinY initiated the deposition of a porous ZnO/eosinY hybrid film, which was carried out for 20 minutes. After the electrodeposition, the films were rinsed with water and dried in a nitrogen flow. To remove the structure-directing agent eosinY out of the pores, the samples were immersed into an aqueous KOH solution of pH 10.5 and were irradiated with the light of two fluorescent tubes, which is known to accelerate the eosinY desorption process, for approximately 48 h. The ZnO film on glass was cut into six pieces and MPc dye adsorption on four of the pieces was done by immersing the ZnO thin film into a ~1 mM solution of the MPc in pyridine containing 50 mM chenodeoxycholic acid for 1 - 24 h. The films were then rinsed with ethanol and dried under compressed nitrogen and stored in the dark. The films were heated at 70°C in an oven for 20 min before photoelectrochemical studies. The other two pieces were kept as control and test pieces.

Photoelectrochemical measurements were performed at the Justus-Liebig University, Giessen Germany. An ORIEL 1000 W xenon arc lamp (intensity = 100 $mW.cm^{-2}$) equipped with a water filter and a UV cut off filter to restrict the illumination to the visible range (385 nm – 900 nm) was employed. The adjustment of the light intensity was achieved using a thermopile (LaserPoint). The illumination to the electrode was controlled using a PRONTOR magnetic E/40 mechanical shutter. The shutter required approximately 15 ms to reach a completely open position as measured with a SIEMENS SFH 219 silicon-PIN-photodiode and was open for 2 sec. The potential and currents were measured with an Iviumstat potentiostat, using a conventional three-electrode arrangement in a 5 ml glass cell with MPc/ZnO hybrid thin film as a window of the cell illuminated from the fluorine-doped tin oxide (FTO) side and used as the working electrode, a Pt counter electrode and $Ag|AgNO_3$ reference electrode

were also used with acetonitrile as internal solvent. A mixture of 0.5 M TBAI and 0.05 M I_2 (in a 1:4 by volume mixture of acetonitrile with ethylene carbonate) was used as an electrolyte.

2.3.4 Optical limiting measurements

Volumes of MPc solution were placed in a quartz cuvette (internal dimensions: 2 mm x 10 mm x 55 mm, 0.7 ml) with a path length of 2 mm (Starna 21-G-2) and irradiated with the laser light (Nd:YAG, 532 nm) starting at a position (- 40 mm) before the focal point of the laser to a position (+ 40 mm) from the focal point. The transmittance of the solution at varying points was recorded and the intensity-dependent absorption coefficient (β_1) computed from the transmittance curve obtained.

2.4 Synthesis

4-Carboxy phthalonitrile was synthesised using a similar method reported in literature using trimellitic anhydride as the starting material [227]. The synthesis of 4-phenylthio phthalonitrile has also been reported before [91].

2.4.1 Synthesis of tris-9 (10), 16 (17), 23 (24)[4-(phenylthio)-2-(carboxy) phthalocyaninato]zinc(II) (ZnPc(COOH)$(SPh)_3$), Scheme 3.1

A mixture of 4-carboxy phthalonitrile (0.750 g, 3.178 mmol) and 4-phenylthio phthalonitrile (0.182 g, 1.059 mmol) was dissolved in pentanol (5 ml) and heated to reflux. Lithium (68.9 mg, 10.59 mmol) was then added in small quantities. The green mixture was left to reflux for 12 h, and then cooled to room temperature. A few drops of glacial acetic acid were added, followed by methanol to precipitate out the Pc, which was then dried and Soxhlet extracted with chloroform to remove symmetric

$H_2(SPh)_4Pc$ which was purified as described in Section 2.4.2. Crude $H_2Pc(COOH)(SPh)_3$ (62.4 mg, ~0.07 mmol) was subsequently dissolved in dry DMF (5 ml) under N_2 and refluxed for 10 min after which DBU (0.25 ml) and then zinc acetate (25.2 mg, 0.12 mmol) were added to the mixture and refluxed for a further 2½ h. After cooling, the metallated Pc was precipitated with water (5 ml) and then thoroughly washed with water to yield 45.1 mg of crude product. The purified product was obtained by dissolving the crude product in minimum pyridine followed by the use of a silica column using DCM as eluent, followed by DMF. The green DMF fraction was then passed through an HP20 resin bead column. The HP20 column was washed with acetone, and the Pc eluted with pyridine, which was evaporated off to obtain a blue-green solid. Yield: 2.13 mg (3 %). UV-vis (DMSO) λ_{max}(nm), (log ε): 690 (5.03), 367 (4.27). FT-IR (cm^{-1}): 687.9 (δ C-S-C), 741.0 (δ Pc ring), 887.9 (δ isoindole & nitrogen mesoatoms), 1031.7 (δ C-H in-plane & isoindole), 1092.4 (δ C-H in-plane), 1282.0 (δ C-H in-plane), 1375.6 (δ pyrrole and nitrogen mesoatoms), 1471.6 (ν isoindole), 1577.8 (ν C=C), 1638.5 (ν C=O), 2916.5 (ν O-H), 3048.1 (ν C-H arom.). Anal. Calc. for $C_{51}H_{28}N_8O_2S_3Zn$: C 64.72, H 2.98; Found: C 65.76, H 3.31%. ^{1}H NMR (THF-d_8): 9.50-9.25 (4H, broad m, Pc-H), 8.75-8.40 (4H, broad m, Pc-H), 8.20-8.00 (1H, m, Pc-H), 7.80-7.60 (3H, m, aromatic-H/Pc-H), 7.60-7.30 (4H, m, aromatic/Pc-H), 7.20-6.85 (6H, broad m, aromatic-H), 6.75-6.30 (6H, broad m, aromatic-H). MALDI-TOF MS m/z: Calc: 946.424 amu. Found: [M+Na] 970.138 amu

2.4.2 Synthesis of tetrakis-2,(3)-[4-(phenylthio) phthalocyaninato] ($H_2Pc(SPh)_4$), Scheme 3.1

The Soxhlet extract containing $H_2Pc(SPh)_4$ (51.3 mg) was purified using a silica column eluted with THF and followed by a silica plug eluted with chloroform. The

green solid was then thoroughly washed with methanol. Yield: 23.6 mg. UV-vis (toluene) λ_{max}(nm), (log ε): 713 (4.84), 678 (4.82), 343 (4.52). FT-IR (cm^{-1}): 687.2 (δ C-S-C), 742.0 (δ Pc ring), 894.5 (δ isoindole & nitrogen mesoatoms), 1282.0 (δ C-H in-plane), 1382.7 (δ pyrrole and nitrogen mesoatoms), 1473.0(ν isoindole), 1579.0 (ν C=C), 3054.26 (ν C-H arom.), 3286.2 (ν N-H). Calc. for $C_{56}H_{34}N_8S_4$: C 71.01, H 3.62, N 11.83, S 13.54; Found: C 70.10, H 3.57, N 11.68. S 12.82%. ^{1}H NMR (THF-d_8): 7.85-7.60 (12H, m, aromatic-H + Pc-H), 7.60-7.45 (12H, m, aromatic-H + Pc-H), 7.45-7.40 (4H, m, aromatic-H/Pc-H), 7.40-7.15 (4H, broad m, aromatic-H/Pc-H), the inner two protons were not observed. MALDI-TOF MS *m/z*: Calc: 947.183 amu. Found: [M-H] 946.189 amu

2.4.3 Synthesis of tetrakis-2,(3)-[4-(phenylthio) phthalocyaninato]zinc(II)] ($ZnPc(SPh)_4$), Scheme 3.1

To synthesise the symmetrical $ZnPc(SPh)_4$, the symmetrical $H_2Pc(SPh)_4$ (20.2 mg, ~0.02 mmol), DBU (0.25 ml) and zinc acetate (10.0 mg, 0.12 mmol) were dissolved in dry pentanol (4 ml) under N_2 and refluxed for 3½ h. After cooling, the metallated Pc was precipitated with water, centrifuged, and purified as for $H_2Pc(SPh)_4$ to obtain a blue-green solid. Yield: 12.1 mg (57 %). UV-vis (DMSO) λ_{max}(nm), (log ε): 692 (5.34), 365 (4.86). FT-IR (cm^{-1}): 682.7 (δ C-S-C), 734.3(δ Pc ring), 886.7(δ isoindole & nitrogen mesoatoms), 1033.9(δ C-H in-plane & isoindole), 1093.4(δ C-H in-plane), 1380.7(δ pyrrole and nitrogen mesoatoms), 1473.1 (ν isoindole), 1579.0 (ν C=C), 3049.1 (ν C-H arom.). Calc. for $C_{56}H_{32}N_8S_4Zn$: C 66.56, H 3.19, N 11.09, S 12.69%; Found: C 66.22, H 2.64, N 10.22. S 11.56 %. ^{1}HNMR (THF-d_8): 9.05-8.90 (4H, broad m, Pc-H), 8.90-8.70 (4H, broad m, Pc-H), 8.05-7.90 (4H, broad m, Pc-H), 7.90-7.75 (8H, m, aromatic-H), 7.45-7.60 (8H, m, aromatic-H), 7.35-7.45 (4H, m, aromatic-H). MALDI-TOF MS *m/z*: Calc: 1010.576 amu. Found: $[M]^+$ 1010.787 amu.

2.4.4 Synthesis of {tetrakis-2,(3)-[4-(phenylthio) phthalocyaninato] germanium (IV)}$(OH)_2$ ($Ge(OH)_2Pc(SPh)_4$), Scheme 3.1

To synthesise the symmetrical $Ge(OH)_2Pc(SPh)_4$, crude $H_2Pc(SPh)_4$ (80.6 mg, ~ 0.09 mmol) was dissolved in dry DMF (5 ml) and heated under N_2. DBU (0.75 ml) and $GeCl_4$ (0.46 ml, 4 mmol) were then added, and the solution allowed to reflux for 2 h. The Pc was precipitated out and then thoroughly washed with water, dried, and passed through a silica column using pyridine as eluent. The first fraction collected was then purified thrice as for $H_2Pc(SPh)_4$ to obtain a dark-green solid. Yield: 4.2 mg (5 %). UV-vis (DMSO) λ_{max}(nm), (log ε): 698 (5.11), 373 (4.63). FT-IR (cm^{-1}): 687.9 (δ C-S-C), 743.5 (δ Pc ring), 1031.7 (δ C-H in-plane & isoindole), 1077.2(δ C-H in-plane), 1282.0 (δ C-H in-plane), 1390.3 (δ pyrrole and nitrogen mesoatoms), 1474.2 (ν isoindole), 1580.3 (ν C=C), 2921.5 (ν C-H arom.), 3045.2 (ν O-H). Anal. Calc. for $C_{56}H_{34}N_8O_2S_4Ge$: C 63.95, H 3.26, N 10.65, S 12.19%; Found: C 63.43, H 3.51, N 8.43, S 11.94%. ^{1}H NMR (THF-d_8): 9.50-9.17 (6H, broad m, Pc-H + OH-H), 8.26-7.98 (4H, broad m, Pc-H), 7.84-7.64 (8H, m, aromatic-H), 7.64-7.40 (16H, m, aromatic-H + Pc-H). MALDI-TOF MS m/z: Calc: 1051.82 amu. Found: [M-OH] 1035.121 amu

2.4.5 Synthesis of gold nanoparticle-MPc conjugate

The synthesis of TOABr functionalised AuNPs (TOABr-AuNP) and their characterisation has been reported before [57] (Scheme 1.5). Briefly, a gold(III) chloride trihydrate solution (25 mM, 4 ml) was vigorously stirred with a toluene solution of TOABr (85 mM, 6 ml). The reducing agent, $NaBH_4$, in aqueous solution (87 mM, 5 ml) was added dropwise for 10 min, and the mixture was stirred vigorously for 20 min. The cherry-red organic phase was separated and washed with deionised

water. The attachment of $ZnPc(SPh)_4$ to AuNPs was achieved by dissolving $ZnPc(SPh)_4$ (0.800 mg, 0.8 µmol) in TOABr-AuNP solution (1.5 ml, 3.18 M) and stirring in the dark, under argon atmosphere for 65 hours for ligand exchange to take place, forming $ZnPc(SPh)_4$-AuNP (Scheme 1.6). A small volume of an aqueous $NaBH_4$ solution was added to the $ZnPc(SPh)_4$-AuNP solution to ensure reduction of any oxidised AuNPs. The dark coloured organic layer was washed with water and then separated twice in a size-exclusion column using toluene as the eluent, to yield the tan-coloured conjugate solution. The conjugate was determined to be free of any unconjugated Pc using silica thin layer chromatography (TLC).

3. RESULTS AND DISCUSSION

Reported in this chapter are the syntheses and spectroscopic characterisation of the metallophthalocyanines, gold nanoparticles and conjugates employed in this work. The photophysicochemical properties of the MPcs and gold nanoparticle conjugates synthesised are discussed. For the MPcs, comparisons are made with respect to the presence of different metal ions, substituents and solvent properties. The photoelectrochemical properties of the low-symmetry MPc synthesised as a sensitiser of nanoporous ZnO is also discussed.

Publications arising from this work

The results discussed in the following chapter have been presented in the articles listed below that have been submitted to peer-reviewed journals.

1. Unquenched fluorescence lifetime for β-phenylthio substituted zinc phthalocyanine upon conjugation to gold nanoparticles, **Shaun Forteath**, Edith Antunes, Wadzanai Chidawanyika, Tebello Nyokong, *Polyhedron* **34** (2012) 114-120.

2. Synthesis and photophysical behaviour of a novel low-symmetry zinc phthalocyanine containing a single carboxylic acid and three phenylthio substituents, **Shaun Forteath**, Edith Antunes, Tebello Nyokong, submitted to *Journal of Luminescence*

3.1 Synthesis and spectroscopic characterisation

3.1.1 Synthesis of phenylthio substituted phthalocyanines

Scheme 3.1 shows the synthetic pathways for the compounds used in this work. Substituted phthalocyanines are normally prepared by the cyclotetramerisation of substituted phthalonitriles. 4-Tetra-substituted phthalocyanines can be synthesised from their 4-substituted phthalonitriles precursors. The symmetrical complexes $ZnPc(SPh)_4$ and $H_2Pc(SPh)_4$ have been reported before [49], but were obtained in this work as by-products of the synthesis of the asymmetric $ZnPc(COOH)(SPh)_3$ complex, hence a different method from the usual synthesis of MPc derivatives. The symmetrical $Ge(OH)_2Pc(SPh)_4$ is reported here for the first time.

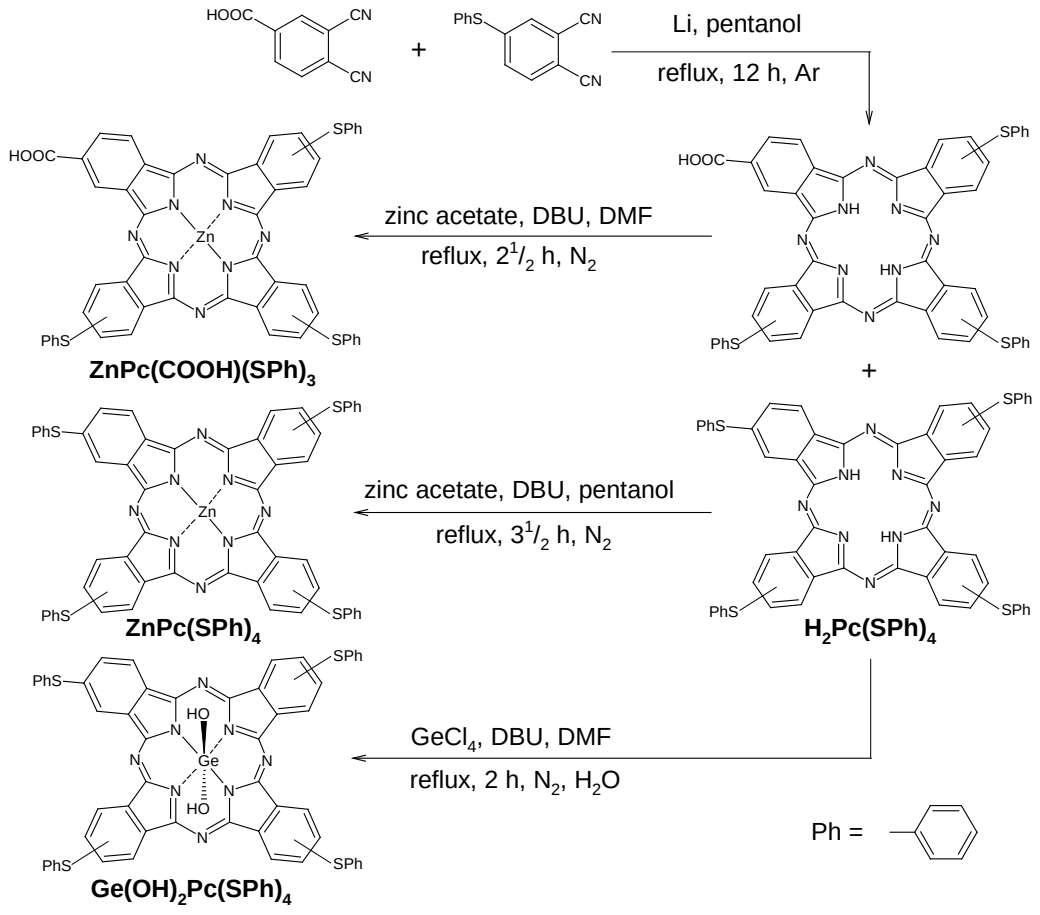

Scheme 3.1. Synthesis of β-phenylthio substituted Pcs

The syntheses of all the complexes gave satisfactory spectroscopic analyses. The MPc complexes synthesised in this study were soluble in organic solvents such as DMF, THF, pyridine and DMSO, with the symmetric complexes also soluble in non-polar solvents like chloroform, toluene and benzene. The unmetallated $H_2Pc(SPh)_4$ was not soluble in the polar solvents, DMSO and DMF. The complexes were characterised by various spectroscopic methods: FT-IR, UV–vis, ^{1}H NMR and mass spectra as well as elemental analysis and are consistent with predicted structures. The ^{1}H NMR spectra of all the complexes showed aromatic ring protons between 6 and 9 ppm. From the FT-IR spectra peaks at 682-688 cm^{-1} correspond to the C-S-C stretch of the phenylthio substituents, with the peak at 1638 cm^{-1} (C=O) confirming the presence of the carboxylic acid group in $ZnPc(COOH)(SPh)_3$, and the peak at 3045 cm^{-1} (OH) confirming the axial ligands of $Ge(OH)_2Pc(SPh)_4$.

3.1.2 UV-vis absorption studies of synthesised phthalocyanines

The ground state electronic absorption spectra (Figure 3.1 A) of $ZnPc(COOH)(SPh)_3$ and $ZnPc(SPh)_4$ in DMSO showed monomeric behaviour, as evidence by a single sharp Q band typical of metallated phthalocyanine complexes in organic solvents. Both spectra are red shifted compared to unsubstituted ZnPc (with a Q band at 672 nm in DMSO, Figure 3.1 A), due to the electron donating effects of the phenylthio groups (Table 3.1). The Q band maximum of $ZnPc(COOH)(SPh)_3$ is at 689 nm and that of $ZnPc(SPh)_4$ is at 692 nm in DMSO (Table 3.1), the latter is red shifted due to the extra phenylthio group. For $ZnPc(SPh)_4$ and $Ge(OH)_2Pc(SPh)_4$ in toluene (Figure 3.1 B) the Q band maxima are at 692 and 704 nm respectively. The B band is split for $Ge(OH)_2Pc(SPh)_4$ with peaks at 357 and 367 nm. For $H_2Pc(SPh)_4$, the Q band is split (680 nm and 713 nm, Table 3.1) due to the unsymmetrical nature of the molecule.

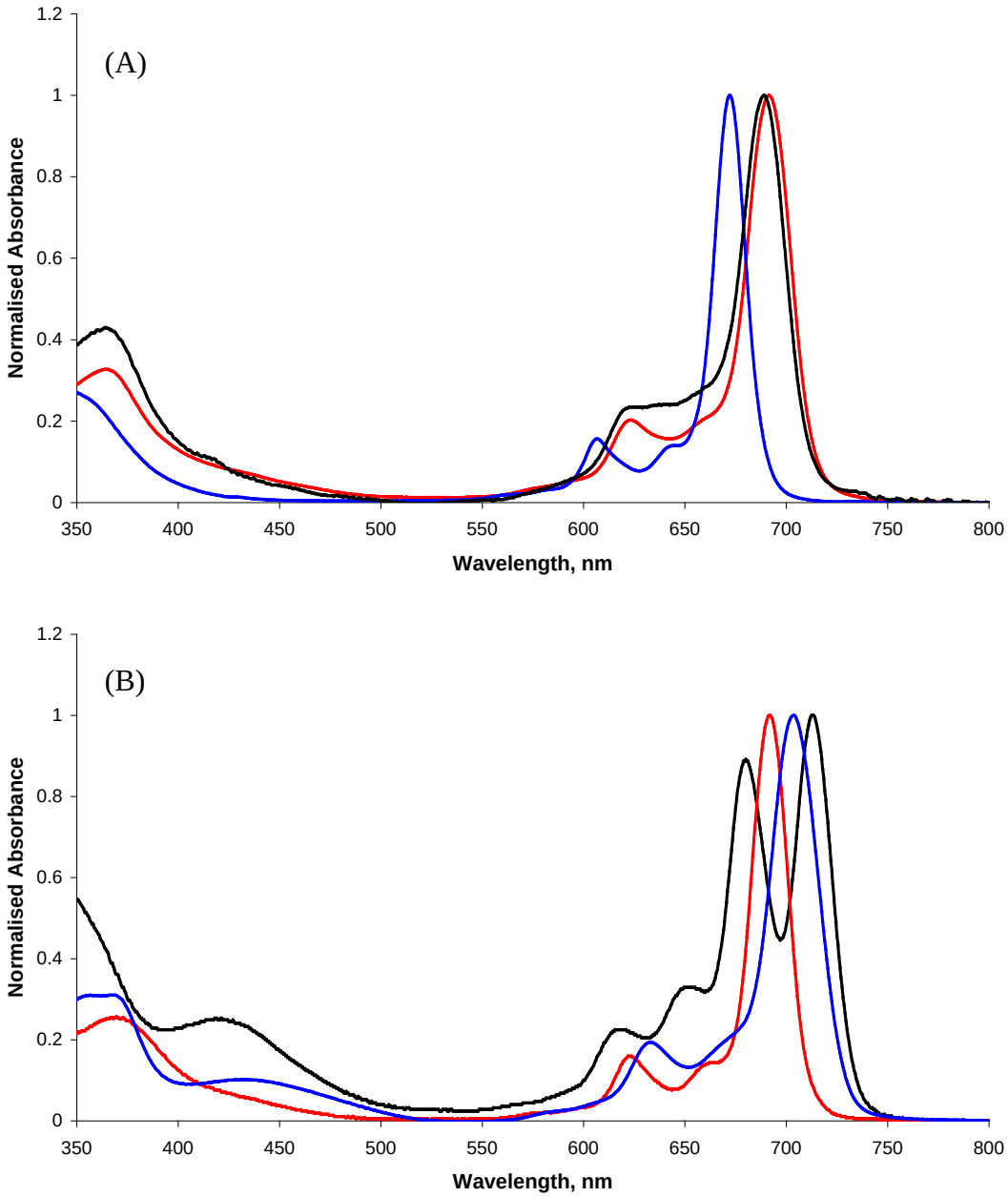

Figure 3.1. UV-vis absorption spectra of 1 x 10^{-5} M (A) ZnPc (blue), $ZnPc(SPh)_4$ (red) and $ZnPc(COOH)(SPh)_3$ (black) in DMSO, and (B) $H_2Pc(SPh)_4$ (black), $ZnPc(SPh)_4$ (red) and $Ge(OH)_2Pc(SPh)_4$ (blue) in toluene.

There is no clear splitting for $ZnPc(COOH)(SPh)_3$, but there is broadening compared to ZnPc and $ZnPc(SPh)_4$ due to the low-symmetry nature of the molecule. $Ge(OH)_2Pc(SPh)_4$ is more red-shifted than $ZnPc(SPh)_4$ due to the higher oxidation state of the Ge(IV) versus Zn(II). A single Q band is observed for $H_2Pc(SPh)_4$ in pyridine (Table 3.1), due to basic nature of this solvent [84]. N bands were observed for $H_2Pc(SPh)_4$, $ZnPc(SPh)_4$ and $Ge(OH)_2Pc(SPh)_4$ in chloroform at 298, 294 and 304 nm respectively.

Table 3.1. Ground state absorption, fluorescence emission and excitation spectral parameters for synthesised Pc derivatives in different solvents.

Complex	**Solvent**	**λ_{abs} (nm)**	**λ_{exc} (nm)**	**λ_{em} (nm)**	**$\Delta_{Stoke's}$ (nm)**
$ZnPc(COOH)(SPh)_3$	DMSO	689	690	700	10
	Pyridine	690	693	700	7
	DMF	686	684	696	12
	THF	682	682	692	10
$ZnPc(SPh)_4$	DMSO	692	692	704	12
	Pyridine	693	694	705	11
	DMF	688	688	700	12
	THF	685	686	695	9
	Benzene	690	691	699	8
	$CHCl_3$	690	693	703	10
	Toluene	692	693	702	9
$H_2Pc(SPh)_4$[a]	Pyridine	692	694	712	18
	THF	678, 710	680, 711	719	8
	Benzene	680, 713	682, 715	721	6
	$CHCl_3$	680, 713	682, 715	723	8
	Toluene	680, 713	681, 714	721	7

Complex	**Solvent**	**λ_{abs} (nm)**	**λ_{exc} (nm)**	**λ_{em} (nm)**	**$\Delta_{Stoke's}$ (nm)**
	DMSO	698	701	710	9
	Pyridine	700	702	710	8
	DMF	700	698	709	9
$Ge(OH)_2Pc(SPh)_4$	THF	697	696	706	10
	Benzene	704	705	714	9
	$CHCl_3$	705	708	717	9
	Toluene	704	704	713	9

[a] Low energy band used to determine Stoke's shift

The electronic absorption spectra of the ZnPc derivatives synthesised in various solvents was analysed using the method described originally by Bayliss [90,228]. The plot of $(n^2 - 1)/(2n^2 + 1)$ versus the Q band maximum wavelength, where n is the refractive index, is shown in Figure 3.2. The linear nature of the plot suggests that the red shifts in the Q band are mainly a result of solvation rather than coordination [71]. The differences in Q band wavelengths in different solvents for $Ge(OH)_2Pc(SPh)_4$ and $H_2Pc(SPh)_4$ (Table 3.1) cannot only be attributed to differences in the refractive index of the solvent, with red shifting not being directly proportional to a higher refractive index. Plots of Q band wavelengths against dipole moment, polarity index and dielectric constants of the solvents were also not directly proportional suggesting that a combination of different solvent properties contribute to the differences in the Q band wavelengths observed.

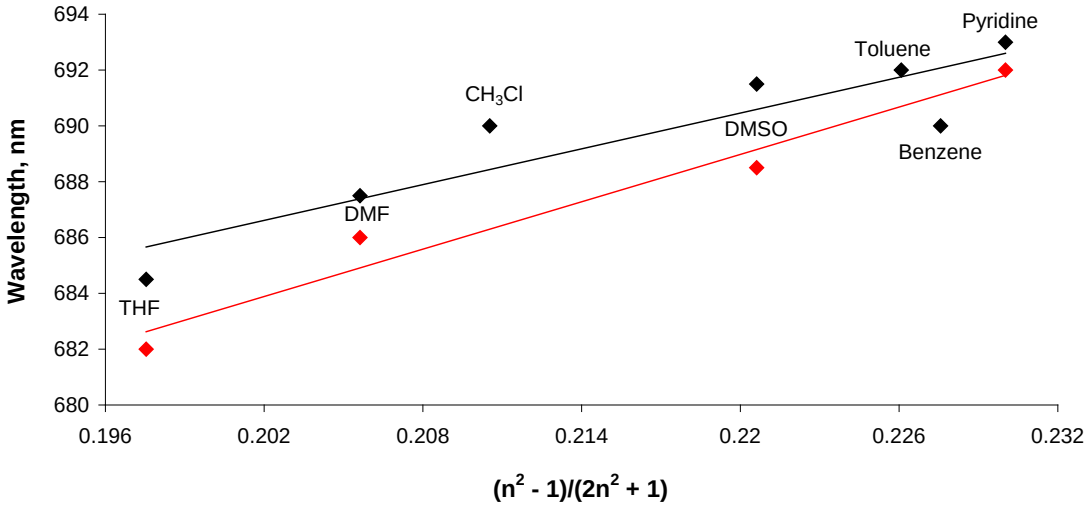

Figure 3.2. Relationship of Q band maximum wavelength of $ZnPc(SPh)_4$ (black) and $ZnPc(COOH)(SPh)_3$ (red) to refractive index of solvent

Plots of absorbance at the Q band against concentration of the synthesised complexes were linear for concentrations below 1×10^{-5} mol.L^{-1} confirming adherence to the Beer-Lambert law (Figure 3.3), with no aggregation detected below this concentration.

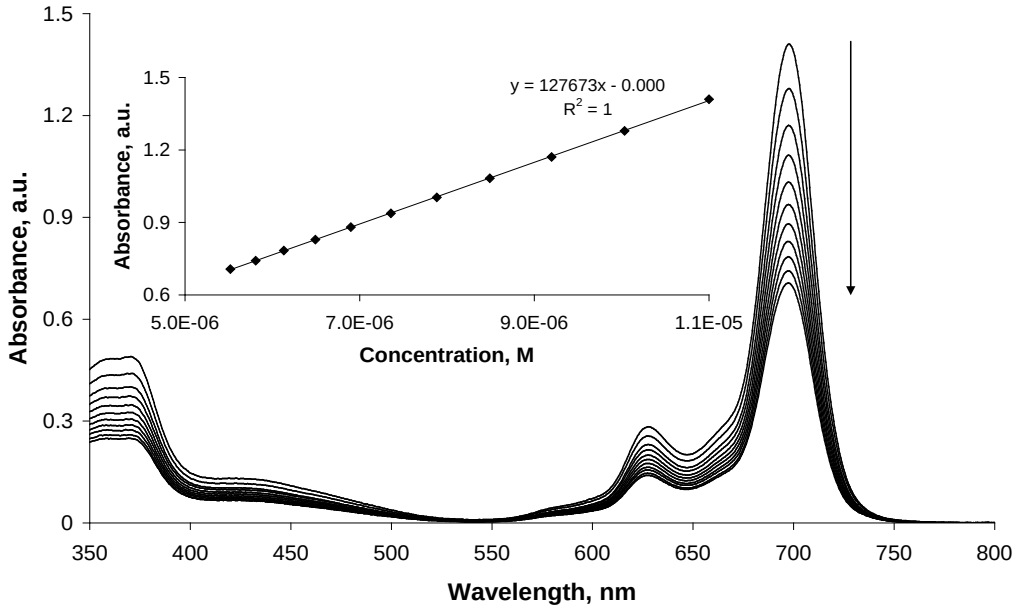

Figure 3.3. Beer's law dependence of $Ge(OH)_2Pc(SPh)_4$ absorption in DMSO

3.2 Photophysical properties

3.2.1 Fluorescence spectra and parameters

Figure 3.4 shows the absorption, excitation and emission spectra of the synthesised complexes in DMSO or toluene. The fluorescence emission peak for $ZnPc(COOH)(SPh)_3$ was observed at 700 nm with the excitation peak being at 690 nm in DMSO (Table 3.1). For $ZnPc(SPh)_4$, $H_2Pc(SPh)_4$ and $Ge(OH)_2Pc(SPh)_4$ in toluene, the emissions were observed at 702, 721 and 713 nm respectively (Figure 3.4 and Table 3.1). The excitation spectra are in agreement with the absorption spectra, with the slight differences between peak wavelengths attributed to the different spectrometers used. For $H_2Pc(SPh)_4$ there is a peak to peak match between excitation and absorption spectra even though the intensities are different due to conformational reorganisation upon excitation. Also for $H_2Pc(SPh)_4$, the fluorescence spectra show one peak as is typical of metal free Pcs which are known to fluoresce with only one main peak in non-aqueous media which has been assigned as the 0-0 transition of the fluorescence [229]. Stokes' shifts are typical of MPc complexes.

The fluorescence quantum yields (Φ_F) of the complexes, calculated using Equation 1.1 and listed in Table 3.2, are typical of monomeric phthalocyanines [71,72,108,230].

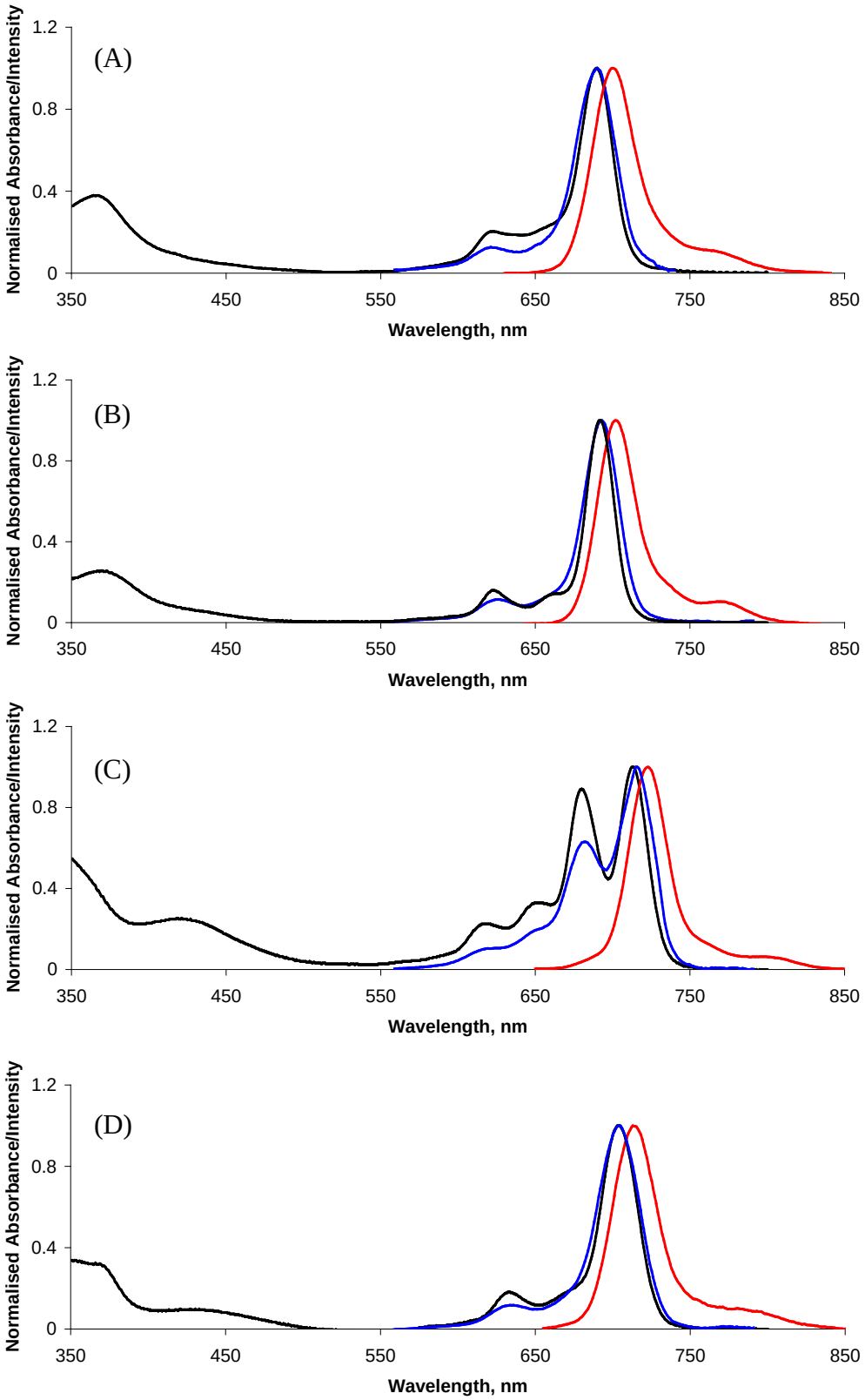

Figure 3.4. Normalised absorbance (black), excitation (blue) and emission (red) spectra of (A) $ZnPc(COOH)(SPh)_3$ in DMSO; (B) $ZnPc(SPh)_4$, (C) $H_2Pc(SPh)_4$ and (D) $Ge(OH)_2Pc(SPh)_4$ in toluene

Table 3.2. Fluorescence quantum yields of synthesised Pcs in different solvents

Complex[a]	DMSO	Pyridine	THF	DMF	$CHCl_3$	Benzene	Toluene
$ZnPc(COOH)(SPh)_3$	0.14	0.11	0.13	0.06			
$ZnPc(SPh)_4$	0.14	0.14	0.15	0.15	0.15	0.13	0.15
$H_2Pc(SPh)_4$		0.14	0.21		0.22	0.22	0.24
$Ge(OH)_2Pc(SPh)_4$	0.17	0.14	0.13	0.11	0.13	0.13	0.14
ZnPcOMP [108]	0.24						
ZnPcOP [71]	0.17						
ZnPcOE [108]	0.19						
ZnPcTMP [119]	0.10						

[a] OMP = octa(methyl-phenoxy); OP = octaphenoxy; OE = octaestrone; TMP = tetramercaptopyridyl. References in brackets.

Factors such as temperature, solvent parameters (polarity, viscosity, refractive index and the presence of heavy atoms in solvent molecule) are known to influence the yield of fluorescence. A decrease in viscosity of the solvent increases the possibility of deactivation of the excited state by external conversion. A chromophore could be rigid in the ground state, but may loosen up after excitation in low viscosity solvents. Except for values in DMSO, the Φ_F values are lower for $ZnPc(COOH)(SPh)_3$ than $ZnPc(SPh)_4$, as expected for symmetry lowered MPcs [119,231]. In DMSO the values of Φ_F for $ZnPc(SPh)_4$ and $ZnPc(COOH)(SPh)_3$, are smaller than for the aryl

substituted derivatives containing oxygen bridges in Table 3.2. This shows that the effects of sulfur could be to quench the singlet state most likely by enhancing intersystem crossing due to the slightly larger sulfur atom compared to oxygen. ZnPcTMP in particular is similar in structure to $ZnPc(SPh)_4$ except the former contains pyridyl instead of phenyl rings, it has a lower Φ_F showing that the slightly larger nitrogen atom could also quench the singlet state by enhancing intersystem crossing. The values for $H_2Pc(SPh)_4$ in different solvents are higher than those for $ZnPc(SPh)_4$ or $Ge(OH)_2Pc(SPh)_4$, with the exception of pyridine, due to the heavy atom effects of Zn and Ge which encourage intersystem crossing.

The fluorescence lifetimes (τ_F) of $ZnPc(COOH)(SPh)_3$, $ZnPc(SPh)_4$ and $Ge(OH)_2Pc(SPh)_4$ in DMSO, and $H_2Pc(SPh)_4$ in toluene were determined (Table 3.3), and a typical TCSPC trace is shown in Figure 3.5. $H_2Pc(SPh)_4$ is not soluble in DMSO, hence toluene was employed for fluorescence lifetime determination. First order kinetics were obeyed for all complexes, showing that only one species is present in each of the solutions, confirming purity of the complexes. The plot of residuals shows that the exponential fit is good, as it is a fairly straight line, with deviations at ~3 ns being due to deviations from the instrument response function and a χ^2 of near unity was obtained.

Table 3.3. Photophysical and photochemical parameters for Pcs in DMSO

Complex[a]	**Φ_F**	**τ_F (ns)**	**Φ_T**	**τ_T (μs)**	**Φ_{Pd} (x10^5)**
$ZnPc(COOH)(SPh)_3$	0.14	2.53 ± 0.01	0.65	331	0.42
$ZnPc(SPh)_4$	0.14	2.56 ± 0.01	0.65	149	0.46
$H_2Pc(SPh)_4$[b]	0.24	5.26 ± 0.01	[c]	13	[d]
$Ge(OH)_2Pc(SPh)_4$	0.17	3.44 ± 0.01	0.33	97	1.75
ZnPc [72]	0.20		0.65 [122]	350	2.61
ZnPcTMP [119]	0.10		0.73	160	0.31
ZnPcOMP [72]	0.24		0.63	370	2.12
$ZnPc(NO_2)_4$ [72]	0.02		0.62	310	
$Ge(Cl)_2PcOMP$ [74]	0.31		0.50	168	
$Ge(Cl)_2PcOP$ [74]	0.12		0.30	340	
$Ge(Cl)_2PcOE$ [74]	0.21		0.20	205	
$Ge(Cl)_2Pc(SO_3^-)_4$ [73]	0.12		0.84	640	8.57

[a] OMP = octa(methyl-phenoxy); OP = octaphenoxy; OE = octaestrone; TMP = tetramercaptopyridyl. References in brackets.

[b] parameters determined in toluene due to lack of solubility in DMSO.

[c] not determined due to lack of standards in toluene.

[d] no change in spectra.

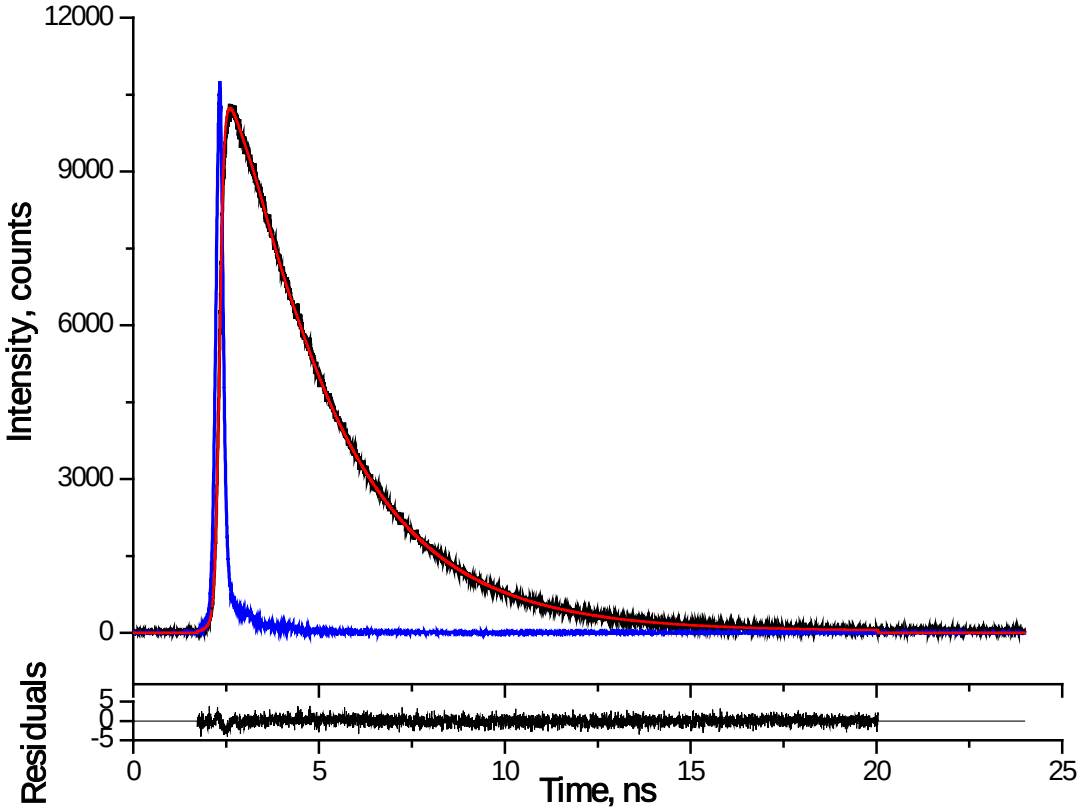

Figure 3.5. Photoluminescence decay curve of $ZnPc(COOH)(SPh)_3$ in DMSO with measurement (black), fit (red) and instrument response (blue).

The τ_F values are typical of MPc complexes [106] and the rate constants for fluorescence (k_F) for the ZnPc derivatives were basically the same, but lower for $H_2Pc(SPh)_4$ and $Ge(OH)_2Pc(SPh)_4$ (Table 3.4).

Table 3.4. Rate constants for excited state deactivation processes in DMSO

Complex	[a]k_F ($x10^7$ s^{-1})	[b]k_{ISC} ($x10^8$ s^{-1})	[c]k_{IC} ($x10^7$ s^{-1})	[d]k_d ($x10^{-2}$ s^{-1})
$ZnPc(COOH)(SPh)_3$	5.53	2.58	8.33	1.27
$ZnPc(SPh)_4$	5.47	2.54	8.20	3.09
$H_2Pc(SPh)_4$	4.18[e]	[f]	[f]	[g]
$Ge(OH)_2Pc(SPh)_4$	4.94	0.96	14.5	18.0

[a]$k_F = \Phi_F/\tau_F$ and is the rate constant for fluorescence.

[b]$k_{ISC} = \Phi_T/\tau_F$ and is the rate constant for intersystem crossing.

[c]$k_{IC} = \Phi_{IC}/\tau_F$ and is the rate constant for internal conversion, where $\Phi_{IC} = 1- (\Phi_F + \Phi_T)$

[d]$k_d = \Phi_{Pd}/\tau_T$ and is the rate constant for photodegradation.

[e] determined in toluene.

[f] not determined due to lack of standards in toluene.

[g] no change in spectra.

3.2.2 Triplet state spectra and parameters

Triplet quantum yield (Φ_T) is the measure of the fraction of absorbing molecules that undergo intersystem crossing (ISC) to the triplet state. The efficiency of a phthalocyanine as a photosensitiser is determined by its triplet state quantum yield and lifetime (τ_T). The triplet quantum yields (Table 3.3) were determined using Equation 1.2 as discussed in Chapter 1. The triplet decay curve of $ZnPc(COOH)(SPh)_3$ is shown in Figure 3.6, and obeyed second order kinetics. This is typical of MPc complexes at high concentrations due to triplet–triplet recombination [232]. Due to lack of standards in toluene and the lack of solubility of $H_2Pc(SPh)_4$ in DMSO, the Φ_T value was not determined for this complex.

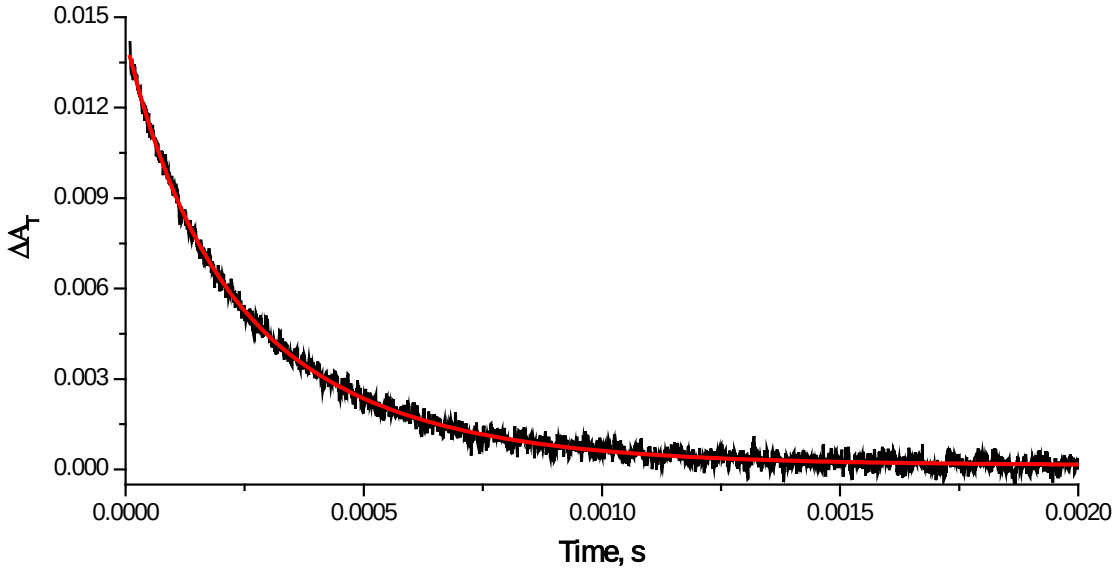

Figure 3.6. Triplet state decay curve of ZnPc(COOH)(SPh)$_3$ in DMSO. Excitation wavelength 679 nm.

The replacement of one phenylthio group with COOH did not have an effect on the Φ_T value comparing ZnPc(COOH)(SPh)$_3$ with ZnPc(SPh)$_4$ in Table 3.3. This is consistent with the similarities in the Φ_F values discussed above. Triplet state lifetime in toluene is low for H_2Pc(SPh)$_4$, this could be related to the viscosity of the solvents as discussed before, where molecules tend to spend more time in the triplet state in highly viscous solvents such as DMSO compared to toluene. The Φ_T values for the aryl substituted ZnPcOMP (Table 3.3) is similar to those of ZnPc(COOH)(SPh)$_3$ and ZnPc(SPh)$_4$. The Φ_T of Ge(OH)$_2$Pc(SPh)$_4$ is similar to that of Ge(Cl)$_2$PcOP [74], lower than that of ZnPc(SPh)$_4$, Ge(Cl)$_2$PcOMP [74] and Ge(Cl)$_2$Pc(SO_3^-)$_4$ [73] but higher than that of Ge(Cl)$_2$PcOE [74] (Table 3.3). The Φ_T of Ge(OH)$_2$Pc(SPh)$_4$ is lower than that of ZnPc(SPh)$_4$, probably due to the slightly larger Zn enhancing intersystem crossing compared to the smaller Ge metal centre. The triplet lifetimes are highly influenced by the presence of oxygen, however in this work the solutions for triplet lifetimes determinations were de-aerated sufficiently before recording of

flash photolysis traces. $ZnPc(COOH)(SPh)_3$ has a higher triplet lifetime than that of $ZnPc(SPh)_4$. The τ_T of the former is close to that of ZnPc, $ZnPc(NO_2)_4$ and ZnPcOMP (Table 3.3) showing that the usymmetrical $ZnPc(COOH)(SPh)_3$ molecule is more favourable for applications as a photosensitiser than the symmetric $ZnPc(SPh)_4$ complex. Table 3.3 shows that in general, the triplet lifetimes values for $ZnPc(COOH)(SPh)_3$ and $ZnPc(SPh)_4$ complexes, are in the reported range for ZnPc complexes. The rate constants for deactivation processes are shown in Table 3.4. The rates of intersystem crossing (k_{ISC}) and internal conversion (k_{IC}) are basically the same for the two ZnPc derivatives, k_{ISC} is however lower for $Ge(OH)_2Pc(SPh)_4$ due to it having a lower Φ_T as described above. The k_{IC} for $Ge(OH)_2Pc(SPh)_4$ is greater than for $ZnPc(SPh)_4$, due to $Ge(OH)_2Pc(SPh)_4$ having a larger quantum yield of internal conversion (Φ_{IC}), indicating that it decays from the T_1 state to the S_0 state more readily than $ZnPc(SPh)_4$.

3.3 Photochemistry

3.3.1 Photodegradation

Photodegradation quantum yield (Φ_{Pd}) determinations were carried out using the experimental set-up described in Chapter 2 and calculated using Equation 1.3. The photodegradation of the synthesised ZnPc derivatives are identified by a decrease in the spectra without formation of new peaks (Figure 3.7) and the Φ_{Pd} were within the range for ZnPc complexes (Table 3.3). The slightly lower Φ_{Pd} for $ZnPc(COOH)(SPh)_3$ (Table 3.3) is possibly due to the electron withdrawing nature of the carboxyl group, which is reported to increase the stability of the Pc to oxidative attack [124,137,138]. The Φ_{Pd} of $ZnPc(SPh)_4$ is of the same order of magnitude compared to ZnPcTMP, which is possibly due to similarities in the structure of the

phenylthio and mercaptopyridyl substituents. The rate constant for photodegradation (k_d, Table 3.4) is higher for the symmetric $ZnPc(SPh)_4$ complex due to the MPc having a shorter triplet state lifetime than the low-symmetry analogue.

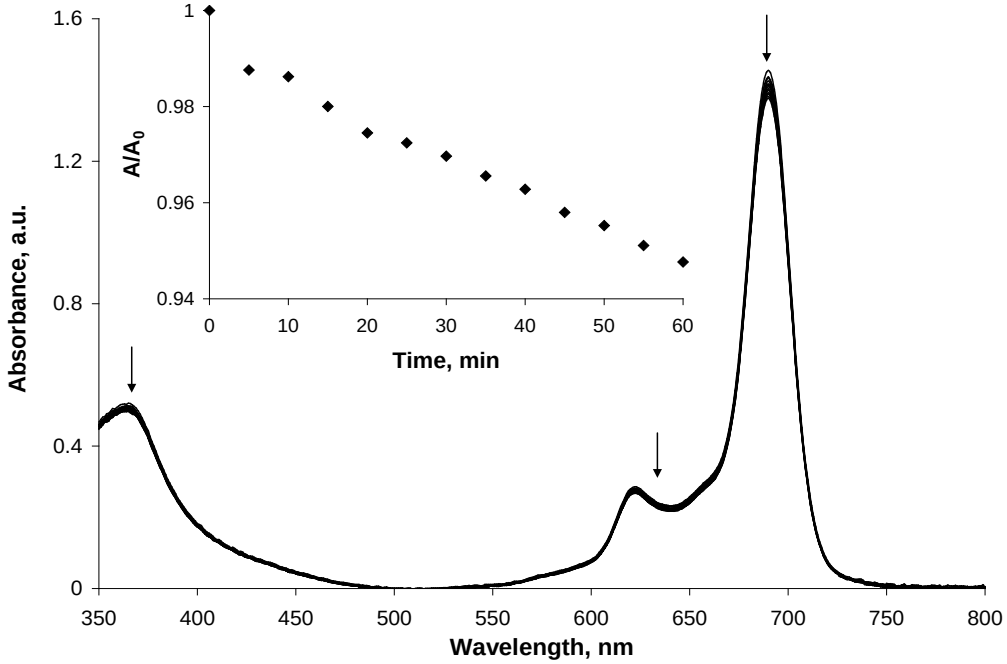

Figure 3.7. Photodegradation of $ZnPc(SPh)_4$ in DMSO after illumination for 5 min intervals (kinetic curve inset). Excitation wavelength 660-740 nm.

3.3.2 Phototransformation

Figure 3.8 A shows the absorption spectra of $Ge(OH)_2Pc(SPh)_4$ in DMSO at 5 minute intervals of illumination. After illumination, there is an initial 16% decrease in Q band intensity with simultaneous increase of absorption in the short-wavelength region around 580 and 600 nm, typical of ring reduction in phthalocyanines [81]. These reduction peaks were obtained within 5 min of photolysis, then decreased as photolysis progressed. A clear photobleaching process was observed after this time. The insert shows the kinetic curve for the photobleaching process. After allowing the

solution to remain in the dark, the Q band is recovered by 10%, with a subsequent decrease in the absorption of the reduction peaks (Figure 3.8 B).

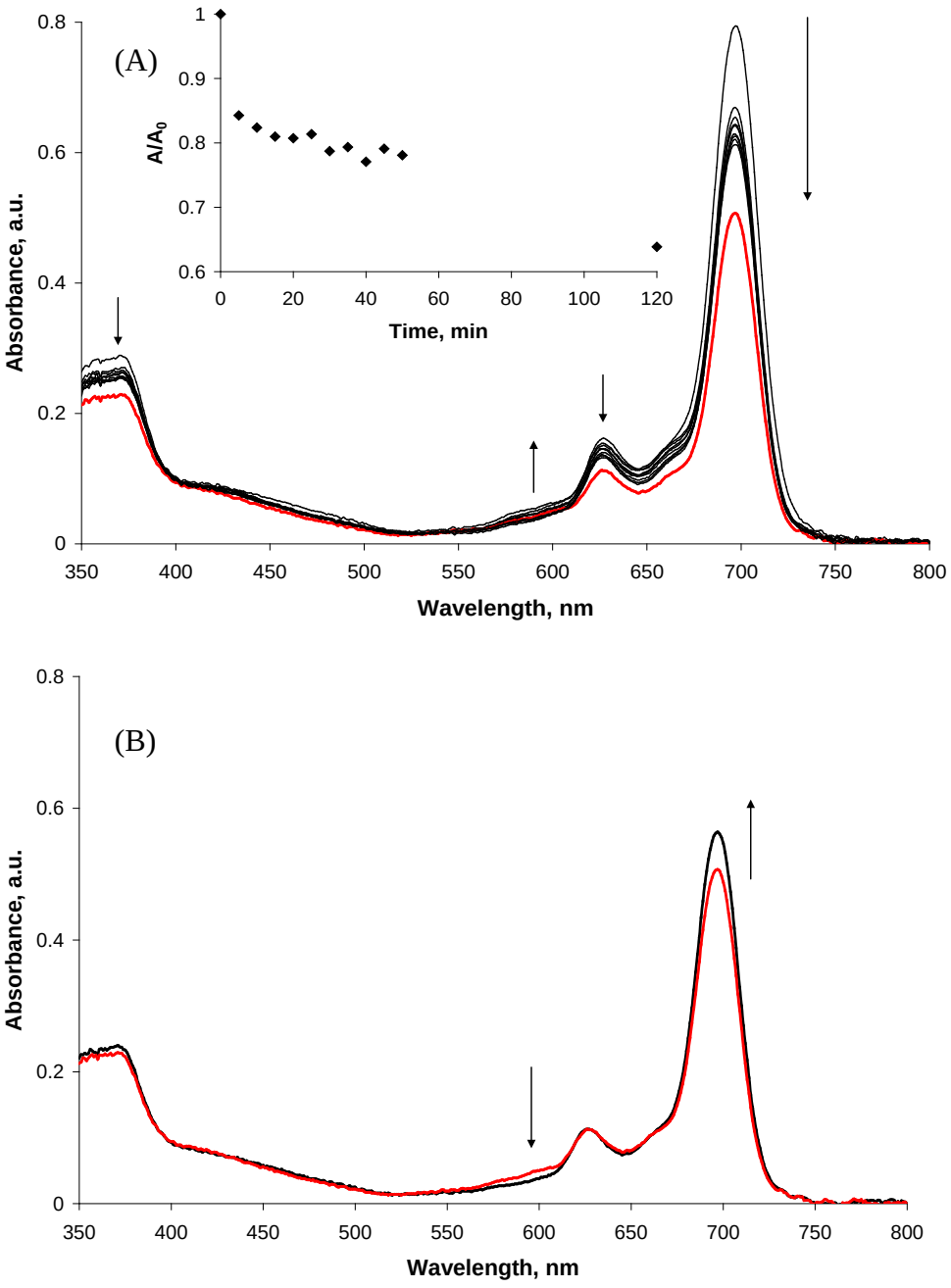

Figure 3.8. Absorption spectra of $Ge(OH)_2Pc(SPh)_4$ in DMSO (A) after illumination for 5 min intervals (black) and after 120 min (red) (kinetic curve inset); (B) after illumination for 120 min (red) and left for 3 min in the dark (black). Excitation wavelength 660-740 nm

Reductive photodegradation has been reported for GePc derivatives [74,136]. Similar new peaks observed have been attributed to the presence of anionic radicals [136] which according to Mack and Stillmann [81] are characteristic of the one-electron reduced species, $M(Pc\text{-}3)^{-}$. Work by other groups [233] have shown that reduction of $(Cl)_2Ge(IV)Pc$ with sodium borohydride resulted in a species which did not retain a Pc moiety, identified as hydroxygermanium(IV) triazabenzcorrole, with a typical sharp band at 400 nm, which was not observed in this work. The reaction mechanism for the photoreduction of the excited GePc derivative (Pc*) has been proposed [74] and is shown in Scheme 3.2:

$$Pc^* + S\text{-}H \rightarrow Pc^{\bullet -} + S\text{-}H^{\bullet +} \quad (1)$$

$$Pc^{\bullet -} + O_2 \rightarrow Pc + O_2^{\bullet -} \quad (2)$$

$$S\text{-}H^{\bullet +} + O_2^{\bullet -} \rightarrow H_2O_2 \quad (3)$$

Scheme 3.2. Proposed mechanism for the photoreduction of GePcs

In this mechanism, electron or hydrogen atom transfer from the solvent (S-H in the Scheme 3.2) to the excited phthalocyanine molecule may be assumed. Interaction of the semi-reduced phthalocyanine radicals with oxygen results in the recovery of the phthalocyanine according to step 2 of Scheme 3.2. The peroxides formed may then oxidise the phthalocyanine ring, by a mechanism known as photooxidation with chemical sensitisation [136]. The Φ_{Pd} was calculated to be 1.75×10^{-5} (Table 3.3), not including the initial decrease due to Pc reduction. This is lower than that observed for $Ge(Cl)_2Pc(SO_3^-)_4$ [73] (Table 3.3). The rate constant of photodegradation (k_d, Table 3.4) of $Ge(OH)_2Pc(SPh)_4$ is higher than for $ZnPc(SPh)_4$ due to its higher Φ_{Pd} and shorter τ_T.

3.4 Optical limiting properties

The linear absorption spectra of phthalocyanine complexes have a Q band in the region of 700 nm, and a B band in the region of 350 nm, with a high linear transmittance window between these two absorption bands, making them attractive as limiters of visible light (~420-650 nm). The triplet absorption maximum is found between the Q and B bands in the UV-vis spectra with the excited state occurring at approximately 520 nm. Irraditaion at 532 nm is therefore a near-resonant excitation [170]. The open-aperture z-scans performed exhibited a reduction in transmission about the focus of the lens. This is typical of induced positive non-linear absorption of the incident light, assumed to be reverse saturable excited state absorption [170]. A sample of typical open-aperture z-scan spectra with normalised transmission plotted as a function of sample position are shown in Figure 3.9.

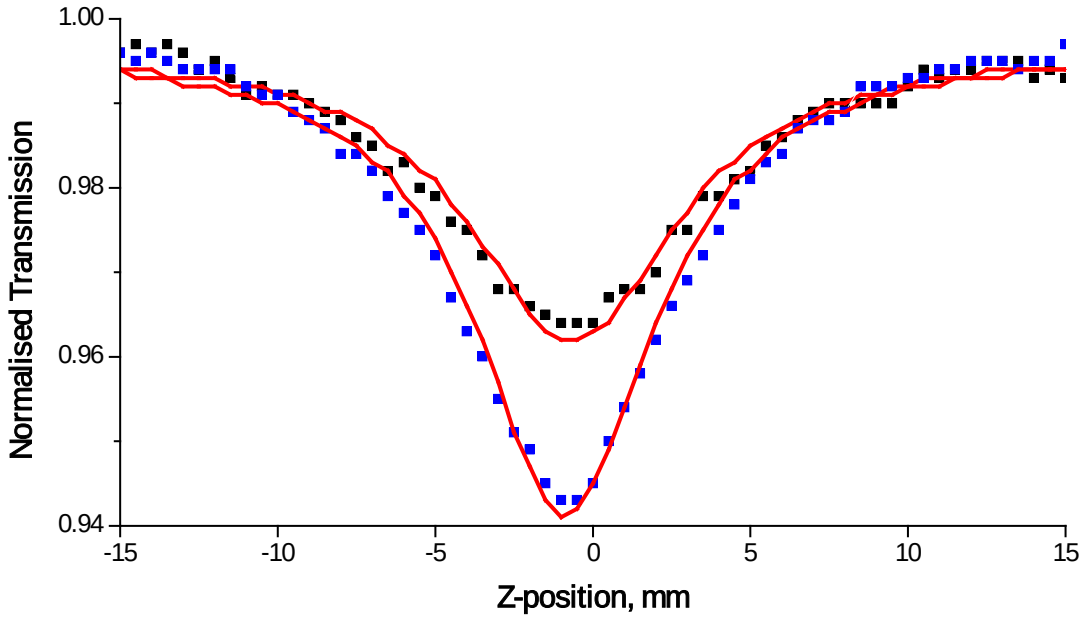

Figure 3.9. Open aperture z-scan spectra of ZnPc(COOH)(SPh)$_3$ (black) and ZnPc(SPh)$_4$ (blue) in DMSO, with fits (red)

No single parameter can be used to describe the efficacy of an optical limiter. A number of optical limiting parameters are summarised in Table 3.5. The linear absorption coefficient (α) was determined as the absorbance at the Q band maxima in the UV-vis spectra, the third-order nonlinear absorption coefficient (β_1) and waist radius at the focus (w_0) were determined by the fitting of the z-scan spectra, the imaginary third-order susceptibility ($\mathrm{Im}\{\chi^{(3)}\}$) and imaginary second-order hyperpolarisability ($\mathrm{Im}\{\gamma\}$) were calculated using Equations 1.10 and 1.11 respectively, the incident laser energy (E) is also shown.

Table 3.5. Optical limiting parameters of synthesised Pcs in different solvents

Complex	Solvent	α (cm^{-1})	E (μJ)	w_0 (μm)	β_1 ($cm.W^{-1}$)	$\mathrm{Im}\{\chi^{(3)}\}$ (esu)	$\mathrm{Im}\{\gamma\}$ (esu)
$ZnPc(COOH)(SPh)_3$	DMSO	1.56	13.4	25.9	1.08×10^{-8}	3.79×10^{-12}	1.13×10^{-31}
$ZnPc(SPh)_4$	DMSO	3.01	15.3	23.8	1.47×10^{-8}	5.18×10^{-12}	1.63×10^{-31}
	Toluene	3.05	15.9	21.8	2.49×10^{-8}	8.96×10^{-12}	3.34×10^{-31}
	THF	3.03	15.0	19.5	1.67×10^{-8}	5.33×10^{-12}	2.75×10^{-31}
$H_2Pc(SPh)_4$	Toluene	1.27	21.0	31.8	6.12×10^{-9}	1.12×10^{-12}	2.58×10^{-32}
	THF	1.16	10.7	30.8	3.12×10^{-9}	1.95×10^{-12}	9.56×10^{-32}
$Ge(OH)_2Pc(SPh)_4$	DMSO	2.73	13.7	28.2	2.38×10^{-8}	8.39×10^{-12}	1.72×10^{-31}
	Toluene	2.67	13.0	19.6	1.85×10^{-8}	6.68×10^{-12}	1.44×10^{-31}

It can be seen that the effective third-order absorption coefficient, β_1, ranges from values of 10^{-9} to 10^{-8} $cm.W^{-1}$, which corresponds to second-order molecular hyperpolarisabilities ($\mathrm{Im}\{\gamma\}$) ranging from on the order of 10^{-32} to 10^{-31} esu. $\mathrm{Im}\{\gamma\}$ can be useful as a comparable value of the molecular response as opposed to the macroscopic response and indicate that the phthalocyanines in this work show promise as optical limiters. The β_1 and $\mathrm{Im}\{\gamma\}$ values for $ZnPc(COOH)(SPh)_3$ in

DMSO are slightly smaller than those for $ZnPc(SPh)_4$ in DMSO. These values for $ZnPc(SPh)_4$ is ~1.4 times greater than that of $ZnPc(COOH)(SPh)_3$, this may be due to the increased conjugation in the extra phenylthio substituent as compared to the low-symmetry analogue. The slightly higher values of $\mathrm{Im}\{\chi^{(3)}\}$ and $\mathrm{Im}\{\gamma\}$ obtained for $Ge(OH)_2Pc(SPh)_4$ in DMSO versus $ZnPc(SPh)_4$ is attributed to the higher molecular weight of the Ge metal centre. The values obtained for $ZnPc(SPh)_4$ are an order of magnitude higher than that of the unmetallated $H_2Pc(SPh)_4$.

The difference between the values obtained in different solvents may be attributed to thermally induced refractive index changes which dominate the changes of the refractive index in the solutions [234]. This is most notable for $ZnPc(SPh)_4$ in toluene having β_1, $\mathrm{Im}\{\chi^{(3)}\}$ and $\mathrm{Im}\{\gamma\}$ values near double that in DMSO. However, nonlinear absorption is still the predominant effect contributing to the third-order nonlinear process. The differences seen for $H_2Pc(SPh)_4$ in THF and toluene may be due to differences in solubility for this complex in these solvents or the intensity of the laser.

The refraction effects indicated by the waist radius, w_0 determined from the fitting, shows that the unmetallated and GePc derivatives have greater refraction effects, showing that it defocuses the laser more effectively relative to the Zn complexes. This is a desirable effect as it spatially disperses the incident pulse, reducing the energy density, which may keep the incident energy density below the damage threshold of the limiting material.

3.5 Photoelectrochemical properties

3.5.1 Preparation of ZnO, MPc readsorption and surface morphology

Deposition of nanoporous ZnO in the presence of eosin Y as a structure directing agent (SDA) was achieved electrochemically as described in the Experimental section and in Chapter 1. A colour change from red to white was observed indicating complete desorption of eosin Y from the ZnO surface (Figure 3.10).

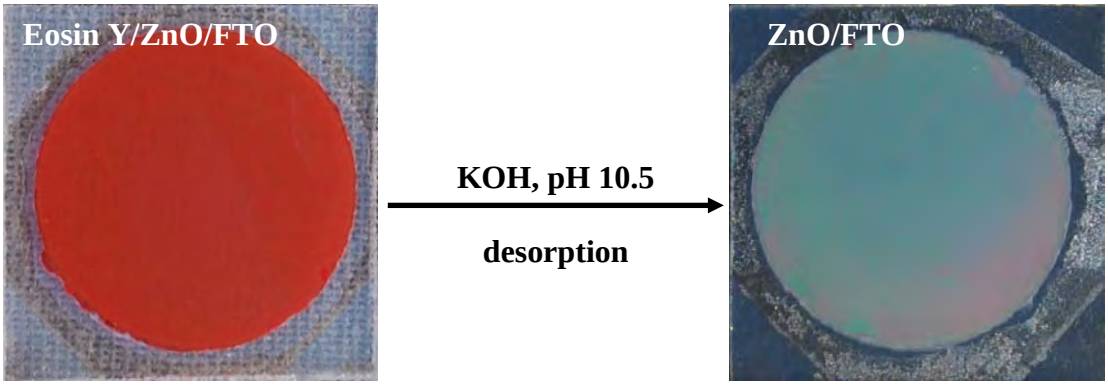

Figure 3.10. ZnO before and after desorption of eosin Y

Figure 3.11 shows the confocal laser microscope and scanning electron microscope (SEM) images of the edge of a ZnO film after desorption of eosin Y. The film thickness was determined to be 4.8 μm. The porous ZnO and nonporous blocking layers are clearly visible on the FTO substrate. Porous substrates are important in DSSCs as they have a high surface area for dye adsorption. After desorption of the SDA by treatment with KOH, the surface area of ZnO increases significantly, with a highly porous ZnO film formed (Figure 3.11). Similar crystal shapes of nanoporous ZnO have been reported using different SDAs [235].

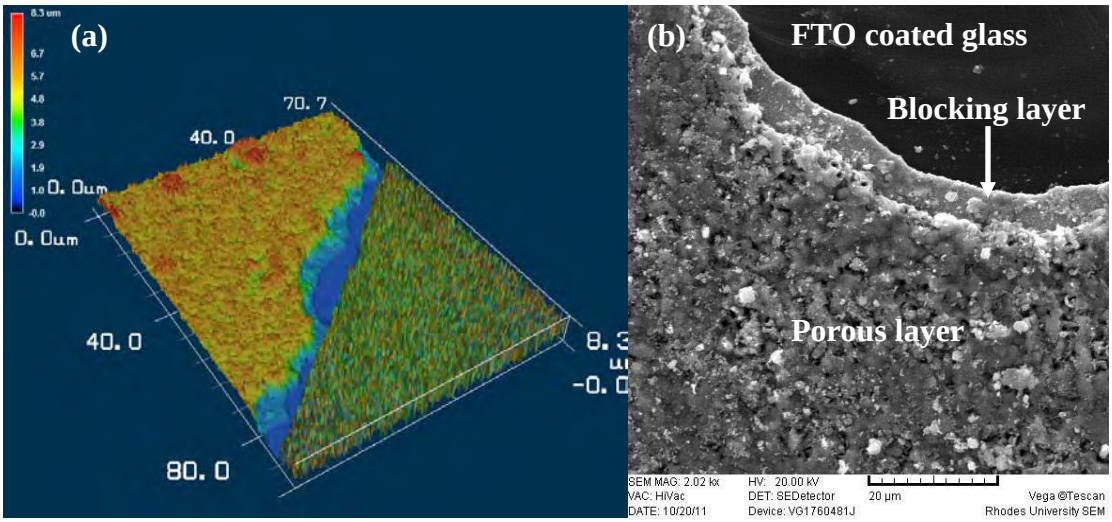

Figure 3.11. Confocal laser microscope image (a) showing FTO coated glass (dark blue), blocking layer (light blue) and porous ZnO (yellow to orange), and (b) SEM image of deposited ZnO with layers labelled.

The $Zn(COOH)(SPh)_3$ dye adsorption was achieved as described in the Experimental section. When the MPc dye molecules were readsorbed on the surface of ZnO after the desorption of eosin Y, an intense blue-green colour was observed suggesting complete coverage of the ZnO by the dye molecules (Figure 3.12). UV-vis spectroscopy was used to characterise the ZnO/MPc films to determine whether there were changes in the electronic structure of the dye molecules on the ZnO surface.

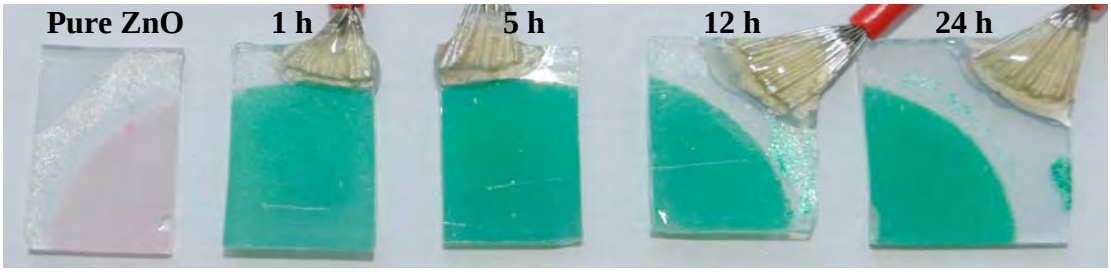

Figure 3.12. ZnO/FTO after adsorption of $ZnPc(COOH)(SPh)_3$ for different times

Figure 3.13 shows the solid state absorption spectra of the ZnPc(COOH)$(SPh)_3$ adsorbed on the ZnO films deposited on FTO. The complex was monomeric in solution, but aggregates are expected in the solid state. New bands were formed due to aggregation of the MPc on the ZnO substrate, as a result of co-facial self-assembly of the Pcs on the surface. The bands in the long wavelength region in the Q band region (680 nm) are due to monomeric species and are of similar intensity to that of the blue-shifted dimeric peaks observed (630 nm), suggesting fairly strong aggregation [97,236]. The amount of dye adsorbed to the ZnO is not directly proportional to the deposition time, this is possibly due to differences between the ZnO film sections used for each deposition time or due to differences in the rinsing of the films after sensitisation.

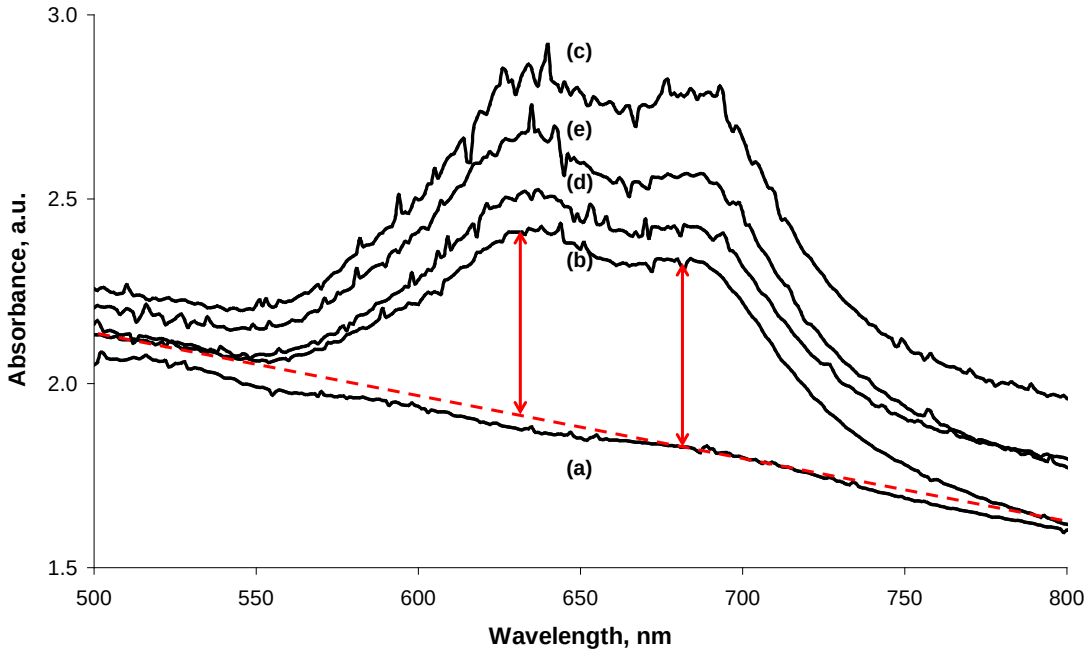

Figure 3.13. Solid state absorption spectra of ZnO/FTO (a), and after 1 h (b), 5 h (c), 12 h (d) and 24 h (e) deposition in ZnPc(COOH)$(SPh)_3$ solution.

Previous reports suggest that the efficiency of the DSSC may be increased by full monolayer coverage of dye molecules on the ZnO surface [237]. Dimers will result in lower efficiencies of photovoltaic cell performance as aggregates are photoinactive [158], with the increased rates of non-radiative recombination and back-electron transfer possibly as a result of strong electronic coupling observed in the aggregates [238,239]. Dye molecules must be in close proximity to each other, with interaction of the molecules required to form the self assembled monolayer hybrid. The confocal laser microscope and SEM images (Figure 3.14) show that there is little visible structural difference between the ZnO film and dye sensitised ZnO surfaces at the specific magnifications.

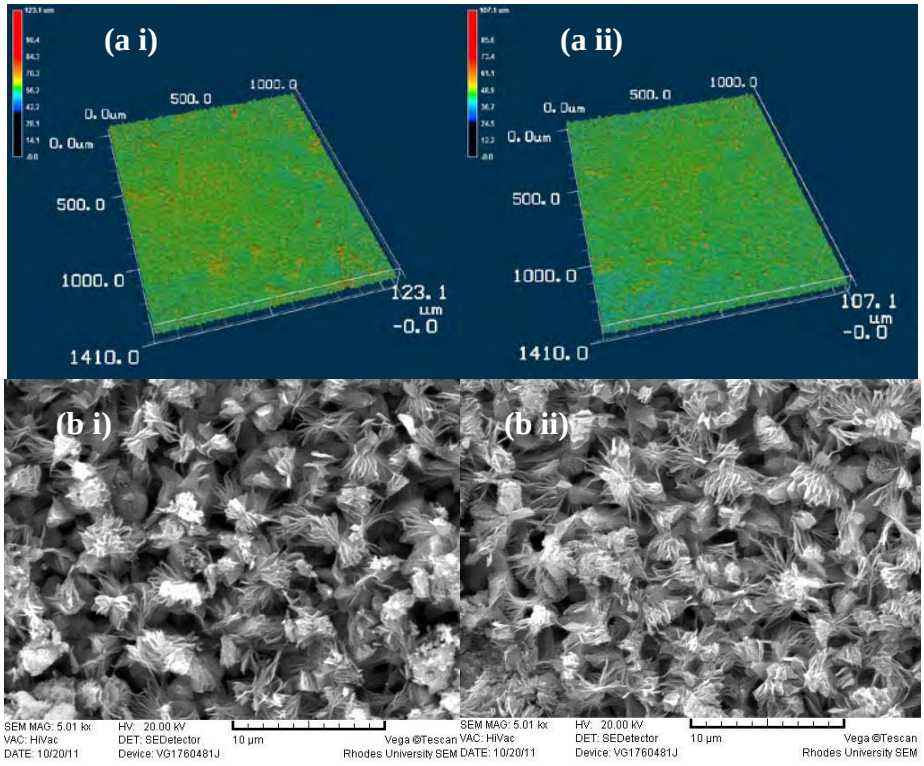

Figure 3.14. Confocal laser microscope (a) and SEM images (b) of porous ZnO on FTO (i) and ZnPc(COOH)$(SPh)_3$ adsorbed on ZnO/FTO for 5 h (ii)

3.5.2 Photoelectrochemical measurements and parameters

Studies have shown that aggregation is one of the limiting factors for MPc use in DSSCs. The synthesised dye used in this report contains a carboxylic substituent since they are known to form an ester-like linkage with free OH groups on the ZnO surface [238,240,241]. The photoelectrochemical measurements were performed at Justus-Liebig University, Germany, using the set-up as described in the Experimental section. Table 3.6 summarises photovoltaic parameters. The incident photon to current conversion efficiency (IPCE), absorbed photon to current conversion efficiency (APCE), fill factor (FF) and overall cell efficiency (η) at different deposition times were calculated using Equations 1.4, 1.5, 1.6 and 1.7 respectively.

Table 3.6. Photoelectrochemical data obtained at an incident photon flux of 10^{16} s^{-1}. cm^{-2} (680 nm red light) (IPCE, APCE) or conditions close to AM 1.5 (white light) (FF, η) for ZnO sensitised with $ZnPc(COOH)(SPh)_3$ for different times

Time (h)/Complex[a]	Abs. (a.u.)	IPCE (%)	APCE (%)	V_{oc} (mV)	I_{sc} ($mA.cm^{-2}$)	FF (%)	η (%)
1	0.480	4.86	7.29	433	0.47	35	0.072
5	0.693	3.74	4.69	440	0.49	34	0.074
12	0.476	4.57	6.85	435	0.49	34	0.072
24	0.605	4.64	6.17	430	0.47	34	0.069
ZnPcOC [154]		14.98	44.1			46	0.33
ZnPcTNCDP [156]		30.9	34.6	420	3.1	37	0.48
OTiPcOC [156]		50.6	62.8			36	0.45

[a] OC = octacarboxy; ZnPcTNCDP structure shown in Figure 1.10. References in brackets.

The IPCE values obtained were low compared to MPcs previously reported (Table 3.6), with the highest external quantum efficiency (IPCE) of 4.86% for 1 h deposition time obtained for ZnPc(COOH)$(SPh)_3$ (Table 3.6). The film under illumination with white light gave the highest photocurrent density of 0.45 mA.cm^{-2} and with illumination at the Q band maximum (680 nm) and an incident photon flux of 10^{16} s^{-1}.cm^{-2}, a photocurrent density of 0.08 mA.cm^{-2} was obtained (Figure 3.14). Lower IPCEs tended to be obtained for the films containing more adsorbed dye (Figure 3.16), due to the higher aggregation tendency leading to charge traps and non-radiative recombination of charges before and after electron injection from the LUMO of the phthalocyanine molecules to the conduction band of the ZnO or to increased recombination of the charges already in the electrolyte.

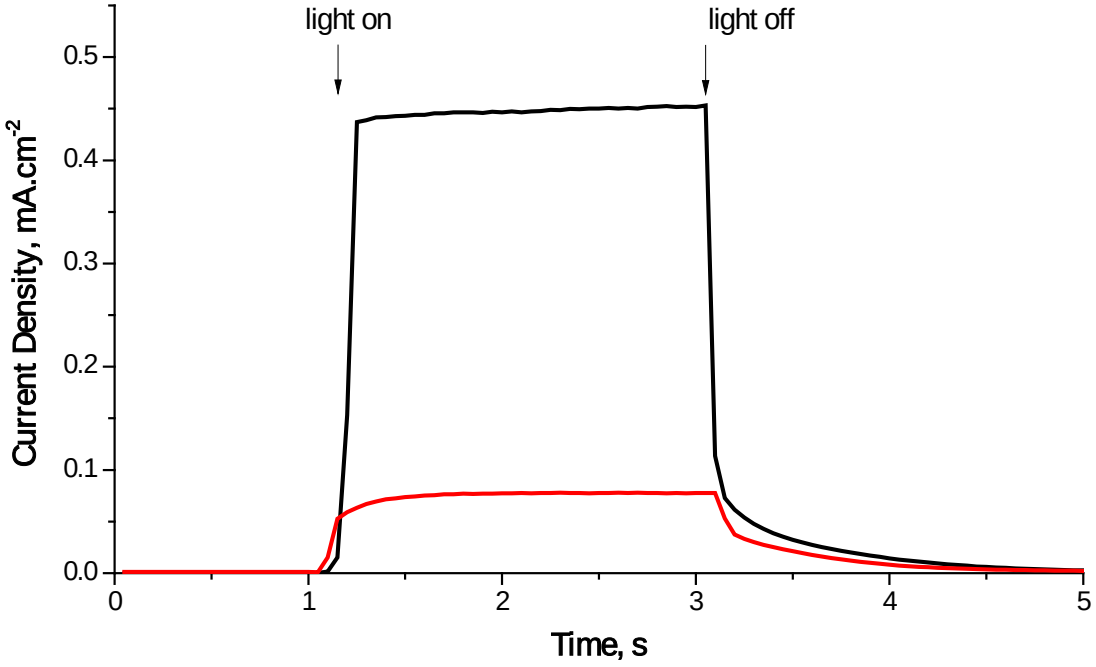

Figure 3.15. Photocurrent transients for ZnPc(COOH)$(SPh)_3$ sensitised ZnO (1 h deposition) under illumination with white light (black), and red light of 680 nm wavelength and incident photon flux of 10^{16} s^{-1}.cm^{-2} (red)

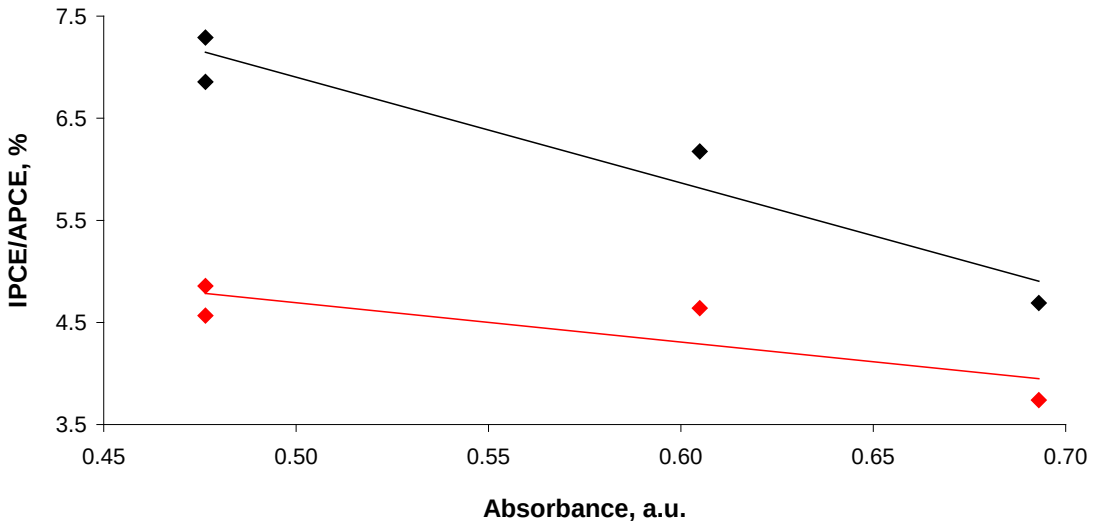

Figure 3.16. Relationship of IPCE (red), and APCE (black) to ZnPc(COOH)(SPh)$_3$ absorption at 680 nm of the sensitised ZnO films.

Similarly shaped time-resolved photocurrent density transients were obtained for the different deposition times indicating that similar relative rates of fast electron injection and reduction of dye regeneration were obtained. Almost rectangular photocurrent responses were obtained, with no overshoot of photocurrent when the light was switched on, showing that the dye molecules are in contact with the electrolyte [242], suggesting full coverage. The absorbed photon to current conversion efficiency (APCE) determines the number of electrons that are generated or converted to the external circuit per photon absorbed on the surface of the electrode, and thus gives an indication of the efficiency of internal processes like injection efficiency. As shown in Table 3.6, the deposition time of 1 h again shows the highest APCE of 7.29% with the absorbance of 0.48. The fact that only 7% of the absorbed photons generate an electron in the external circuit suggests inefficient injection of electrons into the conduction band of the ZnO at a high recombination probability. At higher dye absorption values, injection efficiency was decreased

resulting in a decrease in the APCE (Figure 3.16) suggesting re-adsorption of dye molecules that are not directly linked to the ZnO. The overall cell efficiencies (η) were similar and showed no clear trend (Table 3.6).

Figure 3.17 shows the time-resolved photovoltage curve for the ZnPc(COOH)$(SPh)_3$ sensitised ZnO (1 h deposition) under illumination with white light. A high photovoltage of about 460 mV was obtained. Upon shutter closure, a slow decrease of the photovoltage was observed during the decay period.

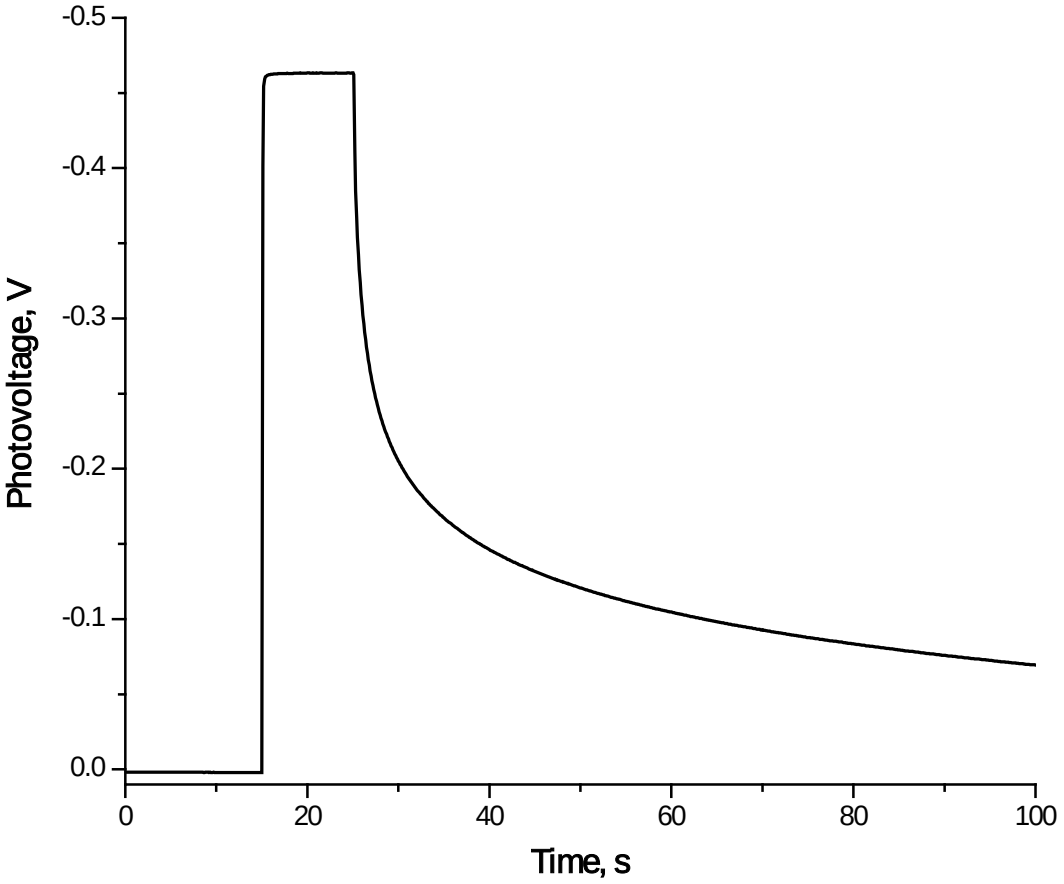

Figure 3.17. Time dependent photovoltage curve of ZnPc(COOH)$(SPh)_3$ sensitised ZnO (1 h deposition) under illumination with white light

Shown in Figure 3.18 is a typical current to voltage (IV) curve in the dark (red) and under illumination with white light (black) for the ZnPc(COOH)$(SPh)_3$ sensitised ZnO film (5 h deposition) giving the short circuit photocurrent (I_{sc}) of 0.49 mA.cm^{-2} and an open circuit voltage (V_{oc}) of 440 mV. Faradaic characteristics were observed for the films, with the highest fill factor of 35% obtained. The electrolyte is being shielded from the ZnO by the dye molecules due to aggregation, resulting in low fill factor values and limiting cell efficiency. This could be improved by using additives in the redox solution of the cell.

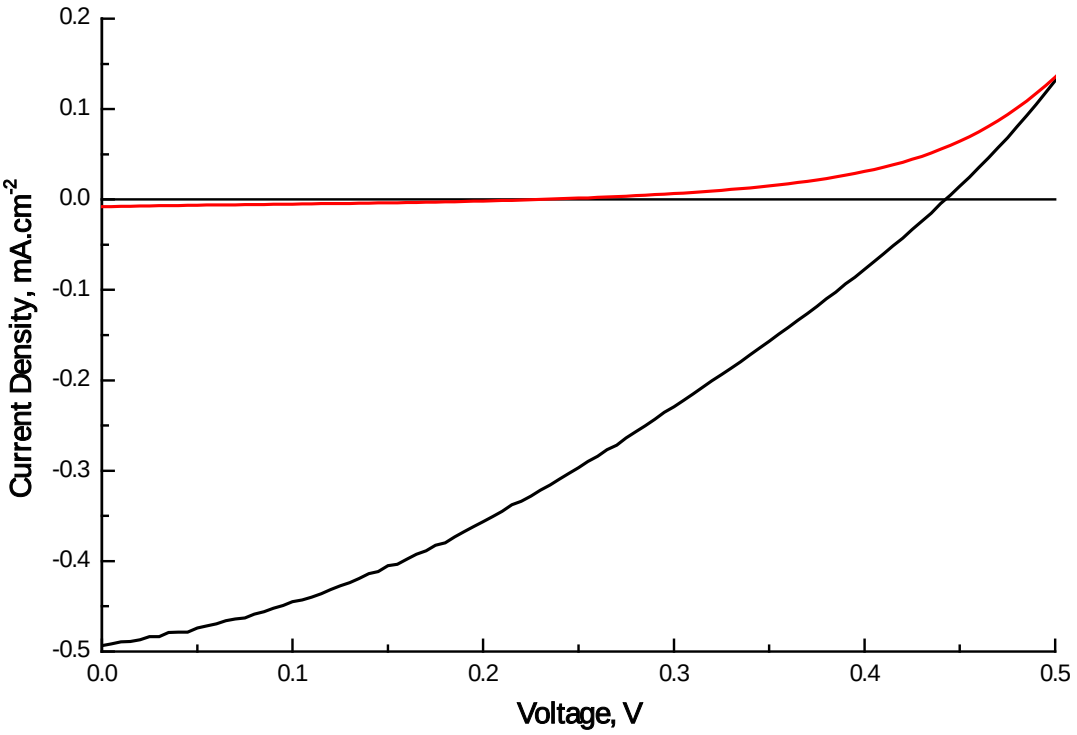

Figure 3.18. Photocurrent density to voltage (IV) curves for ZnPc(COOH)$(SPh)_3$ sensitised ZnO electrode (5 h deposition) in the dark (red) and under illumination with AM 1.5 simulated sunlight (black)

3.6 Conjugation of MPcs to gold nanoparticles

3.6.1. Synthesis and characterisation of AuNPs

The synthesis of TOABr capped AuNPs has been described in the Experimental section. The TEM (Figure 3.19) and AFM (Figure 3.20) images of the synthesised TOABr-AuNPs and ZnPc(SPh)$_4$-AuNP conjugate show a varied size distribution of nanoparticles, with the very large particles (white) in the AFM images being possible agglomerates of nanoparticle or small particles of bulk material.

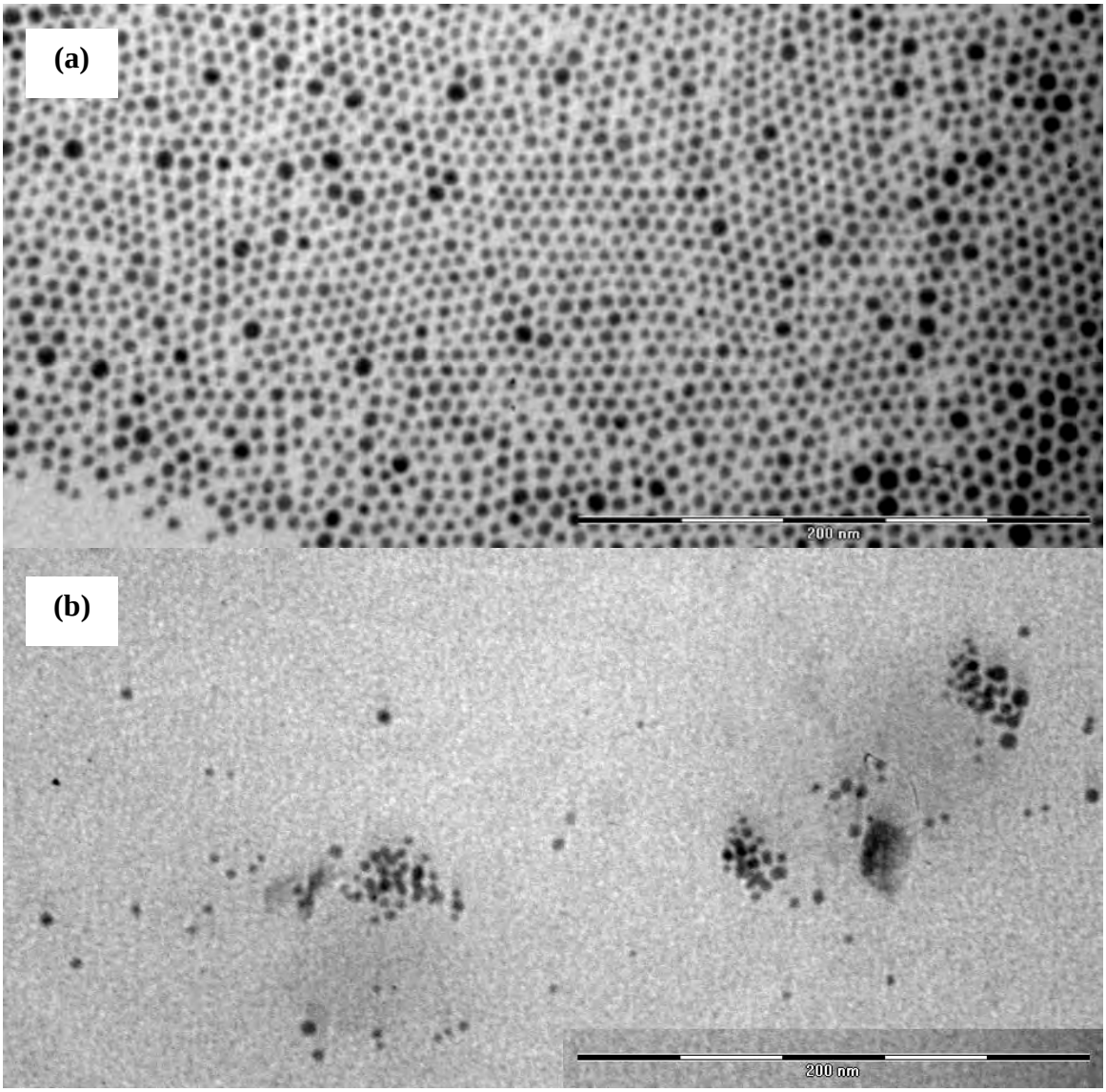

Figure 3.19. TEM images of TOABr-AuNPs (a) and ZnPc(SPh)$_4$-AuNPs (b)

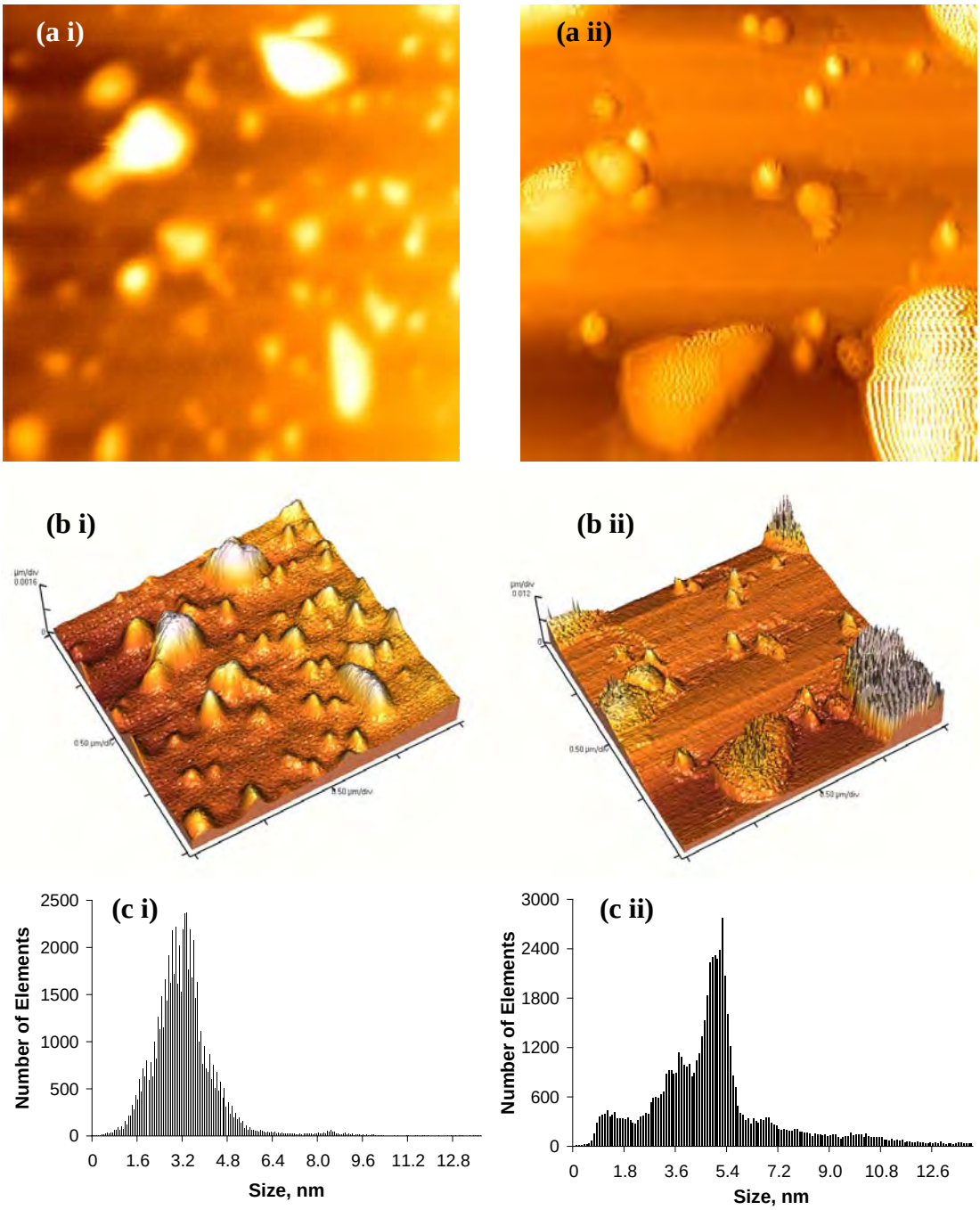

Figure 3.20. 2D (a) and 3D (b) AFM images (height profile), and size distribution histograms (c) of TOABr-AuNPs (i) and ZnPc(SPh)$_4$-AuNPs (ii)

The TOABr-AuNPs have a size distribution of up to > 4.5 nm (Figure 3.20 c i), the size distribution between 2 and 4 nm dominated, with an average size near 3.2 nm, which corresponds well to the size determined using XRD (Figure 3.21).

The average size of the TOABr-AuNPs synthesised was determined by XRD of powdered AuNPs and using the Scherrer equation (Equation 1.14) to be 2.97 nm, the fit obtained is shown in red. The labelled peaks are broad as expected for small crystallite sizes, and correspond well to gold, with the peak indexes given in Figure 3.21.

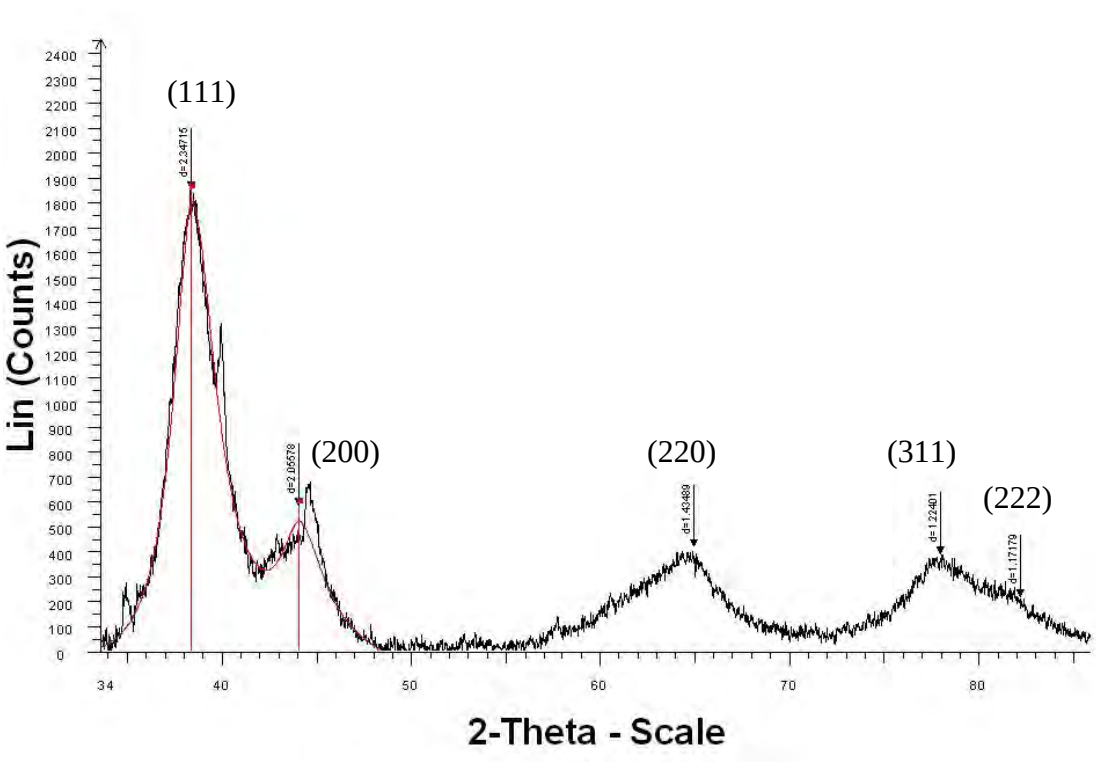

Figure 3.21. X-ray diffraction spectrum of TOABr-AuNPs

The XPS spectrum (Figure 3.22) shows peaks corresponding to C 1s, O 1s, Au 4d and Au 4f electrons. The carbon and oxygen peaks may be due to the presence of the capping agent (TOABr) and oxidised species, or from the tape used for securing the powdered nanoparticles. The resolved XPS spectrum (Figure 3.22 inset) shows the presence of the Au $4f_{5/2}$ and Au $4f_{7/2}$ peaks at 85.1 eV and 81.4 eV respectively, which are shifted as expected for gold nanoparticles compared to bulk gold [243].

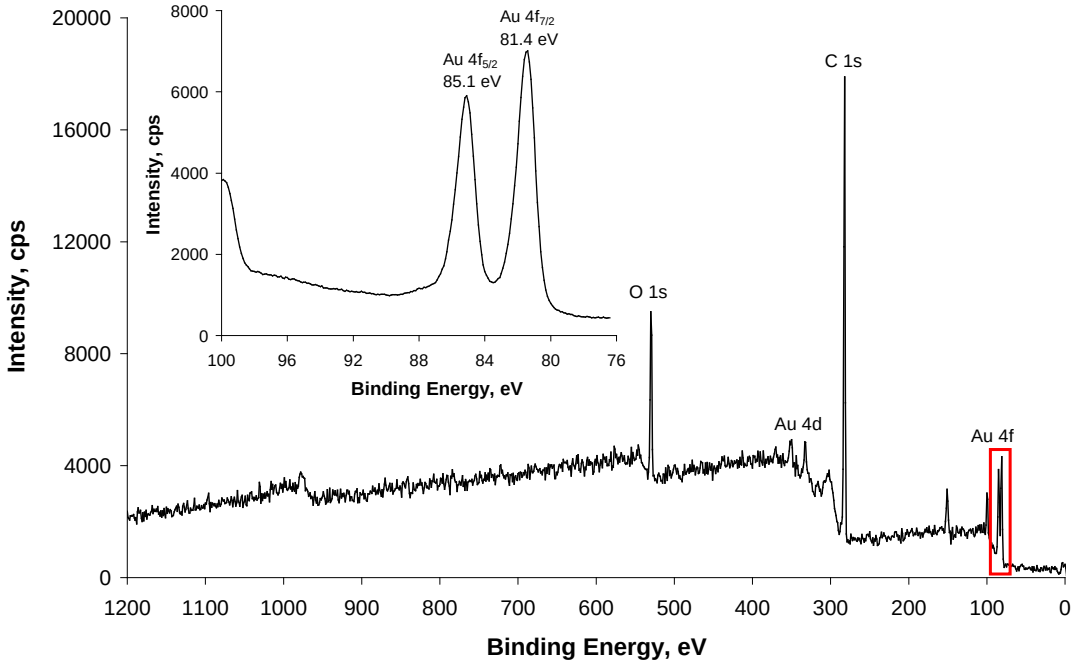

Figure 3.22. XPS spectrum of TOABr-AuNPs. Resolved Au 4f peaks inset.

3.6.2. Synthesis and characterisation of ZnPc(SPh)$_4$–AuNPs conjugates

The conjugation was achieved through ligand exchange described in Chapter 1 and the Experimental section. The AFM histogram in (Figure 3.20 c ii) shows a small increase in the size for ZnPc(SPh)$_4$-AuNP, with a size distribution ranging from 1.2 to > 10 nm and an average of 5 nm, possibly as a result of agglomeration of the ZnPc(SPh)$_4$-AuNP conjugate particles or due to the increase in size due to the Pc molecule contribution. The TEM image shows a similar size distribution of the conjugate particles (Figure 3.19 b) compared to the unmodified AuNPs (Figure 3.19 a), with possible agglomeration also present. The surface plasmon band maximum of TOABr-AuNPs in toluene, is observed at 525 nm (Figure 3.23 A (red)). The ZnPc(SPh)$_4$ has a Soret band at 373 nm and a Q band with the maximum at 692 nm in toluene (Figure 3.23 A (blue), Table 3.7). The Q band of the Pc becomes blue-shifted (684 nm) and broader after the attachment to the gold nanoparticles (Figure 3.23 A (black)). The blue-shifting of the Q band can be attributed to the attachment of the

sulfur atoms to the gold surface, the broadening has been attributed to possible tight packing of the phthalocyanines on the gold [58].

Table 3.7. Spectral and photophysical data of $ZnPc(SPh)_4$ and $ZnPc(SPh)_4$-AuNP conjugate in different solvents

Complex	Solvent	λ_{abs} (nm)	λ_{em} (nm)	Φ_F	λ_1[a] (nm)	λ_2[a] (nm)	τ_1[b] (ns)	τ_2[b] (ns)
	Toluene	692	702	0.15			2.60 ± 0.01 (100%)	
$ZnPc(SPh)_4$	THF	685	696	0.15			2.65 ± 0.01 (100%)	
	$CHCl_3$	690	703	0.15			2.74 ± 0.01 (100%)	
	Toluene	685	698	0.09	694	702	4.23 ± 0.07 (73%)	1.74 ± 0.11 (27%)
$ZnPc(SPh)_4$-	THF	688	696	0.09	696	694	3.76 ± 0.02 (68%)	1.83 ± 0.04 (32%)
AuNP	$CHCl_3$	691	700	0.09	698	700	4.14 ± 0.08 (73%)	1.78 ± 0.19 (27%)

[a] values obtained from TRES spectra

[b] percentage contribution shown in brackets

Phthalocyanines usually form face-to-face-oriented, non-fluorescent H-aggregates, characterized by blue shifted absorption bands, with side-by-side-oriented, fluorescent J-aggregates also possible [101]. Aggregation is unlikely though as the $ZnPc(SPh)_4$ loading on the AuNPs was determined to be approximately 2.1 molecules per AuNP using the absorbance spectra of the conjugate and molar extinction coefficients (Equation 1.12). This is relatively low compared to previous studies [58], but not unexpected due to the comparatively low concentration of $ZnPc(SPh)_4$ used for conjugation. Dye loading may also be low due to the bulky nature of the phenylthio substituent decreasing the ability for conjugation. The surface plasmon band of the gold nanoparticles in the $ZnPc(SPh)_4$-AuNP has the same position (525 nm) as before

the attachment of the phthalocyanines, indicating that the core size of the particles is not affected by the ligand exchange. The bandwidth has however broadened, due to modification of the AuNP surface by Pc molecules. In THF and chloroform (Figure 3.23 B (blue and red, respectively)), the $ZnPc(SPh)_4$ in the conjugate appears to have sharper peaks as compared with that in toluene (Figure 3.23 B (black)).

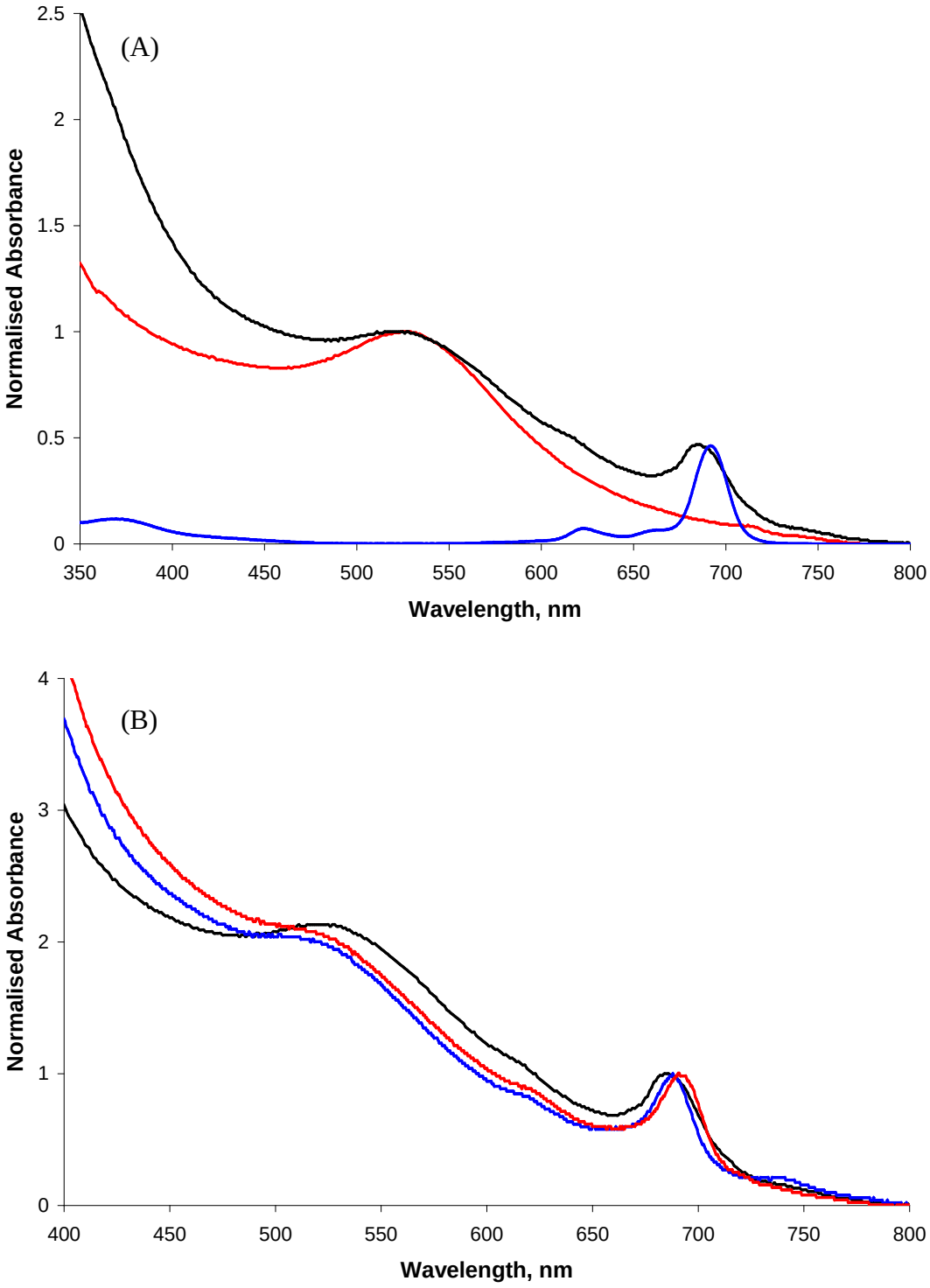

Figure 3.23. Absorbance spectra of (A) TOABr-AuNPs (red), Zn(SPh)$_4$Pc (blue) and Zn(SPh)$_4$Pc–AuNP conjugate (black) in toluene; (B) ZnPc(SPh)$_4$–AuNP conjugate in toluene (black), THF (blue) and chloroform (red)

For $ZnPc(SPh)_4$ in toluene and in the absence of AuNPs, the emission maximum of the Q band was at 702 nm (Table 3.7). The fluorescence peak in $ZnPc(SPh)_4$-AuNP was observed at 699 nm (Figure 3.24), the blue shift corresponds to the blue-shifted absorption peak.

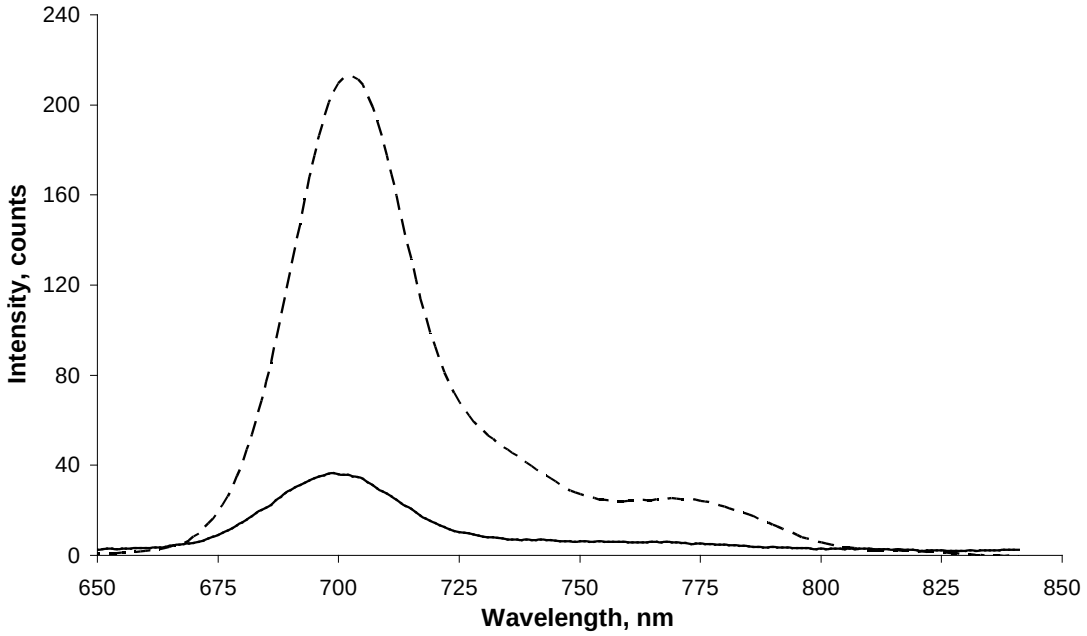

Figure 3.24. Fluorescence spectra of $ZnPc(SPh)_4$ (dashed) and $ZnPc(SPh)_4$-AuNP (solid) excited at equivalent absorbance wavelength of 632 nm

The fluorescence decay curves of $ZnPc(SPh)_4$ and $ZnPc(SPh)_4$-AuNP measured by the TCSPC instrument are shown in Figure 3.25. A dramatic increase in the fluorescence lifetime was observed in the presence of AuNPs (Table 3.7) contradicting the reports that AuNPs quench Pc fluorescence. Two lifetimes were observed for the $ZnPc(SPh)_4$-AuNP, with one lifetime significantly longer and one shorter compared to that of the $ZnPc(SPh)_4$ alone. It is known that AuNPs quench Pc fluorescence [58], but other studies have shown that gold nanoparticles stabilised by thiol or amino derivatised phthalocyanine do not quench the fluorescence [57,225]. In

the case of alkyl thio substituted phthalocyanine, the lack of quenching was attributed to the combination of the long C11 alkyl tether employed and the small gold core. An increased lifetime was reported, but only contributed 2% of overall fluorescence [57], however in this work the increased lifetime contributed considerably more.

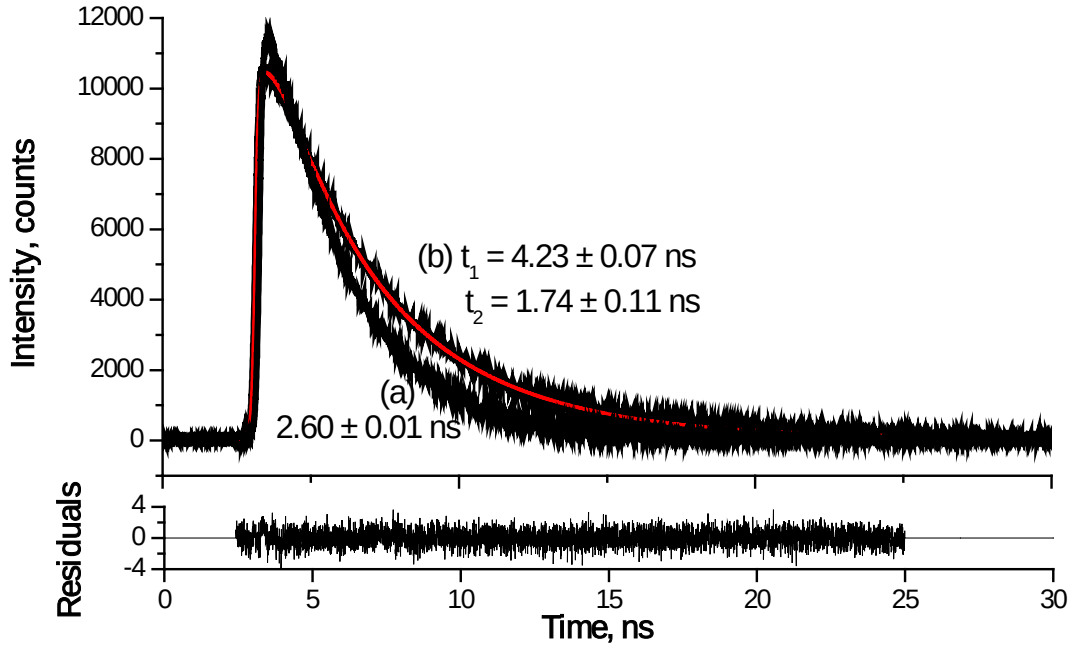

Figure 3.25. Photoluminescence curves of free ZnPc(SPh)$_4$ (a) and ZnPc(SPh)$_4$-AuNP (b) in toluene with bi-exponential fit shown (red). Fluorescence lifetimes inset.

Time-resolved fluorescence spectroscopy (TRES) was conducted, to determine the origin of the lifetimes. Figure 3.26 shows that the two lifetimes are as a result of contributions of fluorescence at 702 nm, which is also the fluorescence maximum of the free Pc in toluene (Table 3.7), and one at 694 nm. The sum of the two spectra (Figure 3.24 c) corresponds well to that of the observed steady state fluorescence maximum (Figure 3.22 (solid)).

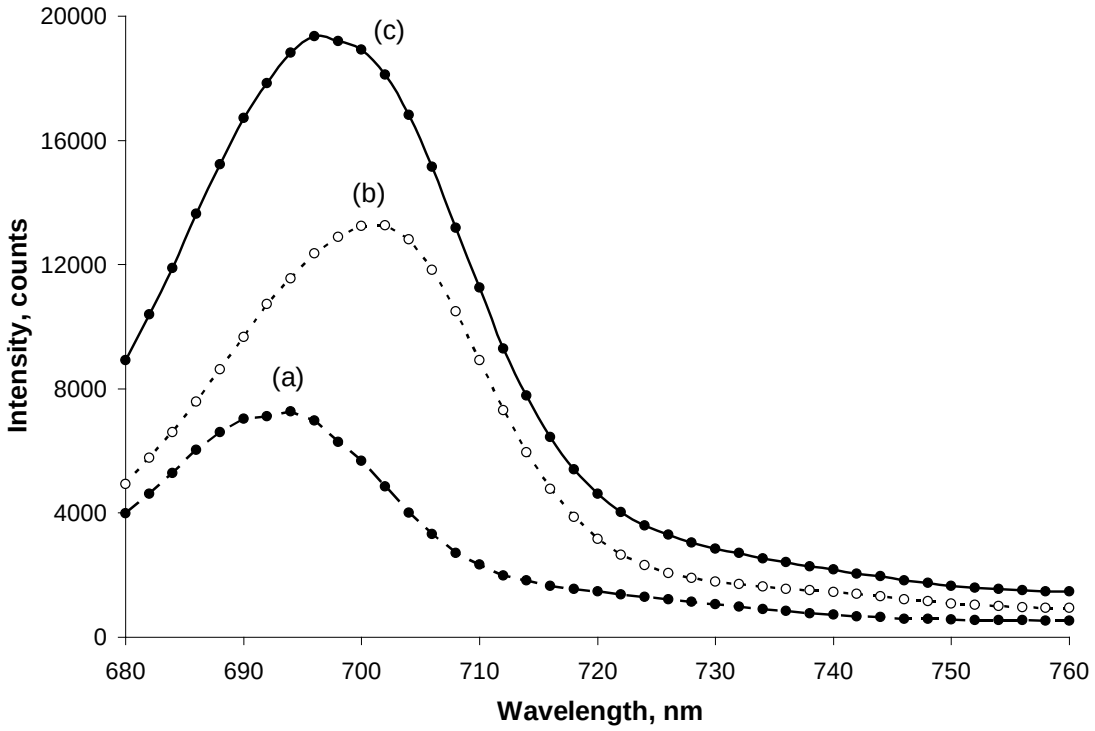

Figure 3.26. TRES spectra of lifetimes of 4.23 ns (a) and 1.74 ns (b), and sum of spectra (c) of conjugate in toluene

The two lifetimes may be as a result of Pc molecules packed differently on the gold surface, with the shorter lifetime possibly due to Pc quenched by interactions with the gold nanoparticles or between the phthalocyanines through aggregation, and the longer lifetime possibly due to Pc molecules which have been stabilised on the AuNP surface. It may also possibly be due to differences in the number of bound sulfur atoms of the phenylthio substituents to the surface of the gold nanoparticle, with Pcs that have more bound sulfur atoms held more rigidly than those that have fewer bound. Since the Pc loading on the AuNPs is also relatively low, it is expected that there would be fewer interactions between Pc molecules which would otherwise decrease fluorescence in the same way as aggregation.

4. CONCLUSIONS AND FUTURE PROSPECTS

This chapter summarises the results obtained for the studies conducted and reported in this thesis and future prospects.

4.1 Conclusions

In conclusion, a number of β-phenylthio substituted Pcs have been successfully synthesised and characterised, including a novel, symmetrical GePc derivative and a novel low-symmetry ZnPc derivative containing a single carboxylic acid group. All the complexes presented in this thesis gave satisfactory spectroscopic results confirming their purity. All the complexes exhibited monomeric behaviour in organic solvents as was evident from their UV-vis spectra characteristic of a high intensity monomeric Q band absorption for the $MPc(SPh)_4$ derivatives and a split Q band for the $H_2Pc(SPh)_4$ derivative. The photophysical and photochemical properties of the MPc derivatives were investigated and compared. Similar fluorescence quantum yields and triplet state quantum yields were observed for the low-symmetry and symmetrical ZnPc complexes, with high triplet state lifetimes obtained.

All of the complexes studied showed promise as optical limiters. They also showed high photostability, with photodegradation quantum yields obtained comparable to other ZnPc and GePc derivatives.

Photoelectrochemical studies of the low-symmetry ZnPc derivative as a sensitiser of ZnO gave a low IPCE value of 4.86% and an APCE of up to 7.29% as compared to values previously reported, due to strong forces of aggregation, with a maximum quantum efficiency of 0.074% obtained.

The higher yielding $ZnPc(SPh)_4$ was successfully conjugated to TOABr capped gold nanoparticles and the fluorescence behaviour of the conjugated MPc investigated. Novel behaviour of increased fluorescence lifetime and decrease in fluorescence quantum yields was observed suggesting both stabilisation of the Pc molecule and energy transfer to the gold nanoparticles.

4.2 Future prospects

Spectroscopic and photophysical studies of the synthesised low-symmetry and symmetrically substituted Pcs conjugated to variously stabilised gold nanoparticles, particularly with agents which improve water solubility, can be explored. The development of MPc-gold nanoparticle conjugates characterised by low toxicity, intense red absorption and good photophysical properties may advance the ongoing research for the treatment of cancer. The optical limiting properties of Pc thin films or polymer-embedded Pcs may also be studied for applications in photo-detector filters.

REFERENCES

[1] R.P. Linstead, *Journal of the Chemical Society* (1934) 1016-1017.

[2] J.M. Robertson, *Journal of the Chemical Society* (1935) 615.

[3] Y. Rio, M. Salomé Rodríguez-Morgade, T. Torres, *Organic and Biomolecular Chemistry* **6** (2008) 1877-1894.

[4] C.G. Claessens, U. Hahn, T. Torres, *The Chemical Record* **8** (2008) 75-97.

[5] M.M. Nicholson, in: Phthalocyanine. Properties and Applications, Vol. 3, VCH, New York, 1993.

[6] G. Mele, *Journal of Catalysis* **217** (2003) 342-334.

[7] D. Wöhrle, O. Suvorova, R. Gerdes, O. Bartels, L. Lapok, *Journal of Porphyrins and Phthalocyanines* **8** (2004) 1020-1041.

[8] M. Emmelius, G. Pawlowski, H.W. Vollmann, *Angewandte Chemie International Edition* **28** (1989) 1445-1471.

[9] R. Rella, A. Serra, P. Siciliano, A. Tepore, L. Troisi, L. Valli, *Thin Solid Films* **284-285** (1996) 870-872.

[10] F. Armand, H. Ferez, S. Fouriaux, O. Araspin, J.-P. Pradeau, C.G. Claessens, E.M. Maya, P. Vazquez, T. Torres, *Synthetic Metals* **10**2 (1999) 1476-1477.

[11] Z. Bao, A.J. Lovinger, A. Dodabalapur, *Applied Physics Letters* **69** (1996) 3066-3068.

[12] A.N. Cammidge, H. Gopee, *Chemical Communications* (2002) 966-967.

[13] M. Kimura, H. Ueki, K. Ohta, H. Shirai, N. Kobayashi, *Langmuir* **22** (2006) 5051-5056.

[14] A.M. Hor, R.O. Loutfy, *Thin Solid Films* **106** (1983) 291-301.

[15] A.W. Snow, W.R. Barger, M. Klusty, H. Wohltjen, N.L. Jarvis, *Langmuir* **2** (1986) 513-519.

[16] B.M. Hoffman, J.A. Ibers, *Accounts of Chemical Research* **16** (1983) 15-21.

[17] P. Turek, P. Petit, J.J. Andre, J. Simon, R. Even, B. Boudjema, G. Guillaud, M. Maitrot, *Journal of the American Chemical Society* **109** (1987) 5119-5122.

[18] D.K.P. Ng, J. Jiang, *Chemical Society Reviews* **26** (1997) 433-442.

[19] R. Koeppe, N.S. Sariciftci, P.A. Troshin, R.N. Lyubovskaya, *Applied Physics Letters* **87** (2005) 244102-244104.

[20] D. Wöhrle, D. Meissner, *Advanced Materials* **3** (1991) 129-138.

[21] G. de la Torre, P. Vázquez, F. Agulló-López, T. Torres, *Chemical Reviews* **104** (2004) 3723-3750.

[22] D. Dini, M. Hanack, *Journal of Porphyrins and Phthalocyanines* **8** (2004) 915-933.

[23] I. Rosenthal, *Photochemistry and Photobiology* **53** (1991) 859-870.

[24] J.D. Spikes, *Journal of Photochemistry and Photobiology B: Biology* **6** (1990) 259-274.

[25] S.B. Brown, E.A. Brown, I. Walker, *The Lancet Oncology* **5** (2004) 497-508.

[26] D. Wöhrle, G. Schnurpfeil, G. Knothe, *Dyes and Pigments* **18** (1992) 91-102.

[27] Y. Chen, Y. Lin, M.E. EI-Khouly, X. Zhuang, Y. Araki, O. Ito, W. Zhang, *Journal of Physical Chemistry* C **111** (2007) 16096-16099.

[28] A. Kempa, J. Dobrowolski, *Canadian Journal of Chemistry* **66** (1988) 2553 - 2555.

[29] M. Quintiliani, E.M. García-Frutos, P. Vázquez, T. Torres, *Journal of Inorganic Biochemistry* **102** (2008) 388-394.

[30] A. Tomoda, S. Saito, S. Ogawa, S. Shiraishi, *Chemistry Letters* **10** (1980) 1277-1280.

[31] P.A. Barrett, D.A. Frye, R.P. Linstead, *Journal of the Chemical Society* (1938) 1157.

[32] E.F. Bradbrook, R.P. Linstead, *Journal of the Chemical Society* (1936) 1744.

[33] A.N. Cammidge, H. Gopee, *Chemistry* **12** (2006) 8609-8613.

[34] E.V. Blackburn, C.J. Timmons, *Journal of the Chemical Society C: Organic* (1970) 175-178.

[35] R.P. Linstead, E.G. Noble, J.M. Wright, *Journal of the Chemical Society* (1937) 911.

[36] D.M. Knawby, T.M. Swager, *Chemistry of Materials* **9** (1997) 535-538.

[37] M. Polat, A. Gül, *Journal of Chemical Research* (1999) 130-131.

[38] S.V. Kudrevich, H. Ali, J.E. van Lier, *Journal of the Chemical Society, Perkin Transactions* **1** (1994) 2767-2775.

[39] H. Kliesch, A. Weitemeyer, S. Müller, D. Wöhrle, *Liebigs Annalen* **1995** (1995) 1269-1273.

[40] Y. Liu, D. Zhu, T. Wada, A. Yamada, H. Sasabe, *Journal of Heterocyclic Chemistry* **31** (1994) 1017-1020.

[41] T. Torres, G. de la Torre, J. García-Ruiz, *European Journal of Organic Chemistry* **1999** (1999) 2323-2326.

[42] G. De La Torre, T. Torres, *Journal of Porphyrins and P hthalocyanines* **1** (1997) 221-226.

[43] N. Kobayashi, R. Kondo, S. Nakajima, T. Osa, *Journal of the American Chemical Society* **112** (1990) 9640-9641.

[44] N. Kobayashi, T. Ishizaki, K. Ishii, H. Konami, *Journal of the American Chemical Society* **121** (1999) 9096-9110.

[45] C.C. Leznoff, P.I. Svirskaya, *Angewandte Chemie International Edition* **17** (1978) 947-947.

[46] M.J. Fuchter, B.J. Vesper, K.A. Murphy, H.A. Collins, D. Phillips, A.G.M. Barrett, B.M. Hoffman, *The Journal of Organic Chemistry* **70** (2005) 2793-2802.

[47] M.J. Fuchter, B.M. Hoffman, A.G.M. Barrett, *The Journal of Organic Chemistry* **70** (2005) 5086-5091.

[48] S.S. Erdem, I.V. Nesterova, S.A. Soper, R.P. Hammer, *The Journal of Organic Chemistry* **73** (2008) 5003-5007.

[49] N. Kobayashi, H. Ogata, N. Nonaka, E.A. Luk'yanets, *Chemistry - A European Journal* **9** (2003) 5123-5134.

[50] A.A. Chernonosov, V.V. Koval, D.G. Knorre, A.A. Chernenko, V.M. Derkacheva, E.A. Lukyanets, O.S. Fedorova, *Bioinorganic Chemistry and Applications* **2006** (2006) 1-8.

[51] V.V. Koval', A.A. Chernonosov, T.V. Abramova, T.M. Ivanova, O.S. Fedorova, D.G. Knorre, *Bioorganicheskaia Khimiia* **26** (2000) 118-125.

[52] A.A. Kuznetsova, L.I. Solov'eva, O.S. Fedorova, *Bioorganicheskaia Khimiia* **34** (2008) 683-695.

[53] V. Vijayanathan, *Synthetic Metals* **114** (2000) 273-278.

[54] R. Zugle, C. Litwinski, N. Torto, T. Nyokong, *New Journal of Chemistry* **35** (2011) 1588-1595.

[55] R.D. George, A.W. Snow, J.S. Shirk, W.R. Barger, *Journal of Porphyrins and Phthalocyanines* **2** (1998) 1-7.

[56] H. Ogata, R. Higashi, N. Kobayashi, *Journal of Porphyrins and Phthalocyanines* **7** (2003) 551-557.

[57] D.C. Hone, P.I. Walker, R. Evans-Gowing, S. FitzGerald, A. Beeby, I. Chambrier, M.J. Cook, D.A. Russell, *Langmuir* **18** (2002) 2985-2987.

[58] A. Kotiaho, R. Lahtinen, A. Efimov, H.-K. Metsberg, E. Sariola, H. Lehtivuori, N.V. Tkachenko, H. Lemmetyinen, *The Journal of Physical Chemistry C* **114** (2010) 162-168.

[59] V.P. Chauke, E. Antunes, W. Chidawanyika, T. Nyokong, *Journal of Molecular Catalysis A: Chemical* **335** (2011) 121-128.

[60] Y. Cheng, J.D. Meyers, A.-M. Broome, M.E. Kenney, J.P. Basilion, C. Burda, *Journal of the American Chemical Society* **133** (2011) 2583-2591.

[61] Y. Cheng, A. C Samia, J.D. Meyers, I. Panagopoulos, B. Fei, C. Burda, *Journal of the American Chemical Society* **130** (2008) 10643-10647.

[62] G. Mbambisa, N. Nombona, T. Nyokong, *Microchemical Journal* **93** (2009) 60-66.

[63] N. Nombona, D.A. Geraldo, J. Hakuzimana, A. Schwarz, P. Westbroek, T. Nyokong, *Journal of Applied Electrochemistry* **39** (2008) 727-736.

[64] K.I. Ozoemena, T. Nyokong, P. Westbroek, *Electroanalysis* **15** (2003) 1762-1770.

[65] F. Matemadombo, T. Nyokong, *Electrochimica Acta* **52** (2007) 6856-6864.

[66] M. Camerin, M. Magaraggia, M. Soncin, G. Jori, M. Moreno, I. Chambrier, M.J. Cook, D.A. Russell, *European Journal of Cancer* **46** (2010) 1910-1918.

[67] N. Nombona, E. Antunes, C. Litwinski, T. Nyokong, *Dalton Transactions* **40** (2011) 11876-11884.

[68] D. Wróbel, A. Boguta, *Journal of Photochemistry and P hotobiology A: Chemistry* **150** (2002) 67-76.

[69] L. Giribabu, Ch. Vijay Kumar, V. Gopal Reddy, P. Yella Reddy, C. Srinivasa Rao , S.-R. Jang, J.-H. Yum, Md.K. Nazeeruddin, M. Grätzel, *Solar Energy Materials and Solar Cells* **91** (2007) 1611-1617.

[70] G. de la Torre, P. Vázquez, F. Agulló-López, T. Torres, *Journal of Materials Chemistry* **8** (1998) 1671-1683.

[71] A. Ogunsipe, *Journal of Molecular Structure* **689** (2004) 89-97.

[72] A. Ogunsipe, J.-Y. Chen, T. Nyokong, *New Journal of Chemistry* **28** (2004) 822-827.

[73] M. Idowu, T. Nyokong, *Journal of Photochemistry and P hotobiology A: Chemistry* **197** (2008) 273-280.

[74] S. Maree, D. Phillips, T. Nyokong, *Journal of Porphyrins and Phthalocyanines* **6** (2002) 17 - 25.

[75] X.-F. Zhang, H.-J. Xu, *Journal of the Chemical Society, Faraday Transactions* **89** (1993) 3347-3351.

[76] A. Beeby, S. FitzGerald, C.F. Stanley, *Journal of the Chemical Society, Perkin Transactions* **2** (2001) 1978-1982.

[77] M. Durmuş, T. Nyokong, *Spectrochimica Acta. Part A, Molecular and Biomolecular Spectroscopy* **69** (2008) 1170-1177.

[78] M.J. Stillman, A.J. Thomson, *Journal of the Chemical Society, Faraday Transactions 2* **70** (1974) 805-814.

[79] A.B.P. Lever, M.R. Hempstead, C.C. Leznoff, W. Llu, M. Melnik, W.A. Nevln, P. Seymour, *Pure and Applied Chemistry* **58** (1986) 1467-1476.

[80] J.R. Darwent, P. Douglas, A. Harriman, G. Porter, M.-C. Richoux, *Coordination Chemistry Reviews* **44** (1982) 83-126.

[81] J. Mack, M.J. Stillman, *Journal of the American Chemical Society* **116** (1994) 1292-1304.

[82] T. Nyokong, Z. Gasyna, M.J. Stillman, *Inorganic Chemistry* **26** (1987) 1087-1095.

[83] M. Gouterman in: The Porphyrins, Part A. Physical Chemistry, Vol. 3, D. Dolphin (Ed.), Academic Press, New York, 1978, pp. 1-165.

[84] M.J. Stillman, T. Nyokong in: Phthalocyanines: Properties and Applications, Vol. 1, C.C. Leznoff, A.B.P. Lever (Eds.), VCH, Cambridge, 1989, pp. 139-247.

[85] K. Kasuga, N. Matsuura, K. Inoue, M. Handa, T. Sugimori, K. Isa, M. Nakata, *Chemistry Letters* **33** (2002) 352-353.

[86] G.A. Kumar, J. Thomas, N.V. Unnikrishnan, V.P.N. Nampoori, C.P.G. Vallabhan, *Journal of Porphyrins and Phthalocyanines* **5** (2001) 456-459.

[87] D.H. Templeton, M.S. Fischer, A. Zalkin, M. Calvin, *Journal of the American Chemical Society* **93** (1971) 2622-2628.

[88] C. Reichar in: Solvents and Solvent Effects in Organic Chemistry, H.F. Ebel (Ed.), VCH, Germany, 1988, pp. 285-338.

[89] N. Kobayashi, H. Konami, in: Phthalocyanines: Properties and Applications, Vol. 4, C.C. Leznoff, A.B.P. Lever (Eds.), VCH, New York, 1999.

[90] W.-F. Law, R.C.W. Liu, J. Jiang, D.K.P. Ng, *Inorganica Chimica Acta* **256** (1997) 147-150.

[91] P. Tau, T. Nyokong, *Dalton Transactions* **60** (2006) 4482-4490.

[92] J. Grodkowski, J.H. Chambers, P. Neta, *The Journal of Physical Chemistry* **88** (1984) 5332-5333.

[93] A. Skorobogaty, T.D. Smith, G. Dougherty, J.R. Pilbrow, *Journal of the Chemical Society, Dalton Transactions* (1985) 651-658.

[94] W.A. Nevin, W. Liu, S. Greenberg, M.R. Hempstead, S.M. Marcuccio, M. Melnik, C.C. Leznoff, A.B.P. Lever, *Inorganic Chemistry* **26** (1987) 891-899.

[95] K. Kasuga, *Coordination Chemistry Reviews* **32** (1980) 67-95.

[96] N. Nensala, *Polyhedron* **17** (1998) 3467-3475.

[97] O.E. Sielcken, M.M. Van Tilborg, M.F.M. Roks, R. Hendriks, W. Drenth, R.J.M. Nolte, *Journal of the American Chemical Society* **109** (1987) 4261-4265.

[98] I. Szymczyk, H. Abramczyk, *Pure and Applied Chemistry* **76** (2004) 183-187.

[99] Z.A. Schelly, D.J. Harward, P. Hemmes, E.M. Eyring, *The Journal of Physical Chemistry* **74** (1970) 3040-3042.

[100] H. Abramczyk, I. Szymczyk, G. Waliszewska, A. Lebioda, *The Journal of Physical Chemistry A* **108** (2004) 264-274.

[101] A.W. Snow in: The Porphyrin Handbook, Vol. 17, K.M. Kadish, K.M. Smith, R. Guilard (Eds.), Elsevier Science, New York, 2003.

[102] A.R. Monahan, J.A. Brado, A.F. DeLuca, *The Journal of Physical Chemistry* **76** (1972) 446-449.

[103] X. Li, D.K.F. Ng, *Tetrahedron Letters* **42** (2001) 5693-5695.

[104] A. Jablonski, *Zeitschrift Für Physik* **94** (1935) 38-46.

[105] P.W. Atkins in: Physical Chemistry, P.W. Atkins (Ed.), 6th ed., Oxford University Press, Oxford, 1998.

[106] K. Ishii, N. Kobayashi in: The Porphyrin Handbook, Vol. 16, K.M. Kadish, K.M. Smith, R. Guilard (Eds.), Elsevier Science, New York, 2003.

[107] N. Kobayashi, K. Nakai, *Chemical Communications* (2007) 4077-4092.

[108] A. Ogunsipe, D. Maree, T. Nyokong, *Journal of Molecular Structure* **650** (2003) 131-140.

[109] S. Fery-Forgues, D. Lavabre, *Journal of Chemical Education* **76** (1999) 1260.

[110] J. Fu, X.-you Li, D.K.P. Ng, C. Wu, *Langmuir* **18** (2002) 3843-3847.

[111] T.W.J. Gadella Jr, R.M. Clegg, T.M. Jovin, *Bioimaging* **2** (1994) 139-159.

[112] X.F. Wang, T. Uchida, D.M. Coleman, S. Minami, *Applied Spectroscopy* **45** (1991) 360-366.

[113] H.C. Gerritsen, *Proceedings of SPIE* **2329** (1995) 260-267.

[114] G.J. Brakenhoff, M. Müller, R.I. Ghauharali, K. Visscher, *Proceedings of SPIE* **2412** (1995) 115-123.

[115] A.D. Scully, A.J. MacRobert, S. Botchway, P. O'Neill, A.W. Parker, R.B. Ostler, D. Phillips, *Journal of Fluorescence* **6** (1996) 119-125.

[116] A.G. Ryder, S. Power, T.J. Glynn, J.J. Morrison, *Proceedings of SPIE* **4259** (2001) 102-109.

[117] J.C. Swarts, M. David Maree, *Journal of Porphyrins and Phthalocyanines* **11** (2007) 613-617.

[118] H. Du, R.-C.A. Fuh, J. Li, L.A. Corkan, J.S. Lindsey, *Photochemistry and Photobiology* **68** (1998) 141-142.

[119] W. Chidawanyika, T. Nyokong, *Journal of Photochemistry and Photobiology A: Chemistry* **206** (2009) 169-176.

[120] N. Nombona, E. Antunes, T. Nyokong, *Dyes and Pigments* **86** (2010) 68-73.

[121] N. Nombona, W. Chidawanyika, T. Nyokong, *Polyhedron* **30** (2011) 654-659.

[122] P. Kubát, J. Mosinger, *Journal of Photochemistry and P hotobiology A: Chemistry* **96** (1996) 93-97.

[123] S. Moeno, T. Nyokong, *Polyhedron* **27** (2008) 1953-1958.

[124] S.E. Maree, T. Nyokong, *Journal of Porphyrins and Phthalocyanines* **5** (2001) 782-792.

[125] J.R. Lakowicz in: Principles of Fluorescence Spectroscopy, 2nd ed., Kluwer Academic, New York, 1999.

[126] R.A. Keller, S.G. Hadley, *The Journal of Chemical Physics* **42** (1965) 2382-2387.

[127] A. Boguta, D. Wróbel, T.J. Hoffmann, P. Mazurkiewicz, *Crystal Research and Technology* **38** (2003) 267-274.

[128] E.S. Dodsworth, A.B.P. Lever, P. Seymour, C.C. Leznoff, *The Journal of Physical Chemistry* **89** (1985) 5698-5705.

[129] L. Oddos-Marcel, F. Madeore, A. Bock, D. Neher, A. Ferencz, H. Rengel, G. Wegner, C. Kryschi, H.P. Trommsdorff, *The Journal of Physical Chemistry* **100** (1996) 11850-11856.

[130] N. Kobayashi, M. Togashi, T. Osa, K. Ishii, S. Yamauchi, H. Hino, *Journal of the American Chemical Society* **118** (1996) 1073-1085.

[131] J.W. Verhoeven, *Pure and Applied Chemistry* **68** (1996) 2223 - 2286.

[132] A. Hirth, A.K. Sobbi, D. Wöhrle, *Journal of Porphyrins and Phthalocyanines* **1** (1997) 275-279.

[133] W. Spiller, H. Kliesch, D. Wöhrle, S. Hackbarth, B. Röder, G. Schnurpfeil, *Journal of Porphyrins and Phthalocyanines* **2** (1998) 145-158.

[134] M.J. Cook, I. Chambrier, S.J. Cracknell, D.A. Mayes, D.A. Russell, *Photochemistry and Photobiology* **62** (1995) 542-545.

[135] T. Nyokong, *Journal of the Chemical Society, Chemical Communications* (1994) 1983-1984.

[136] I. Seotsanyana-Mokhosi, N. Kuznetsova, T. Nyokong, *Journal of Photochemistry and Photobiology A: Chemistry* **140** (2001) 215-222.

[137] H. Xu, T. Shen, Q. Zhou, S. Shen, J. Liu, L. Li, S. Zhou, X. Zhang, Q. Yu, Z. Bi, X. Xiao, *Journal of Photochemistry and Photobiology A: Chemistry* **65** (1992) 267-276.

[138] M.D. Maree, N. Kuznetsova, T. Nyokong, *Journal of Photochemistry and Photobiology A: Chemistry* **140** (2001) 117-125.

[139] N.A. Kuznetsova, V.V. Okunchikov, V.M. Derkacheva, O.L. Kaliya, E.A. Lukyanets, *Journal of Porphyrins and Phthalocyanines* **9** (2005) 393-397.

[140] G. Winter, H. Heckmann, P. Haisch, W. Eberhardt, M. Hanack, L. Lüer, H.-J. Egelhaaf, D. Oelkrug, *Journal of the American Chemical Society* **120** (1998) 11663-11673.

[141] A. Hagfeldt, M. Grätzel, *Accounts of Chemical Research* **33** (2000) 269-277.

[142] J. Moser, *Monatshefte Für Chemie* **8** (1887) 373.

[143] A.E. Becquerel, *Comptes Rendus De l'Académie Des Sciences* **9** (1839) 145.

[144] B. O'Regan, M. Grätzel, *Nature* **353** (1991) 737-740.

[145] A. Fujishima, K. Honda, *Nature* **238** (1972) 37-38.

[146] M. Grätzel, *Journal of Photochemistry and Photobiology C: Photochemistry Reviews* **4** (2003) 145-153.

[147] M.K. Nazeeruddin, A. Kay, I. Rodicio, R. Humphry-Baker, E. Mueller, P. Liska, N. Vlachopoulos, M. Grätzel, *Journal of the American Chemical Society* **115** (1993) 6382-6390.

[148] T. Yoshida, T. Pauporte, D. Lincot, T. Oekermann, H. Minoura, *Journal of the Electrochemical Society* **150** (2003) C608-C615.

[149] T. Yoshida, M. Iwaya, H. Ando, T. Oekermann, K. Nonomura, D. Schlettwein, D. Wöhrle, H. Minoura, *Chemical Communications* **38** (2004) 400-401.

[150] K. Keis, E. Magnusson, H. Lindstr, S.-E. Lindquist, A. Hagfeldt, Solar *Energy Materials and Solar Cells* **73** (2002) 51-58.

[151] T. Yoshida, J. Zhang, D. Komatsu, S. Sawatani, H. Minoura, T. Pauporté, D. Lincot, T. Oekermann, D. Schlettwein, H. Tada, D. Wöhrle, K. Funabiki, M. Matsui, H. Miura, H. Yanagi, *Advanced Functional Materials* **19** (2009) 17-43.

[152] M.K. Nazeeruddin, R. Humphry-Baker, M. Grätzel, D. Wöhrle, G. Schnurpfeil, G. Schneider, A. Hirth, N. Trombach, R. Humphry‐Baker, *Journal of Porphyrins and Phthalocyanines* **3** (1999) 230-237.

[153] J.-J. Cid, M. García-Iglesias, J.-H. Yum, A. Forneli, J. Albero, E. Martínez-Ferrero, P. Vázquez, M. Grätzel, M.K. Nazeeruddin, E. Palomares, T. Torres, *Chemistry* **15** (2009) 5130-5137.

[154] M. Idowu, T. Loewenstein, A. Hastall, T. Nyokong, D. Schlettwein, *Journal of Porphyrins and Phthalocyanines* **14** (2010) 142-149.

[155] Nonomura, Photoelectrochemical Characterization of Dye-Modified ZnO Hybrid Thin Films Prepared by Electrochemical Deposition, Dissertation, 2006.

[156] N. Masilela, N. Nombona, T. Loewenstein, T. Nyokong, D. Schlettwein, *Journal of Porphyrins and Phthalocyanines* **14** (2010) 985-992.

[157] P.Y. Reddy, L. Giribabu, C. Lyness, H.J. Snaith, C. Vijaykumar, M. Chandrasekharam, M. Lakshmikantam, J.-H. Yum, K. Kalyanasundaram, M. Grätzel, M.K. Nazeeruddin, *Angewandte Chemie International Edition* **46** (2007) 373-376.

[158] A. Harriman, M.-C. Richoux, *Journal of the Chemical Society, Faraday Transactions 2* **76** (1980) 1618-1626.

[159] O.K. Varghese, C.A. Grimes, *Solar Energy Materials and Sol ar Cells* **92** (2008) 374-384.

[160] S. Günes, N.S. Sariciftci, *Inorganica Chimica Acta* **361** (2008) 581-588.

[161] R. Boyd in: Nonlinear Optics, Academic Press, San Diego, 1992.

[162] F. Kajzar, J. Messier, C. Rosilio, *Journal of Applied Physics* **60** (1986) 3040-3044.

[163] M. Sheik-Bahae, A.A. Said, T.-H. Wei, D.J. Hagan, E.W. Van Stryland, *The Journal of Quantum Electronics* **26** (1990) 760-769.

[164] H.S. Nalwa, J.S. Shirk in: Phthalocyanines: Properties and Applications, Vol. 4, C.C. Leznoff, A.B.P. Lever (Eds.), VCH, Cambridge, 1996, p. 79.

[165] M.K. Casstevens, M. Samoc, J. Pfleger, P.N. Prasad, *The Journal of Chemical Physics* **92** (1990) 2019-2024.

[166] M.A. Diaz-Garcia, F. Fernández-Lázaroa, G. de la Torre, E.M. Mayaa, P. Vazqueza, F. Agulló-López, T. Torres, *Synthetic Metals* **84** (1997) 923-924.

[167] S. Fang, H. Tada, S. Mashiko, *Applied Physics Letters* **69** (1996) 767-769.

[168] A. Yamashita, S. Matsumoto, S. Sakata, T. Hayashi, H. Kanbara, *Optics Communications* **145** (1998) 141-144.

[169] R. Ramos, P. , E. Blanco, *Journal of Applied Physics* **81** (1997) 7728-7733.

[170] S.M. O'Flaherty, S.V. Hold, M.J. Cook, T. Torres, Y. Chen, M. Hanack, W.J. Blau, *Advanced Materials* **15** (2003) 19-32.

[171] D. Phillips, *Science Progress* **77** (1993) 295-316.

[172] S.G. Bown, C.J. Tralau, P.D.C. Smith, D. Akdemir, T.J. Wieman, *British Journal of Cancer* **54** (1986) 43-52.

[173] M. Auffan, J. Rose, J.-Y. Bottero, G.V. Lowry, J.-P. Jolivet, M.R. Wiesner, *Nature Nanotechnology* **4** (2009) 634-41.

[174] M. Bruchez, M. Moronne, P. Gin, S. Weiss, A.P. Alivisatos, *Science* **281** (1998) 2013-2016.

[175] W.C. Chan, *Science* **281** (1998) 2016-2018.

[176] Y. Bian, X. Chen, D. Wang, C.-F. Choi, Y. Zhou, P. Zhu, D.K.P. Ng, J. Jiang, Y. Weng, X. Li, *Chemistry* **13** (2007) 4169-4177.

[177] S. Wang, N. Mamedova, N.A. Kotov, W. Chen, J. Studer, *Nano Letters* **2** (2002) 817-822.

[178] R. Weissleder, G. Elizondo, J. Wittenberg, C.A. Rabito, H.H. Bengele, L. Josephson, *Radiology* **175** (1990) 489-493.

[179] R. Mahtab, J.P. Rogers, C.J. Murphy, *Journal of the American Chemical Society* **117** (1995) 9099-9100.

[180] A. de la Isla, B. Witold, B. Bernard, M. Estevez, J.R. Rodriguez, S. Vargas, V.M. Castaño, *Materials Research Innovations* **7** (2003) 110-114.

[181] J. Ma, H. Wong, L.B. Kong, K.W. Peng, *Nanotechnology* **14** (2003) 619-623.

[182] C. Mah, I. Zolotukhin, T.J. Fraites, J. Dobson, C. Batich, B.J. Byrne, *Molecular Therapy* **1** (2000) S239-S242.

[183] D. Pantarotto, C.D. Partidos, J. Hoebeke, F. Brown, E. Kramer, J.-P. Briand, S. Muller, M. Prato, A. Bianco, *Chemistry and Biology* **10** (2003) 961-966.

[184] R.L. Edelstein, C.R. Tamanaha, P.E. Sheehan, M.M. Miller, D.R. Baselt, L.J. Whitman, R.J. Colton, *Biosensors and Bioelectronics* **14** (2000) 805-813.

[185] J.-M. Nam, C.S. Thaxton, C.A. Mirkin, *Science* **301** (2003) 1884-1886.

[186] T.K. Shinkai, M. Yanasea, M. Suzukia, H. Hondaa, T. Wakabayashib, J. Yoshidab, *Journal of Magnetism and Magnetic Materials* **194** (1999) 176-184.

[187] R.S. Molday, D. MacKenzie, *Journal of Imunological Methods* **52** (1982) 353-367.

[188] W.J. Parak, R. Boudreau, M. Le Gros, D. Gerion, D. Zanchet, C.M. Micheel, S.C. Williams, A.P. Alivisatos, C. Larabell, *Advanced Materials* **14** (2002) 882-885.

[189] K. Cho, X. Wang, S. Nie, Z.G. Chen, D.M. Shin, *Clinical Cancer Research* **14** (2008) 1310-1316.

[190] A.C.S. Samia, X. Chen, C. Burda, *Journal of the American Chemical Society* **125** (2003) 15736-15737.

[191] J.-Y. Chen, Y.-M. Lee, D. Zhao, N.-K. Mak, R.N.-S. Wong, W.-H. Chan, N.-H. Cheung, *Photochemistry and Photobiology* **86** (2010) 431-437.

[192] J. Li, D. Guo, X. Wang, H. Wang, H. Jiang, B. Chen, *Nanoscale Research Letters* **5** (2010) 1063-1071.

[193] A.C.S. Samia, S. Dayal, C. Burda, *Photochemistry and P hotobiology* **82** (2006) 617-625.

[194] D.K. Chatterjee, Z. Yong, *Nanomedicine* **3** (2008) 73-82.

[195] H.S. Qian, H.C. Guo, P.C.-L. Ho, R. Mahendran, Y. Zhang, *Small* **5** (2009) 2285-2290.

[196] B. Zhao, J.-J. Yin, P.J. Bilski, C.F. Chignell, J.E. Roberts, Y.-Y. He, *Toxicology and Applied Pharmacology* **241** (2009) 163-172.

[197] J. Gil-Tomás, S. Tubby, I.P. Parkin, N. Narband, L. Dekker, S.P. Nair, M. Wilson, C. Street, *Journal of Materials Chemistry* **17** (2007) 3739-3746.

[198] K. Záruba, J. Králová, P. Rezanka, P. Poucková, L. Veverková, V. Král, *Organic and Biomolecular Chemistry* **8** (2010) 3202-3206.

[199] J. Gil-Tomás, L. Dekker, N. Narband, I.P. Parkin, S.P. Nair, C. Street, M. Wilson, *Journal of Materials Chemistry* **21** (2011) 4189-4196.

[200] E.E. Connor, J. Mwamuka, A. Gole, C.J. Murphy, M.D. Wyatt, *Small* **1** (2005) 325-327.

[201] C.N.R. Rao, G.U. Kulkarni, P.J. Thomas, P.P. Edwards, *Chemical Society Reviews* **29** (2000) 27-35.

[202] J. Turkevich, P.C. Stevenson, J. Hillier, *Discussions of the Faraday Society* **11** (1951) 55-75.

[203] S.D. Perrault, W.C.W. Chan, *Journal of the American Chemical Society* **131** (2009) 17042-17043.

[204] M.N. Martin, J.I. Basham, P. Chando, S.-K. Eah, *Langmuir* **26** (2010) 7410-7417.

[205] M. Brust, M. Walker, D. Bethell, D.J. Schiffrin, R. Whyman, *Chemical Communications* (1994) 801-802.

[206] X. Liu, M. Atwater, J. Wang, Q. Huo, *Colloids and Surfaces. B, Biointerfaces* **58** (2007) 3-7.

[207] B. Nikoobakht, M.A. El-Sayed, *Chemistry of Materials* **15** (2003) 1957-1962.

[208] C.J. Johnson, E. Dujardin, S.A. Davis, C.J. Murphy, S. Mann, *Journal of Materials Chemistry* **12** (2002) 1765-1770.

[209] N.R. Jana, L. Gearheart, C.J. Murphy, *The Journal of Physical Chemistry B* **105** (2001) 4065-4067.

[210] J. Pérez-Juste, L.M. Liz-Marzán, S. Carnie, D.Y.C. Chan, P. Mulvaney, *Advanced Functional Materials* **14** (2004) 571-579.

[211] M. Liu, P. Guyot-Sionnest, *The Journal of Physical Chemistry. B* **109** (2005) 22192-22200.

[212] J.E. Millstone, S. Park, K.L. Shuford, L. Qin, G.C. Schatz, C.A. Mirkin, *Journal of the American Chemical Society* **127** (2005) 5312-5313.

[213] T.H. Ha, H.-J. Koo, B.H. Chung, *Journal of Physical Chemistry C* **111** (2007) 1123-1130.

[214] C.S. Ah, Y.J. Yun, H.J. Park, W.-J. Kim, D.H. Ha, W.S. Yun, *Chemistry of Materials* **17** (2005) 5558-5561.

[215] J. Xie, J.Y. Lee, D.I.C. Wang, *Journal of Physical Chemistry C* **111** (2007) 10226-10232.

[216] S. Chen, Z.L. Wang, J. Ballato, S.H. Foulger, D.L. Carroll, *Journal of the American Chemical Society* **125** (2003) 16186-16187.

[217] T.K. Sau, C.J. Murphy, *Journal of the American Chemical Society* **126** (2004) 8648-8649.

[218] X. Kou, S. Zhang, Z. Yang, C.-K. Tsung, G.D. Stucky, L. Sun, J. Wang, C. Yan, *Journal of the American Chemical Society* **129** (2007) 6402-6404.

[219] H. Zhang, Z. Zhou, B. Yang, M. Gao, *The Journal of Physical Chemistry B* **107** (2003) 8-13.

[220] Z.L. Yang, H.Z. Chen, L. Cao, H.Y. Li, M. Wang, *Materials Science and Engineering B: Solid State Materials for Advanced Technology* **106** (2004) 73-78.

[221] A.L. Patterson, *Physical Review* **56** (1939) 978-982.

[222] A. Moores, F. Goettmann, *New Journal of Chemistry* **30** (2006) 1121-1132.

[223] S. Eustis, M.A. El-Sayed, *Chemical Society Reviews* **35** (2006) 209-217.

[224] P. Mukherjee, R. Bhattacharya, N. Bone, Y.K. Lee, C.R. Patra, S. Wang, L. Lu, C. Secreto, P.C. Banerjee, M.J. Yaszemski, N.E. Kay, D. Mukhopadhyay, *Journal of Nanobiotechnology* **5** (2007) 4-16.

[225] K.S. Lokesh, V. Narayanan, S. Sampath, *Microchimica Acta* **167** (2009) 97-102.

[226] D.D. Perrin, L.F. Armarego in: Purification of Laboratory Chemicals, 2nd ed., Pergamon Press, Oxford, 1989.

[227] S.V. Kudrevich, M.G. Galpern, J.E. van Lier, *Synthesis* (1994) 779-781.

[228] N.S. Bayliss, *The Journal of Chemical Physics* **18** (1950) 292-296.

[229] W. Freyer, S. Mueller, K. Teuchner, *Journal of Photochemistry and Photobiology A: Chemistry* **163** (2004) 231-240.

[230] T. Nyokong, E. Antunes in: The Handbook of Porphyrin Science, Vol. 7, K.M. Kadish, K.M. Smith, R. Guilard (Eds.), Academic Press, New York, 2010, pp. 247-349.

[231] J. Mack, N. Kobayashi, *Chemical Reviews* **111** (2011) 281-321.

[232] M.G. Debacker, O. Deleplanque, B. van Vleirberge, F.X. Sauvage, *Laser Chemistry* **8** (1988) 1-11.

[233] M. Fujiki, H. Tabei, K. Isas, *Journal of the American Chemical Society* **108** (1986) 1532-1536.

[234] W. Sun, *Proceedings of SPIE* **4106** (2000) 280-288.

[235] S. Karuppuchamy, *Thin Solid Films* **397** (2001) 63-69.

[236] A.C.H. Ng, X.-you Li, D.K.P. Ng, *Macromolecules* **32** (1999) 5292-5298.

[237] P. Palmgren, B.R. Priya, N.P.P. Niraj, M. Göthelid, *Solar Energy Materials and Solar Cells* **90** (2006) 3602-3613.

[238] K. Nonomura, T. Loewenstein, E. Michaelis, D. Wöhrle, T. Yoshida, H. Minoura, D. Schlettwein, *Physical Chemistry Chemical Physics* **8** (2006) 3867.

[239] D. Schlettwein, T. Oekermann, T. Yoshida, M. Tochimoto, H. Minoura, *Journal of Electroanalytical Chemistry* **481** (2000) 42 - 51.

[240] T. Yoshida, K. Terada, D. Schlettwein, T. Oekermann, T. Sugiura, H. Minoura, *Advanced Materials* **12** (2000) 1214-1217.

[241] M.K. Nazeeruddin, F. De Angelis, S. Fantacci, A. Selloni, G. Viscardi, P. Liska, S. Ito, B. Takeru, M. Grätzel, *Journal of the American Chemical Society* **127** (2005) 16835-47.

[242] T. Oekermann, T. Yoshida, D. Schlettwein, T. Sugiura, H. Minoura, *Physical Chemistry Chemical Physics* **3** (2001) 3387-3392.

[243] S. Shukla, S. Seal, *Nanostructured Materials* **11** (1999) 1181-1193.